Development of Stimuli-Responsive Degradable Block Copolymer Micelles as Smart Drug Delivery Nanocarriers

Behnoush Khorsand Sourkohi

A Thesis
in
the Department
of
Chemistry and Biochemistry

Presented in Partial Fulfillment of the Requirements
for the Degree of Master of Science (Chemistry) at
Concordia University
Montréal, Québec, Canada

July 2013

CONCORDIA UNIVERSITY

School of Graduate Studies

This is to certify that the thesis prepared

By: **Behnoush Khorsand Sourkohi**

Entitled: Development of Stimuli-Responsive Degradable Block Copolymer Micelles as Smart Drug Delivery Nanocarriers

and submitted in partial fulfillment of the requirements for the degree of

Master of Science (Chemistry)

complies with the regulations of the University and meets the accepted standards with respect to originality and quality.

Signed by the final examining committee:

Dr. Judith Kornblatt	Chair
Dr. Christine DeWolf	Examiner
Dr. Peter D.Pawelek	Examiner
Dr. John Oh	Supervisor

Approved by_____

Chair of Department or Graduate Program Director

_____ 2013 _____

Dean of Faculty

Abstract

Polymer-based drug delivery systems offer the potential to increase the bioavailability of drug molecules without leaving toxic byproducts in the body. In particular, micellar aggregates based on amphiphilic block copolymers (ABPs) consisting of a hydrophobic core and a hydrophilic corona can enable the physical encapsulation of poorly water-soluble drugs. These micelles possess several advantages as drug delivery carriers due to their colloidal stability and tunable sizes with narrow size distribution. In addition, their physicochemical properties and small size enable passive tumor targeting through the enhanced permeability and retention effect. Also their chemical flexibility allows them to be tailored for active targeting. One additional benefit of using ABP-based micelles is that they can be engineered to incorporate stimuli-responsive moieties to control release of encapsulated drugs as a result of micellar degradation in response to external triggers such as pH, thiols and temperature. With this knowledge, ABP micelles can be designed with the ability to respond to stimuli that are inherently present in living systems and release their payload before being evacuated from the body. Presence of pH and redox gradients within the body makes them ideal stimuli in the design and development of stimuli-responsive degradable micelles for controlled release of therapeutics.

For better understanding of the structure-property relationship between morphological variance and stimuli-responsive degradation, we have developed new pH-sensitive degradable micelles having pendant t-butyl groups, as well as reductively degradable ABP micelles with single disulfide linkages positioned in the center of triblock copolymers, or with pendant disulfides positioned on the hydrophobic block.

They were synthesized by atom transfer radical polymerization, a dynamic controlled radical polymerization method enabling the synthesis of copolymers with narrow molecular weight distributions and pre-determined molecular weights. Aqueous self-assembly of ABPs resulted in colloidally stable spherical micelles capable of encapsulating hydrophobic model drugs at above critical micellar concentration. Various analytical methods were used to characterize ABPs and their micelles. The resulting micelles in aqueous solutions were destabilized in response to acidic conditions or reductive conditions, which suggests the possibility of enhanced release of encapsulated compounds. Results show that degradable ABPs of varying architectures and designs, upon the proper stimuli, will be dissociated at different rates, leading to a wide range of morphologies and sustained release rates of the encapsulated molecules.

Acknowledgements

First and foremost, I would like to thanks my supervisor Dr. John Oh, for his guidance, patience, support, and enthusiasm in working towards my M.Sc here at Concordia. During the time I spent writing my thesis, his assistance and support were irreplaceable and I appreciate that beyond words. He has been instrumental to my growth as a researcher and to achieving my academic goals, and I am grateful for the opportunities for learning and development that have been afforded to me over the last two years.

I would also like to thank my committee members Dr. Christine DeWolf and Dr. Peter D. Pawelek, for their continued support and guidance, as they were helpful and supportive during each committee meeting in guiding my project with great suggestions and ideas. Their advice has allowed me to overcome many difficulties and have made me a better scientist. Their combined critical minds have provided me with the ability to examine and solve problems in new ways.

Additionally, I would like to thank Dr. Louis Cuccia, who was a constant, pleasant presence throughout my time at Concordia. I have appreciated his kindness, support, and faith.

I was also extremely fortunate to have such amazing lab partners; working with them has been a great experience. I could not have wished for a better group of people with which to spend my time. Andrew, Samuel, Alexander, Nare, Nicky, Priya, Kaiwan, Yasaman, Soyoung - thank you so much. I especially would like to thank Samuel Aleksanian, who I shared many unforgettable times with and for all of his kindness and

help, both inside and outside the lab, and for the fun times we have had. I would also like to thank Dr. Nicky Chan, for time and effort he has extended to me to improve and proofread my thesis. His vast knowledge of polymer chemistry has been both inspirational and exciting. I would also like to thank Avid Hassanpour for her friendship and for the fun and unforgettable times we have had.

I would like to thank my partner Pooya Rahimian for his amazing support, kindness, and tremendous love and for always being in my corner. Finally, I would like to thank my mom Nadereh, my dad Alireza and my brother Behnam, for always having faith in me and encouraging me during hard times. They have always supported everything that I have done, and have been the most significant mentors in my life. Words cannot describe how much I appreciate the love and support you have given me. These people each have taught me to be strong on my way to achieve my dreams and goals.

Dedication

This thesis is dedicated to my parents Nadereh and Alireza, who have enlightened my journey on this earth with their endless love.

Contribution of Authors

The bulk of the research in this thesis was conducted independently under the supervision of Dr. John Oh at Concordia University. The material presented in Chapters 3, 4, and 5 have been accepted and published in a variety of well-respected, peer reviewed journals.

Dr. Rolf Schmidt, in the Centre for NanoScience Research at Concordia University, performed AFM measurements for the research presented in Chapter 4, Dr. Qian Zhang performed the polymer synthesis presented in Chapter 5, and Danièle Gagné and Christian Charbonneau, from the research group at the Université de Montréal performed the flow cytometry and confocal laser scanning microscopy. The preparation and editing of this thesis and of the aforementioned manuscripts were conducted under the supervision of Dr. John Oh.

Table of Contents

Contribution of Authors viii

List of Figures xiii

List of Tables xviii

List of Abbreviations xix

Chapter 1 1

Introduction 1

1.1. Brief overview of the research 1

1.2. Drug delivery in general 1

1.2.1. Pharmacokinetics of drug delivery 1

1.2.2. Routes to elimination of drugs from the body 2

1.2.3. Drug targeting strategies 3

1.3. Polymeric-based drug delivery nanocarriers 4

1.4. Amphiphilic block copolymer micellar aggregates 5

1.4.1. Micelle stability 8

1.4.2. Micelle size 10

1.5. Stimuli-responsive degradation (SRD) strategy 10

1.5.1. pH-responsive degradable micelles 13

1.5.2. Redox-responsive degradable micelles 15

1.6. Scope of the thesis 18

Chapter 2 20

Methodology: Synthesis and Characterization 20

2.1. Brief description 20

2.2. Synthesis and characterization of well-defined ABPs 20

2.2.1 ATRP as a means to synthesize well-defined ABPs 20

2.2.2. Molecular weight determination by gel permeation chromatography (GPC) 23

2.3. Aqueous micellization and characterization 25

2.3.1. Preparation of micellar aggregates in aqueous solution 25

2.3.2. Determination of critical micellar concentration (CMC) 26

2.3.3. Characterization of size and morphology of micellar aggregates 27
2.4. Cellular interaction of ABP-based micelles 29
2.4.1. Cell viability 29
Chapter 3 33
pH-Responsive Degradable Micelles 33
3.1. Introduction 33
3.2. Experimental section 35
3.3. Synthesis of HO-POEOMA-Br macroinitiator 35
3.4. Synthesis of HO-POEOMA-b-PtBMA ABP 37
3.5. Hydrolytic cleavage of t-butyl groups in HO-ABPs 38
3.6. Aqueous micellization of HO-ABPs 39
3.7. Destabilization of HO-ABP micellar aggregates in acidic condition 41
3.8. Physical encapsulation of model drug 42
3.9. Biotinconjugation with biotin and Avidin-HABA assay 44
3.10. Noncytotoxicity of HO-ABP micelles 45
3.11. Conclusions 46
Chapter 4 48
Thiol-Responsive Mono-Cleavable Micelles 48
4.1. Introduction 48
4.2. Experimental section 50
4.3. Synthesis of ss-$(PAP\text{-}Br)_2$ macroinitiator (MI) 50
4.4. Synthesis of ss-ABP_2 triblock copolymer 53
4.5. Aqueous micellization of ss-ABP_2 54
4.6. Reductive cleavage of disulfide linkages in ss-ABP_2 55
4.7. Reductively-degradable ss-ABP_2 micellar aggregates 56
4.8. Conclusions 58
Chapter 5 60
Glutathione-Responsive Micelles Having Pendant Disulfide Linkages 60
5.1. Introduction 60
5.2. Experimental section 63
5.3. Synthesis and aqueous micellization of PEO-b-PHMssEt 63
5.4. Redox-trigger destabilization of PEO-b-PHMssEt micellar Aggregates 64
5.5. Preparation of DOX-loaded micelles 66

5.6. GSH-triggered release of DOX from DOX-loaded micelles 69
5.7. GSH-responsive intracellular release of DOX upon degradation 70
5.8. *In vitro* cytotoxicity of DOX-loaded micelles 72
5.9. Conclusions 73
Chapter 6 75
Conclusion and Future Works 75
Appendix A 80
Experimental Section of Chapter 3 80
A.1. Materials 80
A.2. Synthesis and purification of 2-hydroxyethyl-2′-bromoisobutyrate (OH-iBuBr) 80
A.3. Synthesis of HO-POEOMA-Br macroinitiator (HO-MI) 81
A.4. Synthesis of HO-POEOMA-b-PtBMA (HO-ABP) block copolymer 82
A.5. Aqueous micellization by solvent evaporation 82
A.6. Determination of CMC using a NR probe 83
A.7. Hydrolytic cleavage of t-butyl groups of PtBMA blocks in acidic conditions 83
A.8. pH-responsive destabilization of HO-ABP micelles at low pH 83
A.9. Loading of NR into HO-ABP micelles 84
A.10. Bioconjugation of HO-ABP with biotin 84
A.11. Avidin-HABA binding assay studies 85
A.12. MTT cell viability assay 85
A.13. Supporting figures 86
Appendix B 89
Experimental Section of Chapter 4 89
B.1. Materials 89
B.2. Synthesis of bis[2-(2-bromoisobutyryloxy)ethyl] disulfide (SS-DBr) 89
B.3. Synthesis of ss-$(PAP\text{-}Br)_2$ macroinitiators 90
B.4. Synthesis of ss-ABP_2 triblock copolymers 90
B.5. Aqueous micellization by solvent evaporation 91
B.6. Determination of CMC of ss-ABP_2 in water by tensiometry 91
B.7. Degradation of ss-ABP_2 triblock copolymers and micelles 92
B.8. Supporting figures 93
Appendix C 94
Experimental Section of Chapter 5 94

C.1. Materials 94
C.2. Aqueous micellization by dialysis method 94
C.3. Preparation of DOX-loaded micelles 95
C.4. Determination of loading level of DOX using UV/Vis spectroscopy 95
C.5. GSH-triggered destabilization of PEO-b-PHMssEt micelles 96
C.6. GSH-triggered release of DOX from DOX-loaded micelles 96
C.7. Cell viability using MTT assay 96
C.8. Intracellular DOX release and HeLa cells viability 97
C.9. Cellular uptake using flow cytometry and Confocal laser scanning microscopy (CLSM) 97
C.9.1. Flow cytometry 97
C.9.2. Confocal laser scanning microscopy (CLSM) 98
C.10. Supporting figures 98
References 101
List of publications 105

List of Figures

Figure 1.1. Controlled versus uncontrolled release profile of drugs after administration. 2

Figure 1.2. Passive and active targeting of nanocarriers..... 4

Figure 1.3. Different self-assembled structures formed by ABPs dictated by packing parameter, P. 7

Figure 1.4. Structure of a self-aggregated micelle from diblock copolymers..... 8

Figure 1.5. Schematic illustration of the process of micelle formation and the concept of CMC..... 9

Figure 1.6. Stimuli-responsive degradation of ABP micelles for controlled release of encapsulated hydrophobic drugs..... 11

Figure 1.7. Stimuli responsive ABP micelles with different location of cleavable linkage (X). The figure is slightly modified from the reference (A and B represent polymer blocks and b represent blocks)..... 12

Figure 2.1. Mechanism of normal ATRP process..... 22

Figure 2.2. Mechanism of AGET ATRP process. 23

Figure 2.3. Schematic diagram of a GPC setup for the measurement of polymer molecular weight of polymers. 25

Figure 2.4. Structures of MTT tetrazolium salt and its formazan product..... 30

Figure 2.5. Absorption spectra of MTT and commercially prepared MTT-formazan dissolved in DMSO. Also shown is the spectrum of MTT-formazan produced by incubation of L-DAN cells with MTT (5 mg ml^{-1}) for 4 h. 31

Figure 3.1. Synthesis of HO-ABPs by consecutive ATRP of OEOMA and tBMA in the presence of a HO-terminated ATRP initiator (HO-iBuBr), as well as aqueous

micellization and acid-triggered dissociation of HO-ABP micelles as contolled drug delivery nanocarriers (bpy: 2,2′-bipyridyl, PMAA: poly(methacrylic acid)). 35

Figure 3.2. GPC traces of HO-ABP and HO-POEOMA-Br MI. 38

Figure 3.3. ^{1}H-NMR spectra of HO-MI (a), HO-ABP before (b), and after (c) hydrolytic cleavage of PtBMA block in the presence of trifluoroacetic acid. 39

Figure 3.4. Evolution of fluorescence spectra (a) and fluorescence intensity at 480 nm (b) of NR for aqueous mixtures consisting of NR with various amounts of HO-ABP to determine CMC to be 6.3 μg mL^{-1}. 40

Figure 3.5. DLS diagram and TEM image (inset) with scale bar = 100 nm (a) and diameter over concentration (b) of HO-ABP micelles. 41

Figure 3.6. DLS diagrams (a) and digital images (b) of HO-ABP micelles at pH = 7, 5, and 3 after 4 days. 42

Figure 3.7. Schematic illustration of bioconjugation of HO-ABP with biotin to form biotin-conjugated ABP (a) and UV–Vis spectra of Avidin–HABA complex before and after addition of biotinylated micelles in aqueous solution (b)..... 45

Figure 3.8. Viability of HEK293T and HeLa cells cultured with HO-ABP micelles for 48 hrs..... 46

Figure 4.1. Illustration of synthesis, aqueous micellization, and degradation of mono-cleavable brush-like ss-ABP_2 triblock copolymers labeled with single disulfides in the middle blocks (PMDETA : N,N,N′,N″,N″-pentamethyldiethylenetriamine, Bu_3P: tributylphosphine). 50

Figure 4.2. Kinetic plot (a) and evolution of molecular weight and molecular weight distribution of ss-(PAP-Br)$_2$-1 and ss-(PAP-Br)$_2$-3 (b). The straight line in (b) is the theoretically predicted molecular weight over conversion. 52

Figure 4.3. GPC traces (a) and ^{1}H-NMR spectra in $CDCl_3$ (b) of ss-(PAP-Br)$_2$ and ss-ABP$_2$. 54

Figure 4.4. Surface pressure versus concentration of ss-ABP$_2$ to determine CMC by tensiometry. 55

Figure 4.5. GPC traces of ss-ABP$_2$ before and after reductive cleavage of disulfide linkages in the presence of Bu_3P. 56

Figure 4.6. For ss-ABP$_2$ symmetric triblock copolymers, DLS diagrams based on % volume and AFM images with the size = 10 μm × 10 μm before (a and b) and after (c and d) addition of DTT defined as DTT/disulfide = 1/1 in water (insets; digital images of micellar dispersions in water). 58

Figure 5.1. Preparation of well-controlled PEO-b-PHMssEt via ATRP (PMDETA: N,N,N′,N′,N″-pentamethyldiethylenetriamine). 62

Figure 5.2. Illustration of PEO-b-PHMssEt micelles as effective intracellular drug delivery nanocarriers exhibiting enhanced release of DOX in response to GSH in cancer cells. 63

Figure 5.3. DLS diagram of PEO-b-PHMssEt micelles prepared using dialysis method in water. 64

Figure 5.4. Evolution of DLS diagrams (volume %) of PEO-b-PHMssEt micellar aggregates in aqueous buffer solution as control and in 10 mM aqueous GSH buffer solution over time. 66

Figure 5.5. DLS diagram (a) and TEM images (b) of DOX-loaded micelles of PEO-b-PHMssEt at 2.5 mg/mL concentration prepared by dialysis method (inset of (a): digital picture of DOX-loaded micellar dispersion)..... 67

Figure 5.6. A typical UV/Vis spectrum of DOX-loaded micelles after the removal of water, compared with that of free DOX (19.5 μmol mL^{-1}) in DMF..... 68

Figure 5.7. Release of DOX from DOX-loaded micelles in 10 mM aqueous GSH solution buffered with KH_2PO_4 at pH = 7.0, and aqueous KH_2PO_4 buffer solution at pH = 7.0 as a control. 70

Figure 5.8. Flow cytometric histograms of HeLa cells incubated with DOX-loaded PEO-b-PHMssEt micelles for 2 hrs. 71

Figure 5.9. CLSM images of HeLa cells incubated with DOX-loaded PEO-b-PHMssEt micelles for 24 hrs. The images from left to right show cell nuclei stained by DAPI (blue), DOX fluorescence in cells (red), overlays of two images, and differential interference contrast (DIC) image. Scale bar = 20 μm. 72

Figure 5.10. Viability of HeLa cells incubated with different amounts of empty micelles, DOX-loaded micelles, and free DOX for 48 hrs. Data are presented as average ± standard deviation (n = 12). 73

Figure A.1. For HO-MI-3, kinetic plot (a) and evolution of molecular weight and molecular weight distribution over conversion (b) for ATRP of OEOMA in acetone at 47 °C under $[OEOMA]_0/[HO\text{-}iBuBr]_0/[CuBr]_0/[bpy]_0$ = 50/1/0.5/1; OEOMA/acetone = 1.5/1 wt/wt. The dotted lines in (a) are linear fits, and the straight lines in (b) are the theoretically predicted molecular weight over conversion. 86

Figure A.2. UV spectra of different concentrations of NR in THF to determine its extinction coefficient at λ_{max} = 527 nm. 87

Figure A.3. An example of UV spectra of HO-ABP and NR-loaded HO-ABP micelles dissolved in THF. 87

Figure A.4. DLS diagram of an example of NR-loaded HO-ABP micelles in water. 88

Figure B.1. ^{1}H-NMR spectra of SS-DBr after (a) and before (b) precipitation from hexane (purification). 93

Figure C.1. Evolution of z-average diameter of PEO-b-PHMssEt micelles in aqueous 10 mM GSH solution over time. 98

Figure C.2. UV absorbance at λ= 497 nm of free DOX in outer water during extensive dialysis. 99

Figure C.3. Overlaid UV spectra (a) and absorbance at λ_{max} = 480 nm (b) of DOX at various concentrations (μmol L^{-1}) in DMF to construct a calibration curve. 99

Figure C.4. Absorption (—) and emission (- - -) spectra of 0.01 mg mL^{-1} free DOX, and emission spectrum of 0.2 mg mL^{-1} micellar-encapsulated DOX (····), all in aqueous solution. 100

Figure C.5. Absorption spectra of MTT and commercially prepared MTT-formazan dissolved in DMSO. Also shown is the spectrum of MTT-formazan produced by incubation of L-DAN cells with MTT (5 mg ml^{-1}) for 4 h. 100

List of Tables

Table 1.1. pH sensitive linkages and their hydrolytic products. 14

Table 3.1. Characteristics for ATRP of OEOMA in the presence of OH-iBuBr at 47 ºC in acetone[a] 36

Table 3.2. Encapsulation of NR in HO-ABP micelles at different weight ratios of NR/HO-ABP. 43

Table 4.1. Characteristics of ss-$(PAP\text{-}Br)_2$ difunctional macroinitiators[a] 51

Table 5.1. Loading level of DOX for DOX-loaded PEO-b-PHMssEt micelles prepared by dialysis method over 5 days. 69

List of Abbreviations

ABPs	Amphiphilic block copolymers
AFM	Atomic force microscopy
AGET	Activator generated by electron transfer
ATRP	Atom transfer radical polymerization
BPY	2,2′-bipyridyl
Br-iBuA	2-bromoisobutyric acid
Bu_3P	Tributylphosphine
CLSM	Confocal laser scanning microscopy
CMC	Critical micellar concentration
CRP	Controlled radical polymerization
DAPI	4',6-diamidino-2-phenylindole
D_{av}	Average diameter
DCC	N,N´-dicyclohexyl carbodiimide
DCU	Dicyclohexyl urea
DDS	Drug delivery systems
Dex-LA	Dextran-lipoic acid
D_H	Hydrodynamic diameter
DIC	Differential interference contrast
DLS	Dynamic light scattering
DMAP	N,N-dimethylaminopyridine
DMEM	Dulbecco's modified eagle medium
DMSO	Dimethyl sulfoxide
DOX	Doxorubicin

DTT	Dithiothreitol
EDC	1-ethyl-3-(3-dimethylaminopropyl)carbodiimide
EGFR	Epidermal growth factor receptor
EPR	Enhanced permeability and retention
Et_3N	Triethylamine
EthD-1	Ethidium homodimer
FBS	Fetal bovine serum
GPC	Gel permeation chromatography
GSH	Glutathione
HABA	2-(4-hydroxyphenylazo)benzoic acid
HEK293T	Human embryonic kidney 293T
HEMI	N-(2-hydroxyethyl) maleimide
IV	Intravenous
KHP	Potassium hydrogen phthalate
LA	L-lactide
LE	Loading efficiency
M_n	Number-average molecular weight
MTC	2-(2,4-dinitrophenylthio)ethyl-5-methyl-2-oxo-1,3-dioxane-5-carboxylate
MTT	3-(4,5-dimethylthiazol-2-yl)-2,5-diphenyltetrazolium bromide
MTS	3-(4,5-dimethylthiazol-2-yl)-5-(3-carboxymethoxyphenyl)-2-(4-sulfophenyl)-2H-tetrazolium
M_w	Weight-average molecular weight
NMP	Nitroxide-mediated polymerization
NMR	Nuclear magnetic resonance

NR	Nile red
PAA	Poly(aspartic acid)
PAMAM	polyamidoamine
PAP	Poly(oligo(propylene oxide) monononylphenyl ether acrylate
PC	Polycarbonate
PCL	Poly(ε-caprolactone)
PDI	Polydispersity
PEEP	Poly(ethyl ethylene phosphate)
PEO	Polyethylene oxide
PES	Polyester
PHMssEt	Disulfide-labeled polymethacrylate
PHPMA	poly(N-2-hydroxypropyl methacrylamide)
PMDETA	N, N, N', N'', N''-Pentamethyldiethylenetriamine
PMAA	poly(methacrylic acid)
PMMA	Poly(methyl methacrylate)
POEOMA	Poly oligo(ethylene glycol) monomethyl ether methacrylate
PSt	Polystyrene
PtBMA	poly(t-butyl methacrylate)
RAFT	Reversible addition fragmentation transfer
RES	Reticuloendothelial system
RI	Refractive index
SRD	stimuli-responsive degradation
SS-DBr	Bis[2-(2-bromoisobutyryloxy)ethyl] disulfide difunctional initiator
TBST	Tris-buffered saline tween-20
TEM	Transmission electron microscopy

THF	Tetrahydrofuran
UV/Vis	Ultraviolet Spectroscopy

Chapter 1

Introduction

1.1. Brief overview of the research

My master research is aimed at developing self-assembled micellar aggregates of well-controlled amphiphilic block copolymers (ABPs) with stimuli-responsive degradation (SRD) properties. In response to external stimuli these micelles exhibit enhanced release of encapsulated biomolecules including anticancer drugs, thus offering versatility as multi-functional drug delivery nanocarriers. Several of new ABPs having disulfide and pendant acid-labile linkages were synthesized by atom transfer radical polymerization (ATRP). They were then characterized for aqueous micellization, controlled release and cellular interactions.

1.2. Drug delivery in general

1.2.1. Pharmacokinetics of drug delivery

The science of drug delivery can be described as the application of chemical or biological science to control *in vivo* location of drug molecules for clinical benefits. Figure 1.1 illustrates the release profile of drugs by conventional delivery methods such as injection. When drugs are administrated the drug level abruptly reaches a peak in the blood. However, most of the dose is wasted as only a small fraction of the dose actually hits relevant receptors over time. The drug level then decreases to below the minimum therapeutic level, which represents an ineffective dose until the next administration (dot-

dash line).[1] The ideal pharmacokinetics of drug delivery suggests that sustainable release where drug level in the blood remains constant in the appropriate therapeutic range (solid line) between the maximum toxic threshold, and the minimum therapeutic level would be beneficial compared with conventional drug administrative methods.[2] Effective drug delivery systems (DDS) can offer the ability to maintain the therapeutic dosage within a target zone.

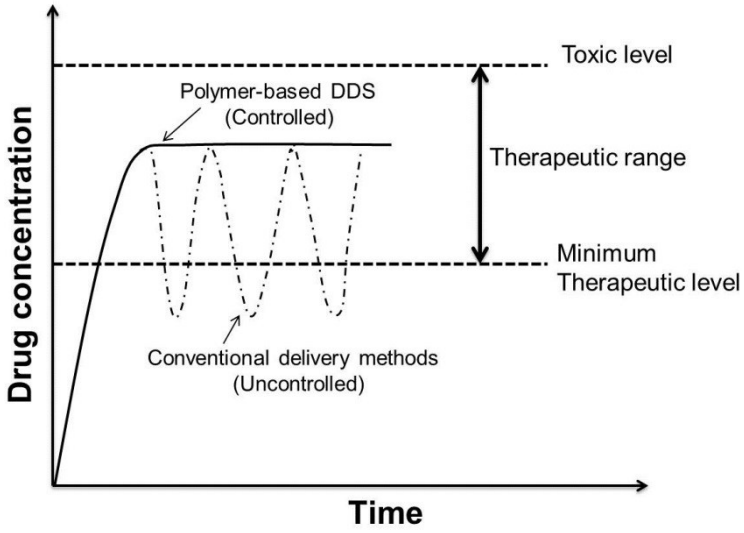

Figure 1.1. Controlled versus uncontrolled release profile of drugs after administration.[1]

1.2.2. Routes to elimination of drugs from the body

Renal excretion and uptake by reticuloendothelial system (RES) are the main routes to the elimination of foreign particles from the body. Renal excretion is the irreversible transfer from plasma into urine. This minor issue can be minimized by designing nanocarriers larger than a certain size (> 8 nm).[3] RES macrophages are the major barrier for the rapid clearance of foreign bodies including drugs from the body after intravenous (IV) administration. Typical macrophages include Kupffer cells in the

liver and fixed macrophages in the spleen, which recognize opsonin proteins.[4] Opsonins are the blood proteins that help macrophages recognize foreign bodies in the blood.[5] DDS coated with opsonins are removed from blood circulation through a process known as opsonization. The extent of opsonization is influenced by size and surface properties of DDS. Large particles and particles with hydrophobic surfaces are rapidly removed by RES macrophages.[6]

1.2.3. Drug targeting strategies

The idea of drug targeting was suggested nearly 100 years ago by Paul Ehrlich, who proposed a hypothetical 'magic bullet' to improve drug delivery in the body.[7] There are two strategies to deliver drugs to specific sites: "passive" and "active" targeting (Figure 1.2). Passive targeting involves the accumulation of particles with diameters < 200 nm in tumors.[8] This process is known to be the enhanced permeability and retention (EPR) effect,[9] utilizing poorly-aligned defective endothelial cells with leaky vasculature. More promising is active targeting that uses specific biological interactions, typically ligand-receptor and antibody-antigen interactions. This strategy requires the synthesis of nanocarriers having functional groups that are utilized for further bioconjugation with cell-targeting species such as peptides, proteins, and antibodies. These biomolecules can recognize receptors over-expressed on specific tumors, facilitating internalization of nanocarriers into cells through receptor-mediated endocytosis.[10]

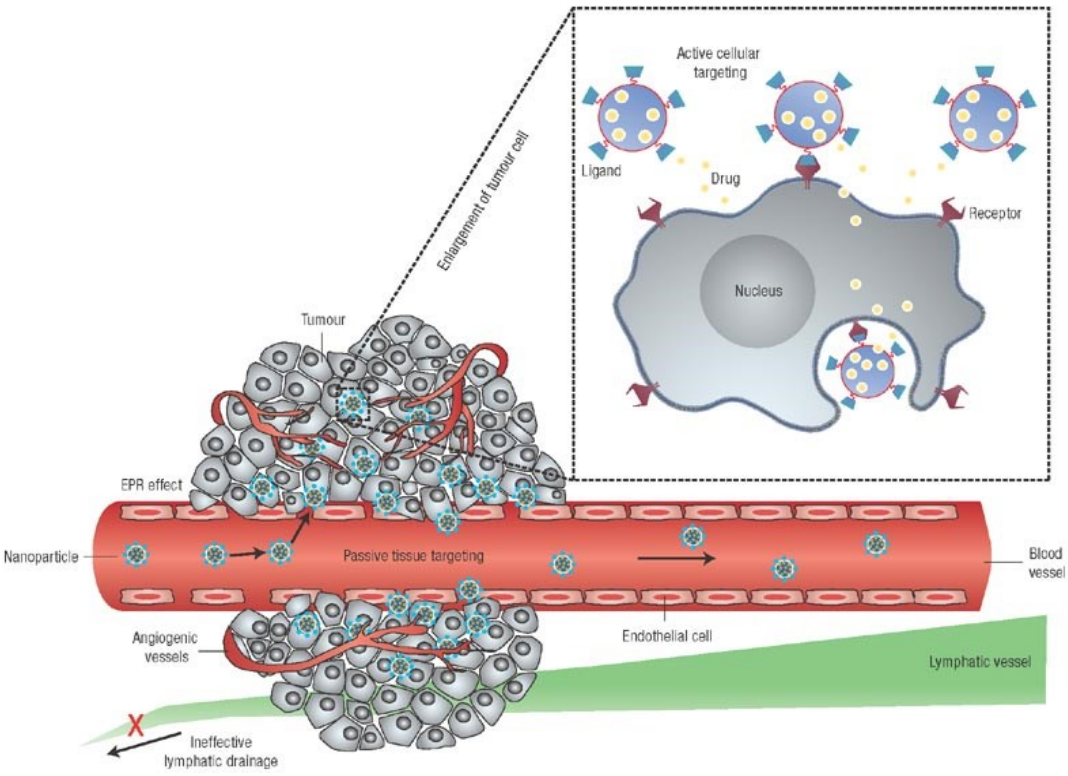

Figure 1.2. Passive and active targeting of nanocarriers.[8]

1.3. Polymeric-based drug delivery nanocarriers

Polymer-based DDS offer great potential to increase bioavailability of drug molecules *in vivo*. They can effectively deliver drugs to targeted sites, thus increasing therapeutic efficiencies.[11] Typical examples of polymer-based DDS include polymer-drug conjugates,[12] dendrimers,[13] microgels/nanogels,[14] and block copolymer aggregates.[15]

Polymer-drug conjugates are called polymer-prodrugs in which drugs are chemically linked to polymers. The polymer-prodrugs can increase water solubility of hydrophobic drugs as well as promote the transport of drugs to targeted areas.[16] However, a drawback involves the use of covalent linkages to conjugate drug molecules

to polymer chains. These stable bonds are not easily cleaved to release drugs. To circumvent this issue, labile linkages such as disulfides have been used.[17]

Dendrimers are well-defined highly branched macromolecules. Typical examples include polyamidoamine (PAMAM) modified with neutral moieties,[18] polyaryl ether and poly(ethylene oxide) (PEO)-based dendrimers.[19] They exhibit unique morphological and physical properties, high biocompatibility and water solubility, thus offering potential as candidates for polymer-based DDS. However, the synthesis of well-defined multi-generation dendrimers remains challenging.

Microgels are a class of hydrogels that are submicron sized crosslinked particles. When the size of microgels is in a nanometer range, they are known as nanogels. These microgels/nanogels possess all features of hydrogels, including tunable chemical and physical structures, good mechanical properties, high water content and biocompatibility. Further, they exhibit tunable size, large surface area for bioconjugation, and hydrophilic interior network.[20] They are suitable for encapsulation of hydrophilic drugs.

My thesis focuses on the design and development of effective micellar aggregates based on amphiphilic block copolymers (ABPs), which will be explained in greater detail.

1.4. Amphiphilic block copolymer micellar aggregates

In recent years, ABP-based micelles have been extensively explored for pharmaceutical applications. The rapid development of ABP-based micelles is because of their ability to form various types of nanoparticles with desirable properties as effective drug nanocarriers. These promising properties of ABPs are initiated as a result of their chemical flexibility and ability to form nanostructure with various morphologies.

ABPs consist of covalently attached hydrophobic and hydrophilic blocks, which can be obtained by polymerization of more than one type of monomers. Typical polymers include polyesters,[21] poly(amino acid) derivatives,[22] and polymethacrylate as hydrophobic block hydrophilic blocks; and PEO, PEO analogues, and polysaccharides as hydrophilic block.[23] As a result of the amphiphilic nature, ABPs undergo self-assembly to form micellar aggregates with various morphologies in aqueous solution. This is to minimize energetically unfavorable interaction of hydrophobic surfaces with water.[24]

These morphologies are dictated by "packing parameter (P)", as defined by the following equation:

$$P = \frac{v}{a_0 l_c}$$

Where "v" is the volume of hydrophobic chains, "a_0" is area of the hydrophilic head group and "l_c" is the length of hydrophobic tail. As seen in Figure 1.3, P values determine the favored morphologies of aggregates: $P \leq {}^{1}/_{3}$ formation for spherical micelles, ${}^{1}/_{3} \leq P \leq {}^{1}/_{2}$ for cylindrical micelles, and ${}^{1}/_{2} \leq P \leq 1$ for vesicles (polymersomes).[25]

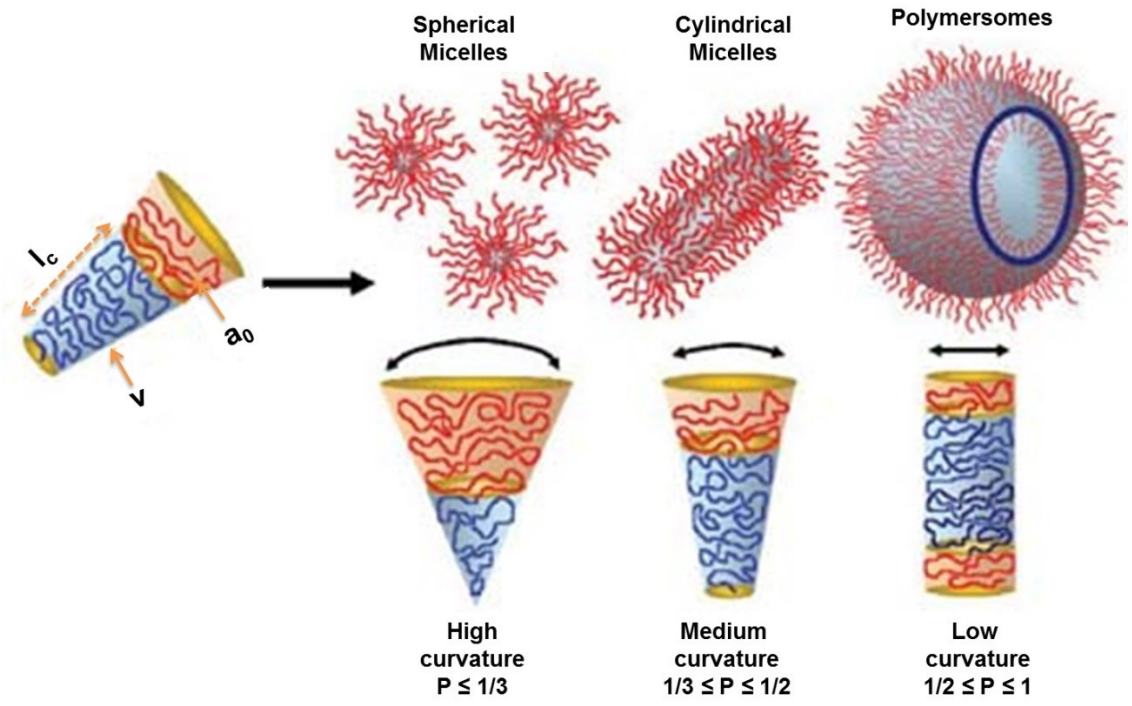

Figure 1.3. Different self-assembled structures formed by ABPs dictated by packing parameter, P.[15]

Self-assembled micelles consist of hydrophobic cores, ensuring encapsulation of hydrophobic therapeutics including anticancer drugs, surrounded with hydrophilic coronas, enduring biocompatibility and aqueous colloidal stability (Figure 1.4).[26] In addition to these features, they possess several advantages; including facile preparation, colloidal stability, tunable sizes with narrow size distribution, as well as protection of drugs from deactivation, preservation of its activity during blood circulation and transport to targeted area. Their physicochemical properties and small size enables passive tumor targeting through the EPR effect,[27] and further they can enhance drug efficiency through active targeting by bioconjugation. For successful applications, a high degree of control over the stability and size of micellar nanocarriers are required.

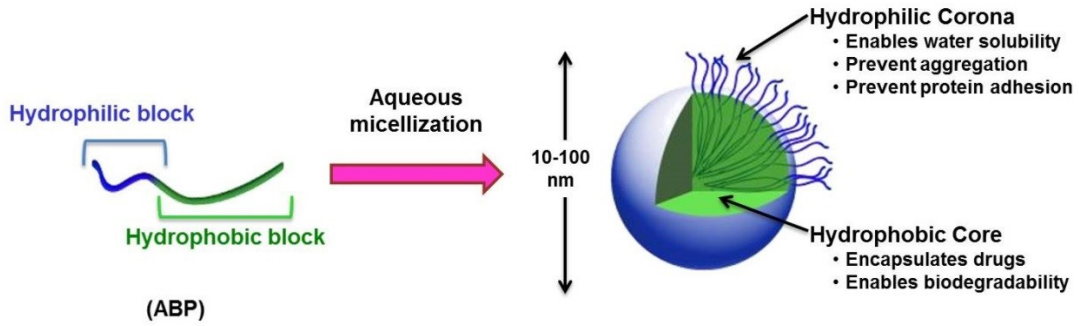

Figure 1.4. Structure of a self-aggregated micelle from diblock copolymers.[28]

1.4.1. Micelle stability

The stability of micellar systems can be evaluated in terms of thermodynamic and kinetic stability. Thermodynamic stability of micelles reflects how micelles form or dissociate at different concentrations. From this point of view, micelle stability can be measured by critical micellar concentration (CMC), which is the concentration at which micellar aggregates first appear. At concentrations below CMC, the existence of polymer chains as unimers or single polymer chains is thermodynamically favored. Upon the increase in concentrations above the CMC, polymer chains prefer to spontaneously self-assemble into micelles to minimize enthalpically less favourable interactions between the hydrophobic segments and water (Figure 1.5).[29]

The important parameters that influence CMC values include the composition of block copolymers; such as chain length, chemical structure/interaction parameters between the different blocks and water, as well as cross-linking of block segments. For example, an increase in hydrophobic chain length decreases CMC, due to greater energy minimization when hydrophobic chains assemble.[30] In general, ABPs have low CMCs ranging from 10^{-6} to 10^{-7} M compared to low molecular weight surfactants whose CMC range from 10^{-3}

to 10^{-4} M.[31] The low CMC is advantageous for *in vivo* applications, in that micelles are stable upon dilution in blood.

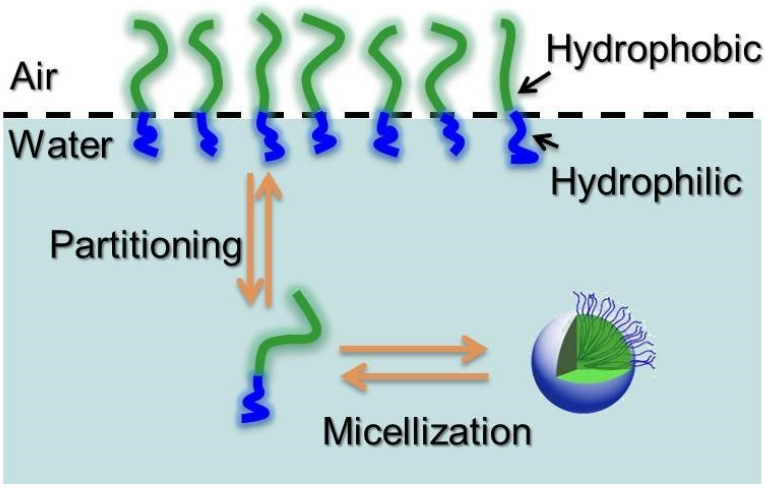

Figure 1.5. Schematic illustration of the process of micelle formation and the concept of CMC.

The kinetic stability of a polymer micelle undergo extremely different processes in assembly and disassembly.[32] For copolymer micelles the nature of the hydrophobic core plays an important role in the kinetic stability. In micelles that exist in environments that are below the glass transition temperature of the core forming polymer, the core of the micelle can be a solid matrix, which would lead to high kinetic stability. The polymer chains in this matrix are essentially immobile and so even when the micelle falls below the CMC, chain mobility is limited and the micelle cannot easily disassemble. So the mobility of the polymer chains, which is T_g dependent, and the degree of entanglement, which is length dependent, are extremely important in tailoring the kinetic stability of a micelle.[33] Another factor that can play an important role in the kinetic stability is the amount of solvent in the core, which can aid in chain mobility and suppress the T_g. Also

the kinetic stability of micelles depends on the size of hydrophobic block and mass ratio of hydrophilic to hydrophobic blocks.[34]

1.4.2. Micelle size

Micelle size is an important property which largely influences the circulation time and organ distribution of DDSs. The size of micelles is controlled by several factors such as the length of core forming block and corona forming block.[34] Polymer based DDS usually range in size from 10 to 100 nm, and as such are less susceptible to RES clearance. They are also small enough to pass through small capillaries in the body (those less than 5 μm), giving them access to small capillaries.[35] Further, their size falls within the optimal range for circulation and retention within tumor tissue by the EPR effect.

1.5. Stimuli-responsive degradation (SRD) strategy

Advanced techniques allow for the synthesis of ABPs with chemical flexibility which can be engineered to incorporate stimuli-responsive degradable moieties. These degradable covalent linkages make nanocarriers capable of undergoing changes in one or more physical properties in response to external triggers; thereby triggering the programmed release of encapsulated biomolecules, particularly anticancer therapeutics (Figure 1.6) while facilitating the removal of empty vehicles after release. This stimuli may either be physiological (i.e. pH, thiols or specific enzymes) or physical stimuli (i.e. heat, light and ultrasound).[36] After micellar dissociation in response to proper stimuli which can be unique to disease pathology, ABP unimers which fall below the glomerular filtration limit (in terms of molecular weight) will simply be evacuated from the body.

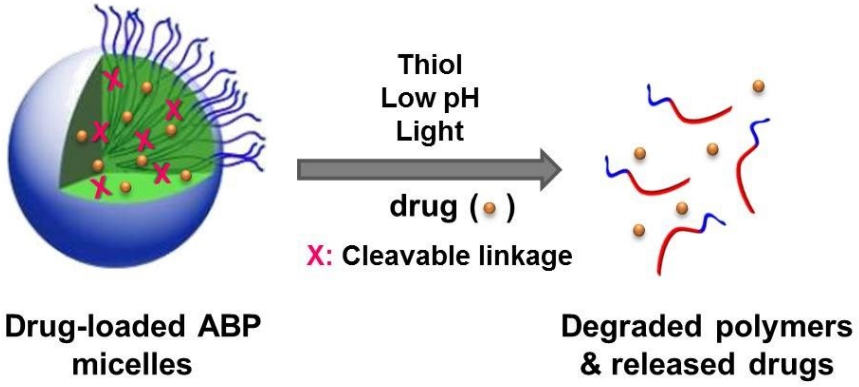

Figure 1.6. Stimuli-responsive degradation of ABP micelles for controlled release of encapsulated hydrophobic drugs.[17]

As seen in Figure 1.7, there are typically four different strategies to design micelles with stimuli-responsive moieties. Based upon the number and location of cleavable linkage (X), they divide to multi-cleavable (A and B) or mono-cleavable micelles (C and D). In addition, the cleavable linkages (X) are located either in their micellar core (A, B and C) or at the interface between micelle core and corona (D).

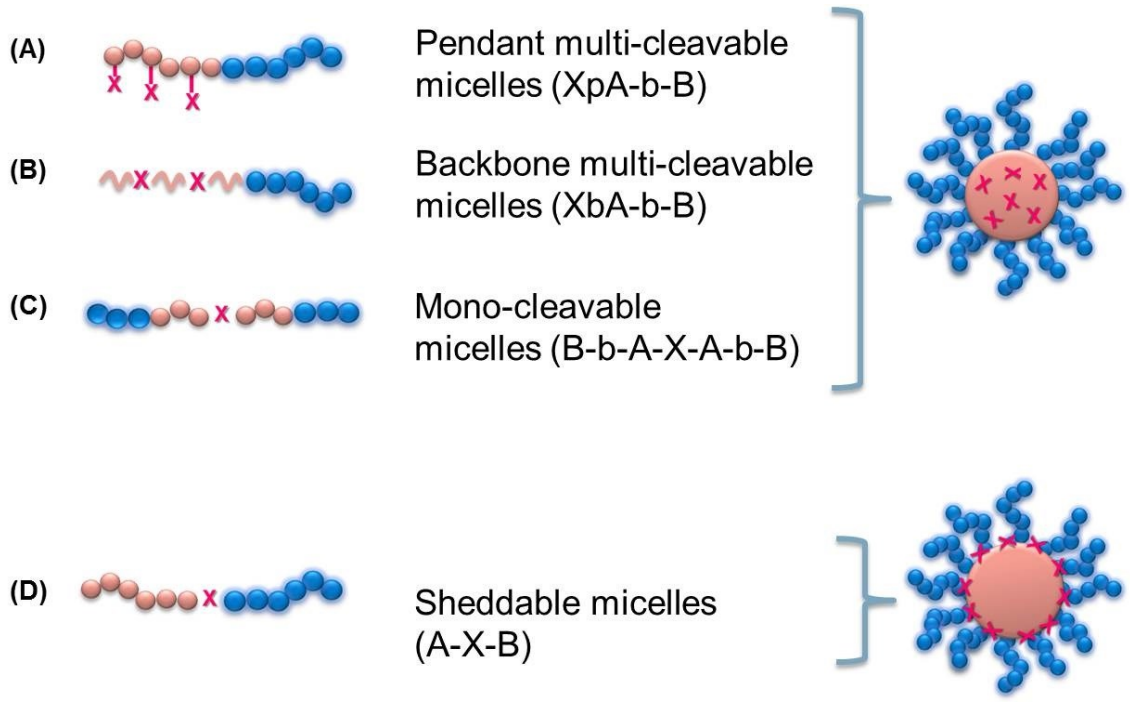

Figure 1.7. Stimuli responsive ABP micelles with different location of cleavable linkage (X). The figure is slightly modified from the reference (A and B represent polymer blocks and b represent blocks).[37]

Pendant multi-cleavable micelles are formed through self-assembly of ABPs having pendant cleavable linkages positioned in the hydrophobic blocks (XpA-b-B).[38] In response to external stimuli, they are destabilized upon the cleavage of pendant degradable groups that increases polarity of hydrophobic blocks. Backbone multi-cleavable micelles have multiple cleavable linkages positioned regularly in the hydrophobic polymer main chains (XbA-b-B).[39] Mono-cleavable micelles are based on amphiphilic triblock copolymers having single cleavage linkages in the middle (B-b-A-X-A-b-B).[40] Both backbone multi-cleavable and mono-cleavable micelles are degraded through the loss of hydrophobic cores. For mono-cleavable micelles, the degraded polymers are still amphiphilic, and thus could re-aggregate to smaller-sized assembled

structures. While all these type of micelles are designed to have cleavable linkages in the hydrophobic cores, sheddable micelles contain cleavable linkages at the interfaces of hydrophobic cores and hydrophilic coronas being shed upon the cleavage of cleavable groups.[17]

In the following section, the development of pH and thiol-responsive degradable block copolymer micelles are reviewed which are of interests to my research.

1.5.1. pH-responsive degradable micelles

pH-sensitive systems have been widely studied because of pH gradients within the body.[41] For example, at organ level, along gastrointestinal (GI) tract, pH changes from acidic in the stomach (pH = 2) to more basic in the intestine (pH > 7). At tissue level, tumor tissue exhibits slightly acidic pH (5.0 to 6.5). In the subcellular compartment level, endosomes and lysosomes are also in acidic pH (5.0 to 5.5).[41] While stable in normal physiological conditions, pH-sensitive degradable micelles are destabilized in acidic environment leading to site-specific release of encapsulated drugs in a controlled manner. The sensitivity of pH-responsive ABP micelles results from their "titratable" groups (pK_a from 3-11), which undergoes ionization upon changing the pH[42] or from their labile linkages which are cleaved under mild acidic conditions (pH < 6). Table 1.1, summarizes pH-sensitive covalent linkages as well as their corresponding hydrolytic products.

Table 1.1. pH sensitive linkages and their hydrolytic products.[41]

Name	Structure	Ref
Ester	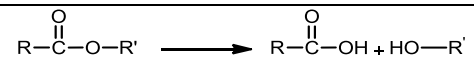	[43]
Hydrazone	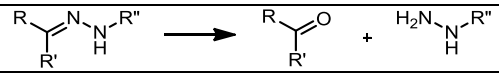	[44]
Carboxy dimethylmalic anhydride	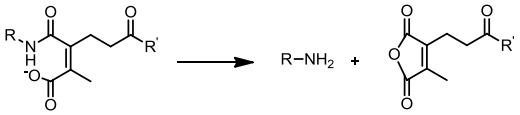	[45]
Orthoester	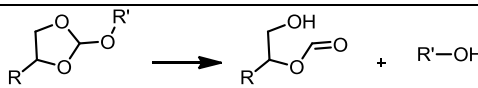	[46]
Imine		[47]
Vinylether		[48]
Acetal	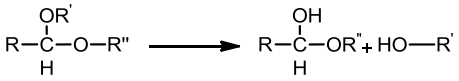	[49]

Extensive studies have been done on the development of pH-responsive degradable micelles. To obtain acid-responsive degradable micelles, different acid labile linkages such as orthoester, hydrazone, cis-acotinyl and acetal have been positioned either in the main chain, at the side chain, or at the terminal of core forming block.[50] Several examples of acid-responsive degradable micelles have been reported. Acid-sensitive ABPs, composed of PEO as the shell forming block and polycarbonate (PC) block having pendant orthoester groups as core forming block (PEO-b-PC) have been synthesized. The self-assembled micelles of PEO-b-PC degraded in acidic pH to the corresponding hydroxyl polycarbonates.[51] Attachment of hydrophobic drugs via acid sensitive linkages to the core forming block of a copolymer is another strategy for developing pH-sensitive DDS.[52] In this system cleavage of the linkage facilitates drug

release. For example pH-sensitive drug delivery nanocarriers was developed by conjugating doxorubicin (DOX) to the end group of PEG-PLA through an acid sensitive hydrazone or cis-aconityl bond.[53] pH-sensitivity of cis-aconityl bonds was actually 10 times higher than hydrazone linkages, but cleavage of this linkage form chemically modified DOX after release; whereas through cleavage of hydrazone bonds, DOX could be released without any change in therapeutic properties. Also another acid-sensitive ABP micelle was developed by grafting DOX to a PEO-polyaspartate through hydrazone linkages. Upon cleavage of hydrazone linkages, the release of DOX was enhanced when decreasing the pH value from 7.4 to 3.0.[54] Recently acetals as acid-labile linkages have been exploited for design of pH-responsive micelles.[49] In particular, trimethoxybenzylidene acetals attached either to the side chain of poly(aspartic acid) (PAA) segment of PEG-PAA block copolymers[49] or to the periphery of dendron of PEG-dendritic block copolymers showed unique sensitivity toward mildly acidic pH.[52] Micellar aggregates were effectively disrupted due to the hydrolysis of acetals and thus enhanced release of encapsulated Nile Red (NR) or DOX under mildly acidic conditions.

1.5.2. Redox-responsive degradable micelles

The existence of reduction potential gradients between intracellular and extracellular compartments makes reductive electron transfer an ideal stimulus in design and development of redox-responsive degradable nanomaterials for drug delivery applications.[55] Disulfides are cleaved in reducing environments or through disulfide-thiol exchange reaction. Disulfide-thiol chemistry is especially applicable for *in vivo* drug delivery applications due to the presence of glutathione (GSH), a low molecular weight tripeptide containing a pendant thiol group that is found in extracellular fluids at a

concentration of ≈10 μM.[56] GSH exist at higher level in cytosol (≈10 mM).[57] More importantly, the cytosolic level of GSH in some tumor cells is several times higher than in normal cells.[58] This large difference in GSH concentration between healthy and cancerous cells can be used to selectively deliver anti-cancer therapeutics to affected areas.

A number of disulfide-containing polymeric micelles have been extensively explored as controlled delivery nanocarriers of anticancer drugs. For example, disruption of a shell-sheddable micelle consisting of poly(ethylene glycol)-ss-poly(ε-caprolactone) (PEG-ss-PCL) in a reductive environment resulted in 60% DOX release within 4 hrs, as compared to 20% DOX release over one month from PEG-b-PCL.[59] Also recently, dextran-block-poly(ε-caprolactone) diblock copolymers containing a disulfide bond between hydrophilic and hydrophobic segments was developed. In the absence of a reducing environment, only 27% of the loaded DOX was released over 11 hrs, as compared to almost 100% discharge in a reducing environment.[60] In a very similar case, a thiol-responsive shell detachable block copolymer composed of PCL block and poly(ethyl ethylene phosphate) (PEEP) block having single disulfide in middle of blocks (PCL-ss-PEEP) was synthesized. The PCL-ss-PEEP micelles exhibited the fast cleavage of disulfide linkages in response to GSH, taking 2 hrs to reach almost complete drug release.[61] Redox-responsive micelles formed from hyperbranched multi-arm copolyphosphates having disulfides were synthesized. The disulfide linkages were cleaved in the presence of dithiothreitol (DTT), enhancing the release of encapsulated DOX.[62] Thiol-responsive micelles of poly(amido-amine) labeled with disulfides and grafted with PEO exhibited the slow cleavage of disulfide linkages in response to DTT,

taking > 120 hrs to reach > 80% degradation.[39] Redox-responsive micelles based on polyester-based polymethacrylate ABPs (ssPES-b-POEOMA or ssABPs, OEOMA: oligo(ethylene glycol) monomethyl ether methacrylate) having disulfide linkages repeatedly positioned on polyester backbones (ssPES) were synthesized. The reductive cleavage of disulfide linkages in reducing conditions resulted in the degradation of ssPES homopolymers. With the increasing amounts of disulfide linkages in ssPES–OH and reducing agents their degradation rate was significantly enhanced.[63]

In order to increase the stability of micelles against premature dissociation of micelles, cross-linked micelles have been developed. However, such a covalent crosslinking strategy can limit the release rate of encapsulated drugs. In order to overcome this drawback, introduction of stimuli-responsive cleavable linkages have been proposed. Recently, a block copolymer consisting of pendant disulfide-labeled methacrylate (PHMssEt) and PEO (PEO-b-PHMssEt) was synthesized. This copolymer self-assembled to form micellar aggregates, which can undergo disulfide core-crosslinking in the presence of catalytic amounts of DTT (< 1 eq). Micelles were destabilized and released the NR by increasing the concentration of DTT (5 eq DTT).[64]

The brief review of literatures demonstrates that stimuli-responsive degradable micelles can be made as successful proof of concepts. These examples are merely a glance at the various numbers of novel and efficient strategies to synthesize versatile stimuli-responsive degradable micelles toward drug delivery. Smart micelles can be made from surprisingly simple polymers, although this may be due to a reluctance to utilize more complex polymeric structures due to fear of unknown toxicity and regulatory delays. Standardization of polymers used might actually aid in commercialization, as

more effort will be devoted to finding a simple synthesis process, making it easier to make micelles that meet current good manufacturing practices. Regardless of all the improvements in the design of stimuli-responsive degradable micelles as DDSs, there is still a need to better understand the structure–property relationship between morphological variance and stimuli-responsive degradation in order to optimize the design of polymeric nanocarriers. A more thorough understanding of the use and placement of different stimuli responsive degradation triggers will help promote the efficiency of DDSs. In addition, implementation of more precise triggers, such as those which response to specific biomolecules will further enhance the effectiveness of targeted delivery, and is an ongoing area of research.

1.6. Scope of the thesis

My master research will be presented in the following four chapters. Chapter 2 describes the methodology for the synthesis and characterization of stimuli-responsive degradable ABPs and their self-assembled structures, as well as their cellular interactions.

Chapter 3 is devoted to the synthesis of a hydroxyl-terminated pH-responsive degradable ABPs and evaluation of its effectiveness as micellar drug carriers. Well-defined hydroxyl-terminated poly(oligo(ethylene oxide) monomethyl ether methacrylate)-b-poly(t-butyl methacrylate) (OH-POEOMA-b-PtBMA) was synthesized. The pendant tert-butyl groups of these ABPs were cleaved in acidic conditions, resulting in pH-triggered destabilization of the micelles in aqueous solution. Their facile bioconjugation was demonstrated by conjugation with biotin. The competitive assay results suggest that > 93% polymer chains in micelles were conjugated with biotin molecules.

Chapter 4 explores a novel brush-like triblock copolymers consisting of a hydrophobic polymethacrylate block having pendant oligo(propylene oxide) and a hydrophilic polymethacrylate block having pendant oligo(ethylene oxide) (ss-(PAP-b-POEOMA)$_2$). Thiol-responsive disulfide linkages were positioned in the middle of the triblock copolymers, thus resulting in the formation of the mono-cleavable micelles by self-assembly in aqueous solution. The cleavage of the disulfide linkages in micellar cores in response to thiols resulted in dissociation of micelles to smaller-sized assembled structures in water.

Chapter 5 describes self-assembly of a thiol-responsive pendant multi-cleavable micelles consisting of a pendant disulfide-labeled polymethacrylate core (PHMssEt) and a hydrophilic poly(ethylene oxide) (PEO) corona (PEO-b-PHMssEt) block copolymer. In response to cellular GSH, the cleavage of pendant disulfide linkages of these PEO-b-PHMssEt ABPs resulted in the destabilization of these micelles, which enhanced the release of encapsulated doxorubicin (DOX) of anticancer drug. Their cellular interactions including intracellular viability after cellular uptake were examined.

Finally, chapter 6 consists of concluding remarks and suggestions for future works.

Chapter 2

Methodology: Synthesis and Characterization

2.1. Brief description

This chapter describes the methodology of synthesis and characterization of well-defined amphiphilic block copolymers (ABPs) and their aqueous micellar aggregates for biological and biomedical applications. Different techniques and instruments employed in my research are also briefly described. The detailed experimental procedure for chapter 3, 4 and 5 are summarized in appendix A, B and C.

2.2. Synthesis and characterization of well-defined ABPs

2.2.1 ATRP as a means to synthesize well-defined ABPs

In order to synthesize polymers with complex macromolecular architectures such as block copolymers for drug delivery applications, it is crucial to have strict control over molecular weight, molecular weight distribution, and chemical composition of polymer chains. Traditionally, living anionic polymerization has allowed for synthesis of well-controlled block copolymers with narrow molecular weight distribution (M_w/M_n < 1.1).[65] This polymerization requires the growth of all polymer chains at the same time with no undesirable side reactions such as chain transfer or irreversible termination.[66] However, carbon-centered terminal anions exhibit a high sensitivity to traces of impurities. Such high sensitivity renders anionic polymerization incompatible with several functional monomers and is difficult to implement industrially. Alternatively,

controlled radical polymerization (CRP) techniques have been recently developed, combining the control of anionic polymerization as well as the versatility of conventional free radical polymerization. They work based upon two main principles: (1) reversible termination, as demonstrated by nitroxide-mediated polymerization (NMP)[67] and atom transfer radical polymerization (ATRP);[68] and (2) reversible transfer, utilized in reversible addition fragmentation chain transfer (RAFT) polymerization.[69] In this thesis, most block copolymers were synthesized by ATRP.

ATRP was independently discovered by Mitsuo Sawamoto[70] and Krzysztof Matyjaszewski[68] in 1995. This technique works through the end-capping of a polymer chain with halogen which can reversibly undergo homolytic cleavage (Figure 2.1). The mechanism of normal ATRP involves the transfer of halogen atoms from dormant polymer chains (P_n-X) to transition metal complexes (Cu(I)/L) as activators, yielding active chain ends (P_n* radicals) and deactivators (X-Cu(II)/L). These (P_n*) radicals species can undergo propagation with the rate constant of propagation (k_p), to grow polymeric chains. Alternatively, the radical species can be deactivated by halogen transfer from deactivators to yield dormant species (P_n-X). This reversible equilibrium process of activation and deactivation is shifted towards deactivation, as the rate constant of deactivation is much larger than the rate constant of activation ($k_{deact} >> k_{act}$). This shift can minimize the concentration of radicals and chain transfer reactions, thus suppressing bimolecular irreversible termination.

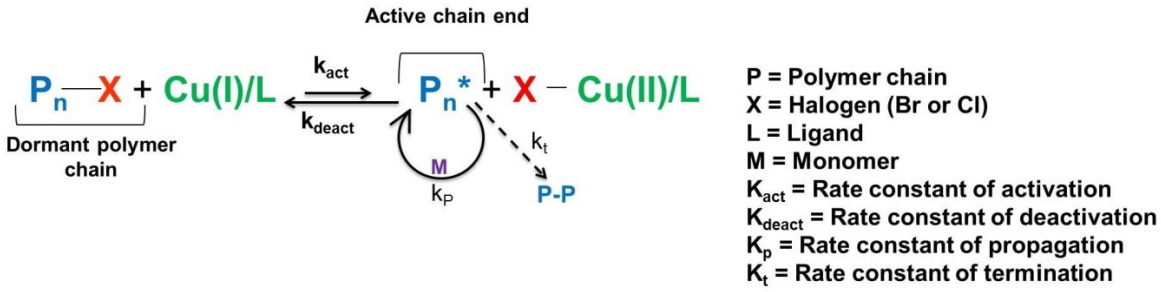

Figure 2.1. Mechanism of normal ATRP process.

One of the key advantages of ATRP for designing various molecular architectures and nanostructure morphologies is that the resulting polymer chains retain halogen moieties at the chain end. These terminal halogens can facilitate the reactivation of the chain end for functionalization or use as macroinitiator for subsequent polymerization, resulting in various architectures of block copolymers with predetermined molecular weight and narrow molecular weight distribution. Also by utilizing functionalized alkyl halides as initiators, along with post polymerization modification of the terminal halogen atom, different functionalities can be easily introduced to both chain ends.

In addition to normal ATRP, Activator Generated by Electron Transfer (AGET) is a facile variant of ATRP. AGET ATRP provides all the benefits of normal ATRP with the additional advantage that more oxidatively-stable Cu(II) complexes are used in the reaction mixture. This process begins with the use of Cu(II) deactivators, which react with reducing agents, generating Cu(I) activators. The polymerization then proceeds as in normal ATRP conditions with the added alkyl halide. Typical reducing agents include ascorbic acid or tin(II) ethylhexanoate (Figure 2.2).[71]

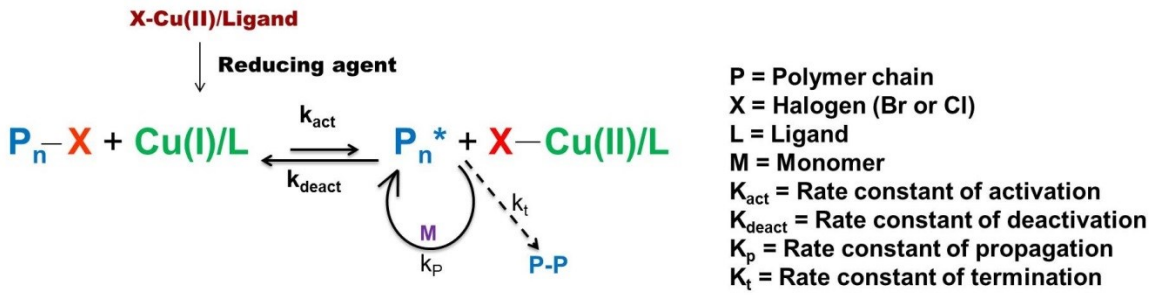

Figure 2.2. Mechanism of AGET ATRP process.

In my research, normal ATRP was conducted in the presence of ATRP initiator, monomer, metal catalyst (CuBr(I)), ligand, and proper solvent. The resulting mixture was deoxygenated by three freeze-pump-thaw cycles. The reaction flask was filled with nitrogen and then CuBr(I) was added to the frozen solution. The flask was sealed, evacuated with vacuum and backfilled with nitrogen. The mixture was thawed and the flask was then immersed in a preheated oil bath to start the polymerization. The polymerization was stopped by exposing the reaction mixture to air.

For AGET ATRP, a mixture consisting of ATRP initiator, monomer, oxidatively-stable metal catalyst (CuBr(II)), ligand, and proper solvent was deoxygenated by purging with nitrogen for 30 min at room temperature. The flask was immersed in a preheated oil bath. A nitrogen-purged solution of reducing agent ($Sn(Oct)_2$) in solvent was added to start the polymerization. The polymerization was stopped by exposing the reaction to air.

2.2.2. Molecular weight determination by gel permeation chromatography (GPC)

The average molecular weight (MW) is a fundamental characteristic of block copolymers which dictates most of their properties. The molecular weight of a polymer can be defined as the number-averaged molecular weight (M_n) and weight-averaged

molecular weight (M_w). M_n is the average molecular weight on the basis of the number of molecules (N_i) in a particular weight class (M_i): $M_n = \sum N_i M_i / \sum N_i$. An average on the basis of the weight fraction (W_i) of molecules in a particular weight class (M_i) is M_w: $M_w = \sum N_i M_i^2 / \sum N_i M_i$. The ratio of M_w/M_n is defined as the polydispersity index (PDI) which is a useful indicator of the breadth of the distribution of molecular mass in a given polymer sample. $PDI = M_w/M_n$.

Gel permeation chromatography (GPC) is a simple and effective method to determine molecular weight of polymers. A typical GPC consist of one or more columns packed with porous microparticles of highly crosslinked polymers connected to various detectors. A polymer solution is injected into a solvent stream that flows through the GPC columns (Figure 2.3). Polymer chains are separated according to their hydrodynamic volumes, which is a function of molecular weight and molecular conformation in solution and affects the elution time through the columns. Longer polymer chains will have a larger hydrodynamic volume, and as such are unable to pass through small void spaces in the porous microparticles packed into a separation column. This gives longer polymer chains a shorter elution/retention time, while shorter polymer chains will possess a longer retention time. Using detectors typically measuring refractive index (RI) or light scattering signals, polymer concentration in the eluent at different elution times is detected. A GPC system is calibrated with a series of standard samples of known molecular weights to relate elution time with molecular weight or intrinsic viscosity. Typical standards include polystyrene (PSt), poly(ethylene glycol), and poly(methyl methacrylate) (PMMA).

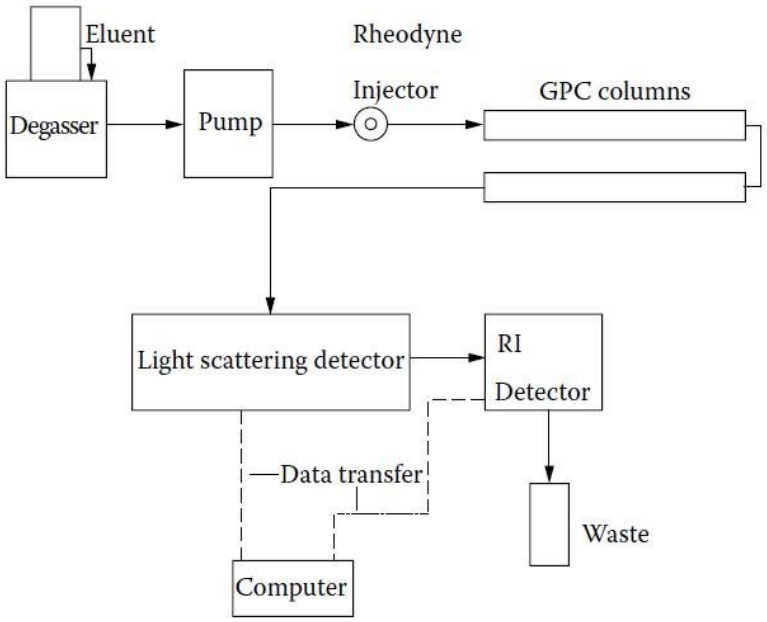

Figure 2.3. Schematic diagram of a GPC setup for the measurement of polymer molecular weight of polymers.[72]

In my research, a GPC equipped with a Viscotek VE1122 pump, a RI detector and three PolyAnalytik columns (PAS-103L, 105L, 106L, designed to determine molecular weight up to 2,000,000 g mol^{-1}) were used with THF as an eluent at 30 °C at a flow rate of 1 mL min^{-1}. Linear PMMA standards were used for calibration. Aliquots of polymer samples were dissolved in THF and the clear solutions were filtered using a 0.25 μm PTFE filter to remove any THF-insoluble species. A drop of anisole was added as a flow rate marker.

2.3. Aqueous micellization and characterization

2.3.1. Preparation of micellar aggregates in aqueous solution

Depending on the physicochemical properties including the solubility of block copolymers, there are several methods that allow for the formation of micellar

aggregates. These methods include direct dissolution, solvent evaporation and dialysis method. Direct dissolution involves dissolving copolymer directly in water. This procedure is applicable for moderately hydrophobic copolymers.[24] Both, solvent evaporation and dialysis methods are accomplished by using organic solvents. The solvent evaporation method is based on dissolving block copolymers in a volatile organic solvent. Water is then slowly added to the solvent to form micelles, and evaporation of the solvent results in the formation micellar aggregates. The Dialysis method involves dissolving copolymers in water miscible organic solvents followed by extensive dialysis against water. Eventually, organic solvents are replaced with water, triggering self-assembly to form micelles.[73]

2.3.2. Determination of critical micellar concentration (CMC)

CMC is the concentration at which micellar aggregates first appear. At the CMC, a distinct transition of several physical properties is observed due to the formation of micellar aggregates. Typical methods to determine CMC of block copolymers include tensiometry[74] and fluorescence spectroscopy.[75]

Tensiometery utilizes the measure of surface tension of aqueous polymer solutions. At low concentrations, the surface tension does not change; however with an increasing concentration, it abruptly increases. Upon further increase, the tension slowly increases. This increase is visible on a plot of surface pressure versus solution concentration. Using this method the CMC is determined as the concentration when the transition of pressure occurs.

Also fluorescence spectroscopy has widely been used to determine the CMC of polymeric micelles. Nile Red (NR) is a fluorescent probe typically used to determine

CMC. It generally excites at 485 nm and emits at 525 nm. Its fluorescence is strongly influenced by the polarity of its environment. In this method, the change in fluorescence intensity of NR at various concentrations of the polymer is monitored.[76] This characterization method works based upon the fact that as a result of poor water solubility of NR, its fluorescence emission is significantly lower in water; however, when NR is entrapped in the hydrophobic micellar core, its fluorescence becomes much more intense.[76] The CMC can be easily estimated from changes of the NR fluorescence intensity as a function of micellar concentration. The transition onset of fluorescence intensity is defined as the CMC.

In my research, CMC of amphiphilic block copolymers in water have been determined using both methods. A DeltaPi Surface Tensiometer from Kibron was calibrated using air and water at room temperature and used to measure the change in surface tension of different polymer solutions. Alternatively, the fluorescence spectra of various polymer solutions containing NR were recorded on a Varian Cary Eclipse fluorescence spectrometer.

2.3.3. Characterization of size and morphology of micellar aggregates

Dynamic light scattering (DLS) is a common technique for determining the size of particles in colloidal dispersions. DLS measures the intensity of light scattered by particles in dispersions at a given angle upon radiation of light. Brownian motion of particles in solution causes changes in scattered light intensity. Analysis of these intensity fluctuations allows for the determination of hydrodynamic diameter of particles through the Stokes-Einstein equation.

$$D_H = \frac{K_B T}{6\pi \eta D} \times 2$$

Where K_B is the Boltzmann constant; T is absolute temperature; η is viscosity and D is diffusion constant. The diffusion of particles is essentially controlled by temperature, viscosity of the solvent and the size of the particles. If the temperature and solvent are constant and known, the variation in the intensity of the scattered light is directly related to the "size" of the molecule. The larger the molecules, the slower they move.

In my research, particle size of micellar aggregates was measured by DLS using two different particle size analyzers. Initially a model DynnaPro Titan from Wyatt Technology at fixed scattered angle of 90° at 25 °C was used. In this case, DLS measurements provide average diameter (D_{av}), which is defined as follows, $D_{av} = \sum D_i/N$, where D_i is the diameter of the particle i and N is the total number counted. The bulk of the measurements were conducted using a Malvern Instruments Nano S ZEN1600 equipped with a 633 nm He-Ne gas laser at a fixed scattering angle of 173° at 25 °C. All micellar dispersions were filtered by a 0.45 μm polyethersulfone (PES) filter to remove large aggregates formed during aqueous micellization.

Transmission electron microscopy (TEM) is used to study the morphologies of micellar aggregates in dehydrated states and can provide an absolute measurement of particle size. TEM involves a transmission of a beam of electrons through a dried sample in a high-vacuum environment. Regional differences in electron densities give contrast to form images.

In my research, TEM images were taken using a Philips CM200 HR-TEM, operated at 200 kV electrons and equipped with thermionic LaB6 cathode filament, anti-contamination cold finger, Genesis EDAX system, and AMT V600 2k × 2K CCD camera. The point-to-point resolution and the line resolution of the machine are 0.24 nm and 0.17 nm, respectively. To prepare specimens, samples were dropped onto the TEM copper grids (400 mesh, carbon coated), then grids were dried in air. In this case, particle size was analyzed using ImageJ program.

2.4. Cellular interaction of ABP-based micelles

2.4.1. Cell viability

For biomedical applications polymeric materials should be non-toxic to cells. A variety of methods to estimate cell viabilities are available ranging from the most routine trypan blue dye exclusion assay to highly complex analysis of individual cells using RAMAN microscopy.[77] The cost, speed, and complexity of equipment required play an important role in determining the assay used.

Trypan blue is a simple method to determine cell viability. Trypan blue is normally excreted from live cells. If cells take up trypan blue, they are considered non-viable. Cell viability is calculated as the ratio of number of viable cells to the total number of cells within the grids on the counting cell slide (hemocytometer).[78]

Tetrazolium-based assays are standard colorimetric methods, including 3-(4,5-dimethylthiazol-2-yl)-2,5-diphenyltetrazolium bromide (MTT) and 3-(4,5-dimethylthiazol-2-yl)-5-(3-carboxymethoxyphenyl)-2-(4-sulfophenyl)-2H-tetrazolium (MTS) assays. Tetrazolium-based assays have several advantages over other methods,

including simplicity, reproducibility and fast data generation.[79] These assays are based upon the functionality of the mitochondrial dehydrogenase of viable cells to reduce a tetrazolium-based compound. This enzyme is able to cleave the tetrazolium rings of the MTT dye and form blue formazan crystals (Figure 2.4) and the MTS dye into water-soluble formazan product. Dead cells rapidly lose the ability to reduce tetrazolium products. The production of the colored formazan products are directly proportional to the number of living cells.[80]

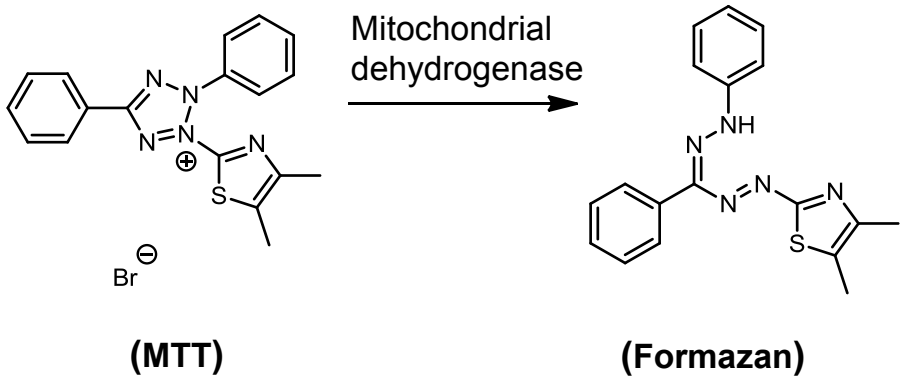

Figure 2.4. Structures of MTT tetrazolium salt and its formazan product.[81]

Figure 2.5 shows the absorption spectra of MTT and MTT-formazan produced by incubation of L-DAN cells in presence of MTT. Also absorption spectrum of commercial prepared MTT-formazan is shown in Dimethyl sulfoxide (DMSO). Commercial formazan (from Sigma) exhibits two absorption maxima at 510 and 570 nm. However, formazan produced by cells shows maximum absorption at 560 nm.[82]

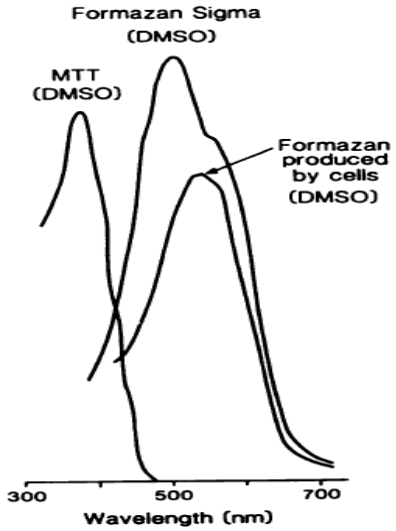

Figure 2.5. Absorption spectra of MTT and commercially prepared MTT-formazan dissolved in DMSO. Also shown is the spectrum of MTT-formazan produced by incubation of L-DAN cells with MTT (5 mg ml-1) for 4 h.[82]

LIVE/DEAD viability assay is a fluorescence-based method. Calcein AM and ethidium homodimer (EthD-1) are optimal fluorescence probes for this assay, which are used to measure intracellular esterase activity and plasma membrane integrity.[83] In this assay, live cells are distinguished upon the functionality of ubiquitous intracellular esterase. This enzyme is able to convert the almost non-fluorescent calcein AM to the intensely fluorescent calcein, therefore producing green fluorescence in live cells (ex/em ~ 495 nm/ ~ 515 nm). On the other hand, EthD-1 is excreted from live cells and enters cells with damaged membranes. Upon binding to nucleic acids, the fluorescence intensity of the EthD-1 increases, producing red fluorescence in dead cells (ex/em ~ 495 nm / ~ 635 nm).[84] These physical and biochemical properties help to determine the cell viability. This assay is generally faster, less expensive, and more

accurate than alternative methods. However it is more complicated than tetrazolium-based assays and requires fluorescence microscope.

In my research, cell viability was measured using a CellTiter 96 Non-Radioactive Cell Proliferation Assay kit (MTT, Promega). Measurements were performed according to manufacturer's instruction. Briefly, MTT solution (15 μL) was added into each well. DMSO (100 μL) was added into each well in order to dissolve the formed formazan blue crystals, and then the absorbance at λ = 570 nm was recorded using a Powerwave HT Microplate Reader (Bio-Tek). Each concentration was repeated 12 times. Cell viability was calculated as the percent ratio of absorbance of mixtures with micelles to control (cells only).

Chapter 3

pH-Responsive Degradable Micelles

3.1. Introduction

pH-sensitive ABP micelles have been widely studied because of pH gradients in normal and pathophysiological states.[41] While stable in normal physiological conditions, pH-sensitive micelles are destabilized in acidic environments, such as the interior of tumors. Such destabilization facilitates the release of encapsulated drugs in a controlled manner.[85] Current strategies toward the development of pH-responsive micelles involve the synthesis and aqueous micellization of acid-sensitive ABPs. Most these strategies are achieved by either incorporating "titratable" groups, such as amines[86] or carboxylic acids[87] into the copolymers, or utilizing labile linkages, such as hydrazones[53] or ortho esters.[52] The latter is my strategy of interest.

A convenient method to prepare pH-responsive degradable micelles involves the incorporation of pendant pH-sensitive cleavable groups into a hydrophobic block. Hydrolytic cleavage of these groups in acidic environment increases the polarity of the hydrophobic block, causing the micelles to be destabilized. The development of acid-sensitive copolymers consisting of PEO as the hydrophilic block and different hydrophobic blocks functionalized with pendant ortho ester moieties have been reported. Typical hydrophobic blocks include poly(aspartic acid) (PAA),[88] polylysine (PLL) dendrons,[52] and poly(methacrylamide).[89] Despite these advances, the developments of

new types of pH-responsive degradable micelles are needed to better understand structure-property relationship between morphological variance and pH responsive degradation.

This chapter describes new hydroxyl-terminated ABPs having pendant pH-sensitive t-butyl groups, consisting of hydrophilic poly(oligo(ethylene oxide) monomethyl ether methacrylate) (POEOMA) and hydrophobic poly(t-butyl methacrylate) (PtBMA) blocks. These HO-terminated POEOMA-b-PtBMA block copolymers (HO-ABPs) were synthesized by consecutive atom transfer radical polymerization (ATRP) of OEOMA and tBMA in the presence of a HO-functionalized bromine initiator (OH-iBuBr). Figure 3.1 shows the synthetic scheme and rational design of HO-ABPs as potential drug delivery nanocarriers. First, POEOMA was chosen as the hydrophilic block because of its high water solubility and as a biocompatible analog of linear PEO, a material approved by the FDA for clinical use.[90] Second, PtBMA as core-forming block enables the encapsulation of hydrophobic therapeutics. Also it is potentially degradable through hydrolytic cleavage of pendant t-butyl groups to water-soluble poly(methacrylic acid) (PMAA) in acidic conditions. Third, since tBMA was commercially available, the synthesis of new monomers having pendant cleavable groups is not required. Fourth, in order to prove a facile bioconjugation of HO-ABPs with cell targeting biomolecules, here, terminal OH groups were conjugated with biotin (vitamin H) for the synthesis of biotin-terminated ABPs.

This chapter comprises material published in *Journal of Polymer Science Part A: Polymer Chemistry*, **2013**, *51*, 1620-1629. Part of this text is adapted from the original source material.

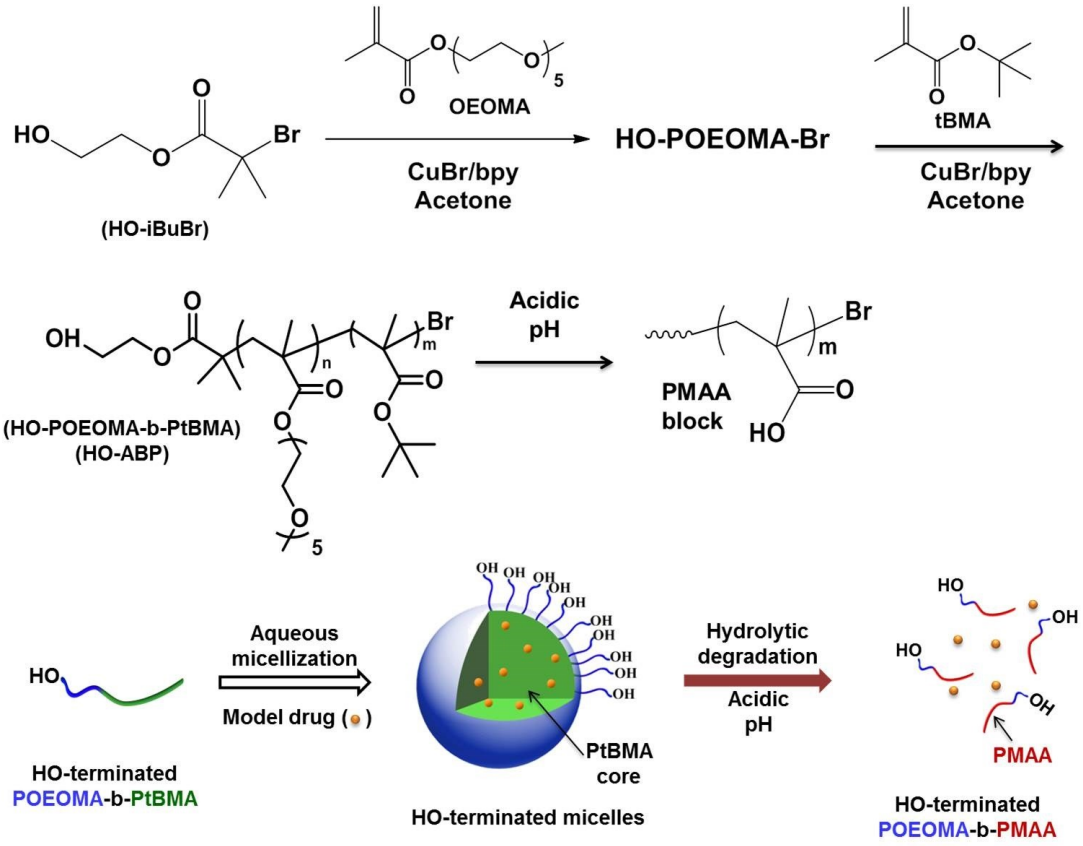

Figure 3.1. Synthesis of HO-ABPs by consecutive ATRP of OEOMA and tBMA in the presence of a HO-terminated ATRP initiator (HO-iBuBr), as well as aqueous micellization and acid-triggered dissociation of HO-ABP micelles as contolled drug delivery nanocarriers (bpy: 2,2′-bipyridyl, PMAA: poly(methacrylic acid)).

3.2. Experimental section

The detailed procedures of synthesis and characterization are described in Appendix A.

3.3. Synthesis of HO-POEOMA-Br macroinitiator

My experiments began with the synthesis of a hydroxyl-terminated ATRP initiator (HO-iBuBr) through a facile carbodiimide coupling reaction. The structure is shown in Figure 3.1 and its detailed synthesis is described in our publication[91] and

elsewhere.[92] Next, a seris of ATRP of OEOMA in the presence of HO-iBuBr in acetone at 47 ºC was carried out under various conditions. The important parameters that significantly influence the kinetics and control of ATRP of OEOMA were investigated. Table 3.1 summarizes the results.

Table 3.1. Characteristics for ATRP of OEOMA in the presence of OH-iBuBr at 47 ºC in acetone[a]

Recipe	Catalyst	Ligand	Time (hrs)	Conversion[b]	$M_{n,theo}$[c] (g mol^{-1})	M_n[c] (g mol^{-1})	M_w/M_n[b]
HO-MI-1	CuBr	PMDETA	2.0	0.81	12,200	15,400	1.22
HO-MI-2	CuCl	PMDETA	2.2	0.80	12,000	15,600	1.39
HO-MI-3	CuBr	bpy	4.0	0.78	11,700	14,300	1.40

[a] $[OEOMA]_0/[HO\text{-}iBuBr]_0/[catalyst]_0/[Ligand]_0 = 50/1/0.5/0.5$ for PMDETA and 1/0.5/1 for bpy; OEOMA/acetone = 1.5/1 v/v.

[b] Determined by GPC with PMMA standards.

[c] Theoretically calculated molecular weight: $M_{n,theo} = [OEOMA]_0/[HO\text{-}iBuBr]_0 \times MW(OEOMA) \times conversion$.

With the target degree of polymerization (DP) defined as the initial ratio of $[OEOMA]_0/[HO\text{-}iBuBr]_0 = 50$, ATRP of OEOMA in the presence of CuBr/N,N,N′,N″,N″-pentamethyldiethylenetriamine (PMDETA) (HO-MI-1) and CuCl/PMDETA (HO-MI-2) proceeded rapidly, reaching 80% conversion in 2 hrs. This result suggests no significant difference in kinetics for catalysts complexed with PMDETA. However, CuBr/PMDETA complex gave better control with $M_w/M_n < 1.22$, compared with CuCl/PMDETA active complex in this system. Polymerization with CuBr/bpy (HO-MI-3) proceeded more slowly; reaching 78% conversion in 4 hrs (Appendix A, Figure A.1.). To synthesize well-defined HO-POEOMA-Br macroinitiators (HO-MI-Br) with a short chain length, the recipe HO-MI-3 was then repeated while polymerization time was shortened to 30 minutes. The resulting polymer was purified by precipitation from hexane to remove unreacted OEOMA monomers, followed by passing

it through a column filled with basic aluminum oxide to remove residual Cu species. The gel permeation chromatography (GPC) results indicate that the resulting HO-POEOMA-Br had molecular weight, M_n = 9,500 g mol^{-1} with molecular weight distribution as narrow as M_w/M_n = 1.22 (Figure 3.2). ^{1}H-NMR was used to determine the DP (Figure 3.3a). A NMR signal at 1.4 ppm corresponds to two methyl protons (a) and the singlet appeared at 3.3 ppm corresponds to methoxy protons. From the integral ratio of peaks [(b/3)/(a/6)] (Figure 3.3a), the DP of HO-POEOMA-Br (HO-MI-Br) was determined to be 19.

3.4. Synthesis of HO-POEOMA-b-PtBMA ABP

In the presence of the dried, purified HO-POEOMA$_{19}$-Br MIs, ATRP of tBMA was conducted in acetone at 47 °C under the conditions of $[tBMA]_0/[HO\text{-}POEOMA\text{-}Br]_0/[CuBr]_0/[bpy]_0$ = 200/1/0.5/1. The GPC trace evolved to a higher molecular weight region with M_n = 20,800 g mol^{-1} and M_w/M_n = 1.24 (Figure 3.2). From the integral ratio of [(c/9)/(b/3)] with the DP = 19 for HO-POEOMA-Br, the ^{1}H-NMR integration was used to determine the DP of the PtBMA block to be 67 (Figure 3.3b). The GPC and ^{1}H-NMR results suggest the successful synthesis of well-controlled HO-POEOMA$_{19}$-b-PtBMA$_{67}$ (HO-ABP) with narrow molecular weight distribution (M_w/M_n < 1.24).

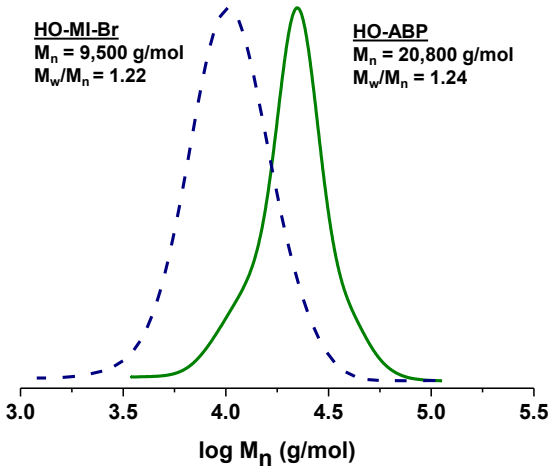

Figure 3.2. GPC traces of HO-ABP and HO-POEOMA-Br MI.

3.5. Hydrolytic cleavage of t-butyl groups in HO-ABPs

The cleavage of pendant t-butyl groups in PtBMA blocks of HO-ABP in the presence of trifluoroacetic acid was examined. Figure 3.3c shows the ^{1}H-NMR spectrum of the hydrolyzed polymers in DMSO-d_6. The signal at 1.5 ppm, resulting from t-butyl protons completely disappeared. Further, solubility change was observed; while HO-ABP was dissolved in $CDCl_3$ before hydrolysis, it had poor solubility and precipitated in chloroform after hydrolysis. These results suggest significant hydrolysis of t-butyl ester groups of PtBMA blocks to form pendant acid moieties.

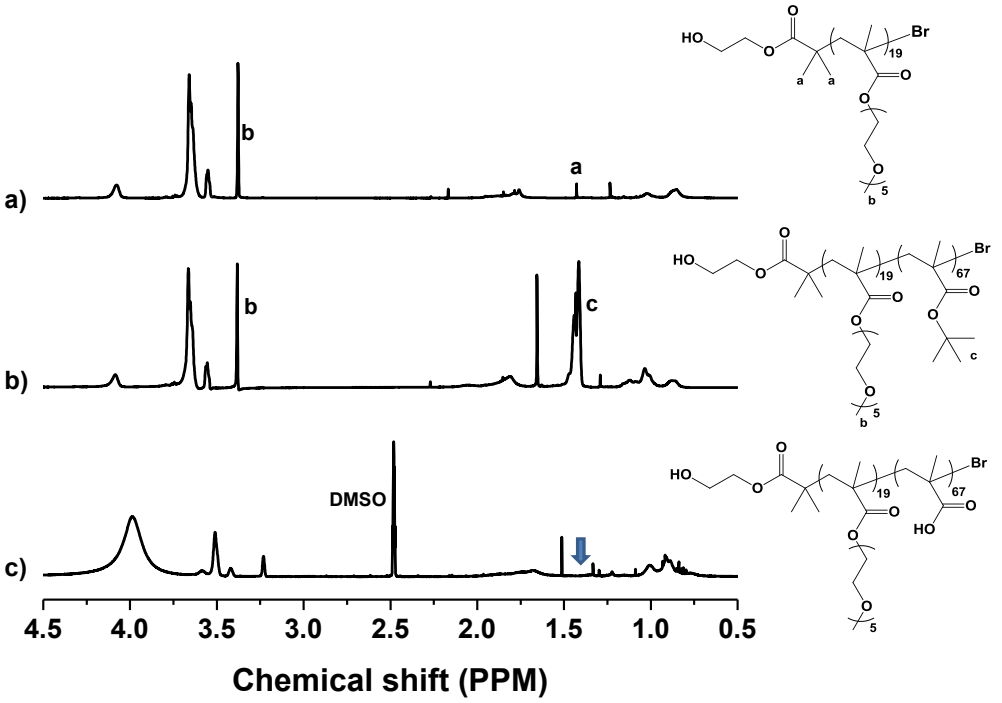

Figure 3.3. ^{1}H-NMR spectra of HO-MI (a), HO-ABP before (b), and after (c) hydrolytic cleavage of PtBMA block in the presence of trifluoroacetic acid.

3.6. Aqueous micellization of HO-ABPs

A solvent evaporation method[93] was used to form HO-ABP micelles consisting of a hydrophobic PtBMA core surrounded with hydrophilic POEOMA corona in aqueous solution. Its critical micellar concentration (CMC) was determined using a fluorescence spectroscopy technique with Nile Red (NR) probe. A series of mixtures consisting of a constant concentration of NR and various amounts of HO-ABP ranging from 10^{-5} to 0.08 mg mL^{-1} in aqueous solution was prepared by solvent evaporation method. Figure 3.4a shows overlaid fluorescence spectra of NR in the solution measured at λ_{ex} = 592.05 nm after the removal of THF by evaporation and free NR by filtration. The weak

fluorescence intensity at lower concentrations of HO-ABP show that the NR was not encapsulated. However, a steady increase in fluorescence intensity was observed by increasing the concentration of HO-ABP, indicating the formation of micelles (Figure 3.4b). Each dataset was fitted to linear regression. From two obtained equations, the CMC of HO-ABP was determined to be 6.3 µg mL^{-1}.

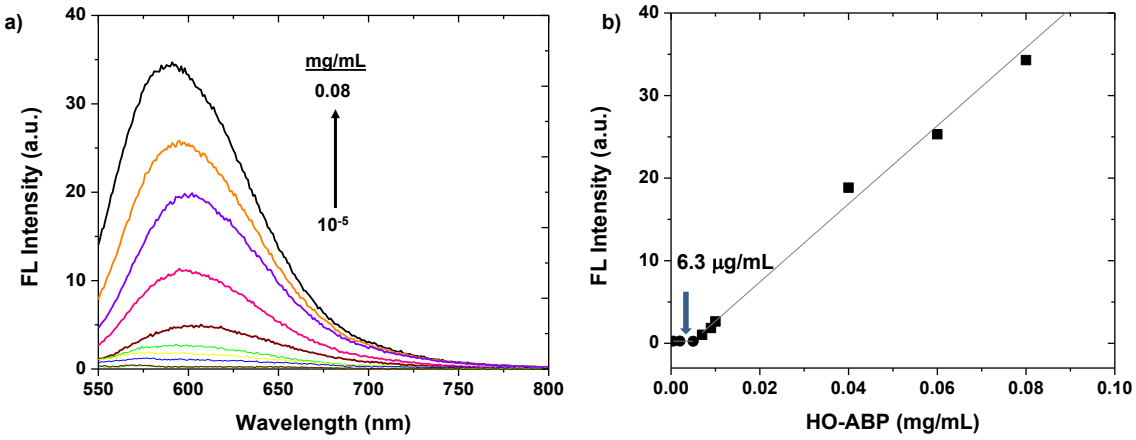

Figure 3.4. Evolution of fluorescence spectra (a) and fluorescence intensity at 480 nm (b) of NR for aqueous mixtures consisting of NR with various amounts of HO-ABP to determine CMC to be 6.3 µg mL^{-1}.

Due to the amphiphilic nature of HO-ABP, the purified polymer self-assembled to form colloidally stable micellar aggregates in aqueous solution. At the concentration of 50 µg mL^{-1}, above CMC, dynamic light scattering (DLS) results show the formation of micelles with a monomodal size distribution of 28.8 ± 0.1 nm in diameter. DLS data was collected from a single sample measured 3 times with 12 runs in each measurement. The average and standard deviation were calculated using the data collected from the 3 measurements (Figure 3.5a). Further, the micelle size remained similar over micellar concentration ranging from 0.05 to 5 mg mL^{-1} (Figure 3.5b). The morphology of micelles

was then studied using transmission electron microscopy (TEM) measurement. TEM microscopic image indicates the average diameter of dried micelles = 12.5 ± 2.5 nm (inset in Figure 3.5a). The micelle size was smaller by TEM than by DLS; the difference is attributed to the dehydrated state of the micelles for TEM measurements.[94]

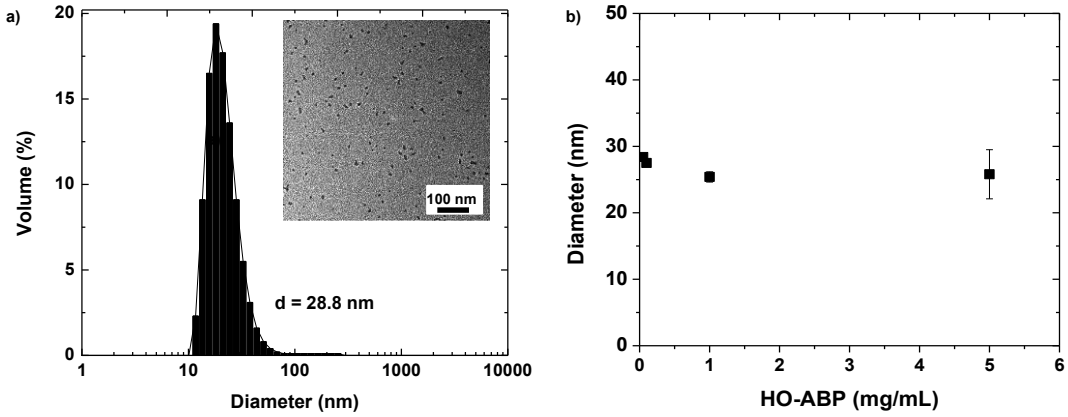

Figure 3.5. DLS diagram and TEM image (inset) with scale bar = 100 nm (a) and diameter over concentration (b) of HO-ABP micelles.

3.7. Destabilization of HO-ABP micellar aggregates in acidic condition

pH-responsive degradation of HO-ABP micelle was examined by following the change in micelle size at different pH values using DLS. Micellar dispersion was prepared at the concentration of 5 mg mL^{-1}. Its aliquots were adjusted to pH = 5 and 3 using an aqueous potassium hydrogen phthalate (KHP) buffer solution at pH = 3. The size of micelles in the control sample at pH = 7 did not change and the dispersion remained transparent, as shown in Figure 3.6. After 4 days, at pH = 5, the DLS results indicate a slight increase in the micelle size from 28.8 to 29.7 nm, with the occurrence of a new population of large aggregates (> 1 μm). The micellar dispersion became cloudy,

suggesting the formation of large aggregates. By decreasing the pH further to 3, the average diameter of micelles increased more significantly from 28.8 to 34.6 nm with a larger population of large aggregates (Figure 3.6). DLS data was collected from a single sample measured 3 times with 12 runs in each measurement. The D_n was calculated using the data collected from the 3 measurements. Such a variation of micelle size in acidic environments could be due to hydrolytic cleavage of pendant t-butyl groups, resulting in the formation of hydrophilic PMAA blocks.

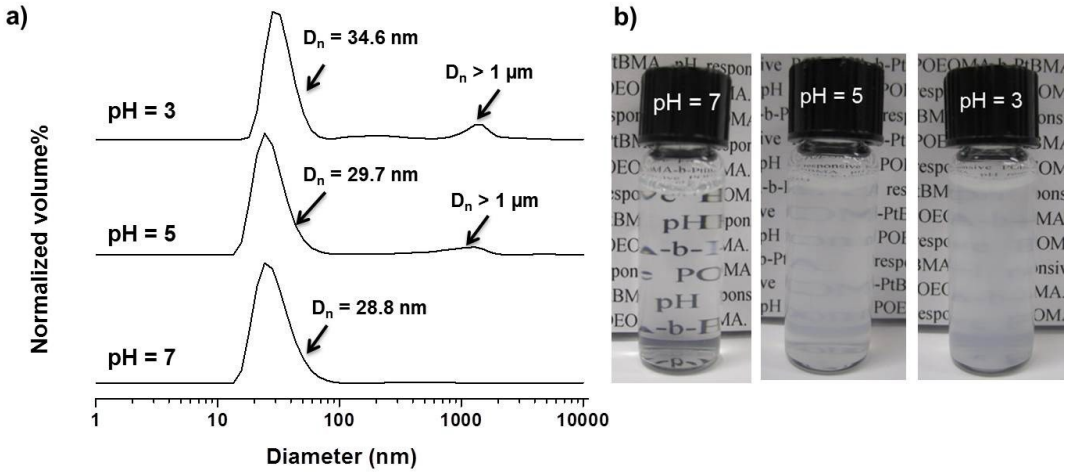

Figure 3.6. DLS diagrams (a) and digital images (b) of HO-ABP micelles at pH = 7, 5, and 3 after 4 days.

3.8. Physical encapsulation of model drug

To examine applicability of self-assembled HO-ABP micelles as a potential drug delivery carrier, the encapsulation of model drugs was examined. Physical entrapment is a facile method to load small drugs in micelles.[95] Here, the physical encapsulation of NR as a hydrophobic model drug was examined to investigate the effect of the weight ratio of

NR/HO-ABP on physical loading. Micellization of HO-ABP with NR in water through the solvent evaporation method yielded NR-loaded micelles. After removal of excess NR by centrifugation and subsequent filtration, the micelles were concentrated by rotary evaporation. The residues were dissolved in THF, and using the Beer-Lambert equation with the absorbance at λ_{max} = 527 nm and the extinction coefficient ε = 37,300 M^{-1} cm^{-1} (Appendix A, Figure A.2.),[91] the loading level and loading efficiency (LE) of NR in micelles were determined. All samples were performed in triplicate.

As presented in Table 3.2, with the weight ratio of NR/HO-ABP = 1.0/10 at 0.5 mg mL^{-1} concentration of HO-ABP micelles, the loading level was 0.4% with LE = 4.1%. With a decreasing ratio of NR/HO-ABP to 0.2/10 wt/wt at higher concentration of HO-ABP micelles (3.3 mg mL^{-1}), the loading level increased to 1.1% and LE to 55.9%. In addition, DLS results indicate that their hydrodynamic diameters remained similar to that of micelles without NR, suggesting no significant effect of the presence of NR on micellization of HO-ABP in aqueous solutions (Appendix A, Figure A.4.).

Table 3.2. Encapsulation of NR in HO-ABP micelles at different weight ratios of NR/HO-ABP.

HO-ABP (mg mL^{-1})	NR/HO-ABP (wt/wt)	Loading[a] (%)	LE[b] (%)	Diameter (DLS) (nm)
0.5	No NR	Control		28.2
0.5	1.0/10	0.4 ± 0.04	4.1 ± 0.4	28.3
3.3	0.2/10	1.1 ± 0.1	55.9 ± 0.1	27.3

[a] Determined by the weight ratio of NR encapsulated in micelles to dried polymers.

[b] Calculated by the weight ratio of NR encapsulated in micelles to the NR initially added.

3.9. Biotinconjugation with biotin and Avidin-HABA assay

Active targeting to specific cells through bioconjugation of delivery vehicles with cell targeting agents is a highly desired property for polymer-based drug delivery nanocarriers.[96] Specific targeting reduces serious side effects common to small drugs, as well as enhances drug efficiency. To assess the applicability of HO-ABP toward targeted delivery, the conjugation of HO-ABP with vitamin H (biotin) was examined. A facile carbodiimide coupling reaction between COOH groups of biotin and OH groups of HO-ABP micelle was employed in the presence of 1-ethyl-3-(3-dimethylaminopropyl)carbodiimide (EDC) for 12 hrs. Unreacted biotin was removed by extensive dialysis against aqueous $NaHCO_3$ solution. The purified biotin-labeled HO-ABP (Biotin-ABP) was collected by rotary-evaporation and used to form biotinylated micelles at concentration of 5.0 mg mL^{-1} through solvent evaporation method (Figure 3.7a).

The bioavailablity of biotin present in the OH-functionalized ABP was evaluated by a competitive Avidin/2-(4-hydroxyphenylazo)benzoic acid (HABA) binding assay via UV/Vis spectroscopy.[97] Avidin is a protein with four binding pockets for HABA as well as biotin. Since Avidin has higher binding affinity to biotin than HABA, HABA in an Avidin-HABA complex can be replaced by biotin. Figure 3.7b shows the UV−Vis spectra of Avidin-HABA complex before and after the addition of biotinylated micelles. Upon the addition of biotin-functionalized ABP micelles, the absorbance at 500 nm decreased by $\Delta A = 0.79$; this specifies Avidin–biotin complexation. Using a calibration curve reported elsewhere,[98] the difference of absorbance allows for the calculated availability of biotin to be 0.93 mg biotin/g polymer.

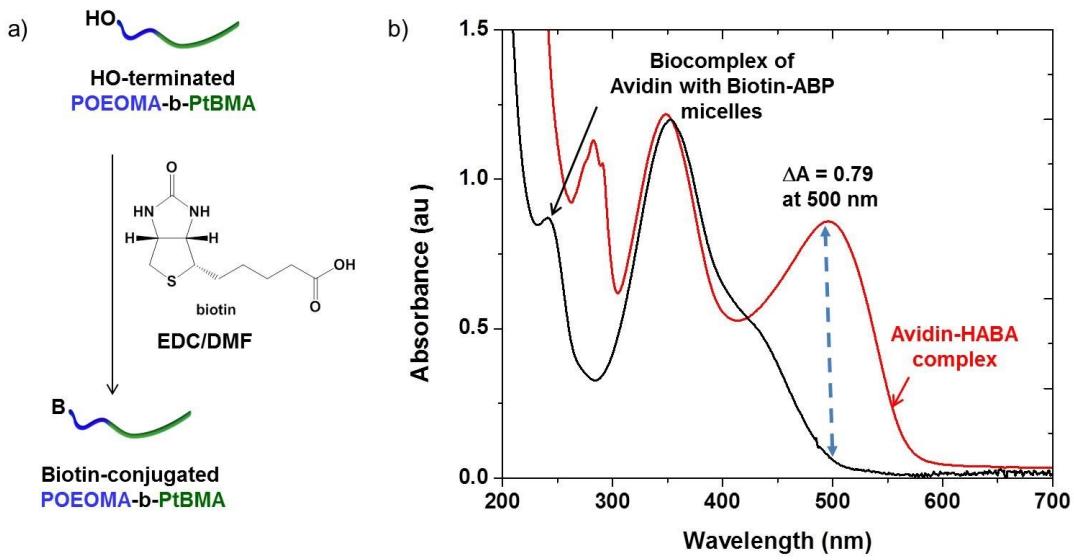

Figure 3.7. Schematic illustration of bioconjugation of HO-ABP with biotin to form biotin-conjugated ABP (a) and UV–Vis spectra of Avidin–HABA complex before and after addition of biotinylated micelles in aqueous solution (b).

3.10. Noncytotoxicity of HO-ABP micelles

A MTT assay was used to assess the cytotoxicity of HO-ABP micelles. Different cell lines including human embryonic kidney (HEK293T) and HeLa cancer cell lines were examined. Both cell lines were incubated with different concentrations of HO-ABP micelles for 48 hrs. Figure 3.8 shows > 95% viability of cells, suggesting the nontoxicity of HO-ABP micelles to different cell lines up to 1 mg mL^{-1}.

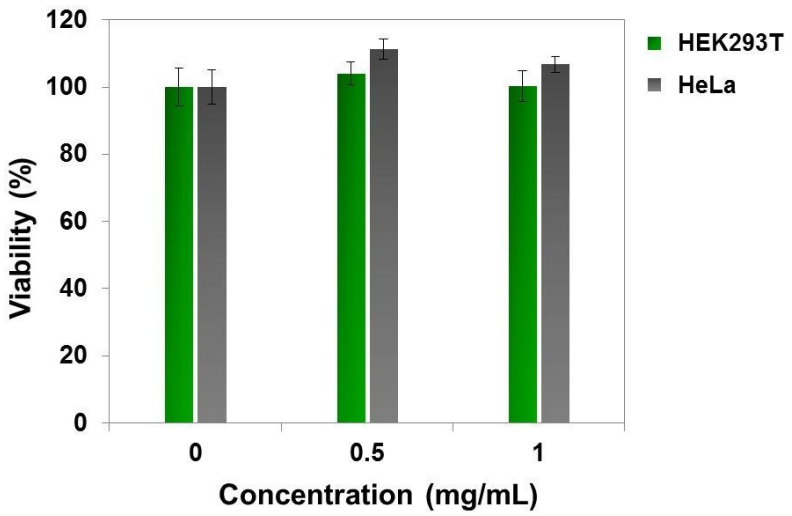

Figure 3.8. Viability of HEK293T and HeLa cells cultured with HO-ABP micelles for 48 hrs.

3.11. Conclusions

Well-defined HO-ABP block copolymers were synthesized by consecutive ATRP of OEOMA and tBMA in the presence of a HO-iBuBr initiator in acetone. The obtained polymers were characterized by ^{1}H-NMR and GPC measurements. Due to the amphiphilic nature, HO-ABPs self-assembled, through aqueous micellization to form spherical micellar aggregates with a diameter = 28.8 nm as determined by DLS and 12.5 nm when measured by TEM. The CMC was found to be 6.3 μg mL^{-1} using a NR fluorescence probe method. The hydrophobic core of micelles enabled the encapsulation of hydrophobic model drugs. The hydrolysis of pendant t-butyl groups of PtBMA in acidic condition resulted in doubly hydrophilic HO-POEOMA-b-PMAA block copolymers. In acidic pH, HO-ABP micelles were destabilized to form large aggregates. As proof of concept, the biotinylated micelles were prepared. The Avidin-HABA assay results indicate that the availability of biotin was 0.93 biotin per HO-ABP chain. These

results, combined with noncytotoxicity, suggest that new HO-terminated ABP micelles have potential as controlled drug delivery carriers in response to acidic conditions.

Chapter 4

Thiol-Responsive Mono-Cleavable Micelles

4.1. Introduction

A strategy toward the development of reduction-sensitive degradable micelles involves the introduction of disulfide linkages into well-defined ABPs.[55] Different number of disulfide linkages are positioned at various locations; such as in main chains, at side chains, or the cross-links.[17, 99] For reductively degradable micelles having disulfides in main chains, backbone multi-cleavable micelles[21, 62, 100] and sheddable micelles[101] have been reported. Their characteristics are described in Section 1.5 in Chapter 1. Mono-cleavable micelles are new and based on symmetric triblock copolymer having single disulfides in the middle blocks. After our publication,[102] several examples of mono-cleavable micelles have been reported. They include multi-armed poly(ε-caprolactone)-b-poly(ethylene oxide) copolymers,[103] comb-like alternating copolymers consisting of styrenic and N-(2-hydroxyethyl) maleimide units[40] and polypeptides with diethylene glycol-L-glutamate N-carboxyanhydride.[104]

This chapter describes the first example of mono-cleavable micelles based on novel comb-type triblock copolymers consisting of hydrophilic POEOMA and hydrophobic poly(oligo(propylene oxide) monononylphenyl ether acrylate (PAP) blocks. As illustrated in Figure 4.1, single disulfide linkages are positioned in the center of the triblock copolymers; thus named POEOMA-b-PAP-ss-PAP-b-POEOMA (ss-ABP_2).

These block copolymers were synthesized by a consecutive ATRP of oligo(propylene oxide) monononylphenyl ether acrylate (AP) in the presence of a difunctional Br-initiator labeled with a disulfide linkage (SS-DBr) and then OEOMA. The resulting ss-ABP_2 self-assembled to form colloidally stable micellar aggregates in aqueous solutions at concentration above the CMC. Their thiol-responsive degradation by cleavage of disulfide linkages in their micelle cores led to a change in morphology to smaller aggregate structures, as confirmed by dynamic light scattering (DLS) and atomic force microscopy (AFM) measurements.

This chapter comprises material published in *Macromolecular Rapid Communications*, **2011**, *32*, 1652-1657. Part of this text is adapted from the original source material.

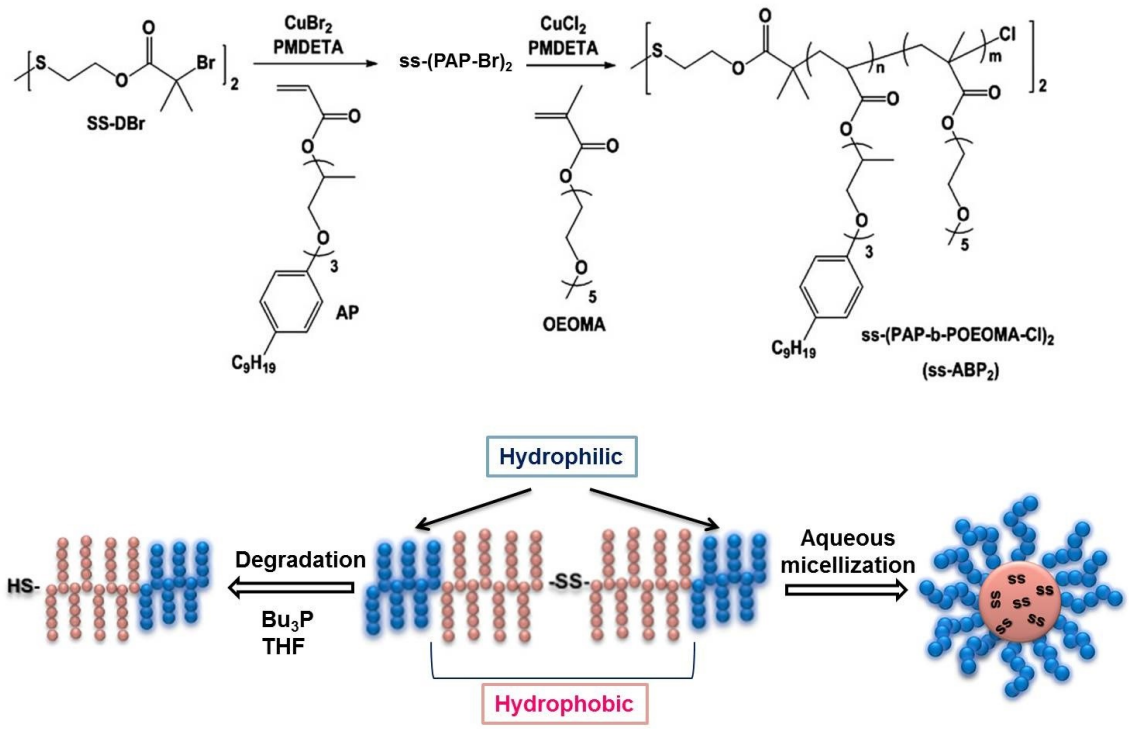

Figure 4.1. Illustration of synthesis, aqueous micellization, and degradation of mono-cleavable brush-like ss-ABP_2 triblock copolymers labeled with single disulfides in the middle blocks (PMDETA : N,N,N′,N″,N″-pentamethyldiethylenetriamine, Bu_3P: tributylphosphine).

4.2. Experimental section

The detailed procedures of synthesis and characterization are described in Appendix B.

4.3. Synthesis of ss-(PAP-Br)$_2$ macroinitiator (MI)

Bis[2-(2-bromoisobutyryloxy)ethyl] disulfide (SS-DBr) difunctional ATRP initiator was synthesized by A. Nelson-Mendez in our group using a carbodiimide coupling reaction (^{1}H-NMR spectra of SS-DBr before and after purification is given in Appendix B, Figure B.1.). Its detailed synthesis is described in our publication[102] and elsewhere.[105] In the presence of SS-DBr initiator, a series of ATRP of AP was

conducted in acetone under various conditions. An Activators Generated by Electron Transfer (AGET)[71] process for ATRP was examined here. With the initial mole ratio of $[AP]_0/[SS\text{-}DBr]_0 = 50/0.5$, important parameters including temperature and $[CuBr_2]_0/[SS\text{-}DBr]_0$ were varied to synthesize well-controlled ss-(PAP-Br)$_2$ MI's. Table 4.1 summarizes the results.

Table 4.1. Characteristics of ss-(PAP-Br)$_2$ difunctional macroinitiators[a]

ss-(PAP-Br)$_2$	$[CuBr_2]_0/[SS\text{-}DBr]_0$	Temp (ºC)	Time (hrs)	Conversion[b]	$M_{n,theo}$[c] (g mol^{-1})	$M_{n,GPC}$ (g mol^{-1})	M_w/M_n[b]
1	0.5/1	60	15.0	0.16	6,700	7,300	1.22
2	0.5/1	80	8	0.36	15,000	11,700	1.51
3	1/1	80	21.0	0.24	10,000	12,000	1.22

[a] $[AP]_0/[SS\text{-}DBr]_0 = 50/0.5$, $[CuBr_2]_0/[Sn(Oct)_2]_0 = 1/1.3$, AP/acetone = 1.5/1 v/v.

[b] Determined by GPC with PMMA standards.

[c] Theoretically calculated molecular weight: $M_{n,theo} = [AP]_0/[SS\text{-}DBr]_0 \times MW(AP) \times$ conversion.

For AGET ATRP with $[CuBr_2]_0/[SS\text{-}DBr]_0 = 0.5/1$ at 60 ºC, conversion reached 16% in 15 hrs, suggesting slow polymerization (ss-(PAP-Br)$_2$-1). The resulting polymer had number average molecular weight M_n = 7,300 g mol^{-1} with a molecular weight distribution as narrow as M_w/M_n = 1.22. When the polymerization temperature was increased from 60 to 80 ºC, conversion increased to 36% in 8 hrs, but the polydispersity index (PDI) also increased to 1.51 (ss-(PAP-Br)$_2$-2), indicating a loss of control during the polymerization. The amount of deactivators of $CuBr_2$ complex as the ratio of $[CuBr_2]_0/[SS\text{-}DBr]_0$ was then increased at the same temperature of 80 ºC (ss-(PAP-Br)$_2$-3) to enhance the rate of deactivation. With a higher concentration of copper species,

conversion reached 24% within 21 hrs. The resulting (ss-(PAP-Br)$_2$-3) polymer had M_n = 12,000 g mol^{-1} with M_w/M_n = 1.22. After purification by removal of unreacted PA monomers and Cu species, the purified (ss-(PAP-Br)$_2$-3) had the degree of polymerization (DP) = 24, calculated from monomer conversion; thus Br-$_{12}$PAP-ss-PAP$_{12}$-Br (ss-(PAP$_{12}$-Br)$_2$).

Kinetics of AGET ATRP AP was further examined. Figure 4.2 shows the results. For both ss-(PAP-Br)$_2$-1 and ss-(PAP-Br)$_2$-3, polymerization proceeded at a steady rate for the first 4 hours. However, the polymerizations slowed significantly for both reactions after the initial burst, possibly due to oxidation of copper(I) activators to copper(II) deactivators as oxygen was introduced during the course of polymerization. As expected in a living polymerization, molecular weight increased linearly with conversion and molecular weight distributions remained low with M_w/M_n < 1.23. These results suggest successful synthesis of well-defined ss-(PAP-Br)$_2$ MIs having single disulfide linkages positioned in the middle.

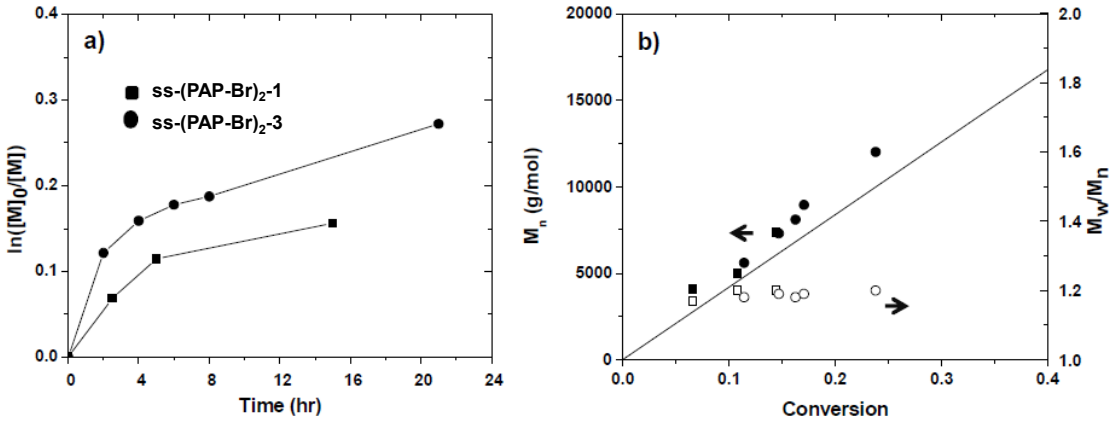

Figure 4.2. Kinetic plot (a) and evolution of molecular weight and molecular weight distribution of ss-(PAP-Br)$_2$-1 and ss-(PAP-Br)$_2$-3 (b). The straight line in (b) is the theoretically predicted molecular weight over conversion.

4.4. Synthesis of ss-ABP_2 triblock copolymer

For the synthesis of well-defined mono-cleavable ss-ABP_2, AGET ATRP of OEOMA was conducted for chain extension of ss-$(PAP\text{-}Br)_2$ with water-soluble POEOMA. To ensure faster initiation than propagation in block copolymerization consisting of polyacrylate-Br MIs and methacrylates, a halogen exchange is required to slow down the polymerization of methacrylates. Otherwise, final block copolymers will be contaminated with the presence of unactivated polyacrylate MIs.[106] Here, $CuCl_2$/PMDETA complex was used to enable better control of ATRP of OEOMA in the presence of ss-$(PAP\text{-}Br)_2$ MIs. The conditions include $[OEOMA]_0/[ss\text{-}(PAP\text{-}Br)_2]_0/[CuCl_2/PMDETA]_0/[Sn(Oct)_2]_0 = 50/0.5/1/1.3$ and OEOMA/anisole = 1.5 v/v at 80 °C. After 2 hrs, GPC traces evolved into a higher molecular weight region with M_n = 15,200 g mol^{-1} and M_w/M_n = 1.23 at 10% conversion (Figure 4.3a). ^{1}H-NMR was used to compare ss-ABP_2 with ss-$(PAP\text{-}Br)_2$ (Figure 4.3b). These results suggest the synthesis of well-defined ss-$(PAP_{12}\text{-}b\text{-}POEOMA_5\text{-}Cl)_2$ symmetric triblock copolymers using the AGET ATRP of OEOMA in the presence of ss-$(PAP\text{-}Br)_2$.

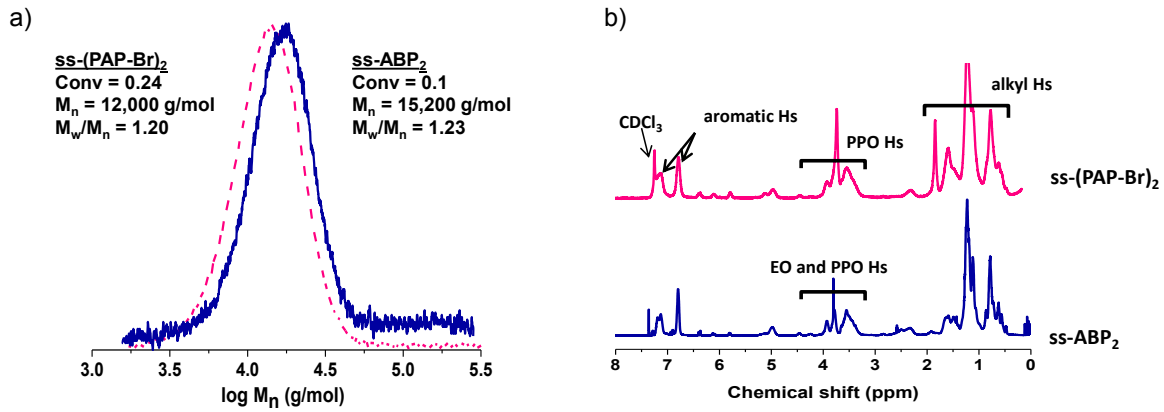

Figure 4.3. GPC traces (a) and ^{1}H-NMR spectra in $CDCl_3$ (b) of ss-(PAP-Br)$_2$ and ss-ABP$_2$.

4.5. Aqueous micellization of ss-ABP$_2$

Owing to its amphiphilic nature, the purified ss-ABP$_2$ formed micellar aggregates consisting of a hydrophobic ss-(PAP-Br)$_2$ core surrounded with short hydrophilic POEOMA coronas. Critical micellar concentration (CMC) was determined using tensiometry. An aqueous stock solution of ss-ABP$_2$ at a concentration of 1.0 mg mL^{-1} was prepared by solvent evaporation method. Aliquots of the stock solution were diluted with various amounts of water. The surface pressure was recorded at different concentrations ranging from 2.8 to 90 µg mL^{-1}. As seen in Figure 4.4, at lower concentrations the pressure of aqueous solutions was as low as < 1 mN m^{-1}. When the concentration increased, the pressure rapidly increased, and then became constant. Each dataset was fitted to linear regression. From two obtained equations, the CMC of ss-ABP$_2$ was determined to be 32 µg mL^{-1}.

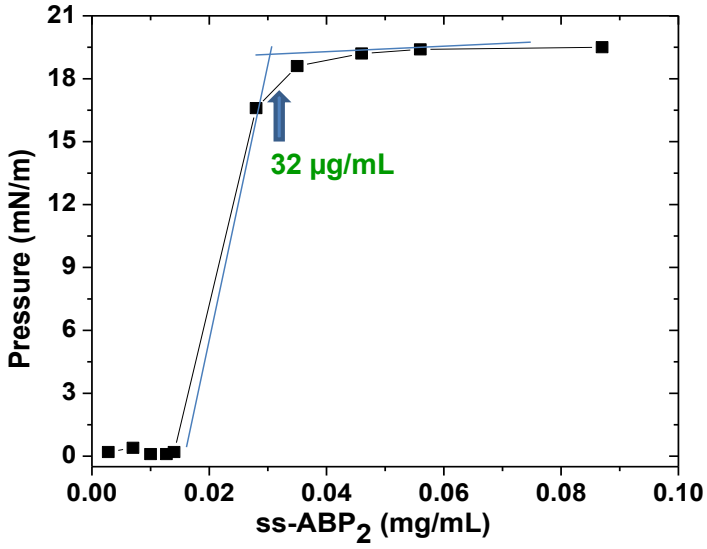

Figure 4.4. Surface pressure versus concentration of ss-ABP_2 to determine CMC by tensiometry.

4.6. Reductive cleavage of disulfide linkages in ss-ABP_2

Reductive cleavage of single disulfide linkages in the middle blocks of ss-ABP_2 triblock copolymers was examined. When all disulfide linkages of ss-ABP_2 are cleaved by reductive reactions under reducing conditions, the degraded products could be thiol-terminated diblock copolymers (HS-PAP-b-POEOMA) with a half molecular weight of ss-(PAP-b-POEOMA)$_2$. For GPC measurements, ss-ABP_2 was dissolved in THF and mixed with tributylphosphine (Bu_3P) at a mole equivalent ratio of Bu_3P/disulfide = 1/1 for 24 hrs. As seen in Figure 4.5, molecular weight of ss-ABP_2 decreased from M_n = 14,500 g mol^{-1} to M_n = 5,500 g mol^{-1}. This result indicates the significant cleavage of disulfide linkages in ss-ABP_2 under reducing conditions.

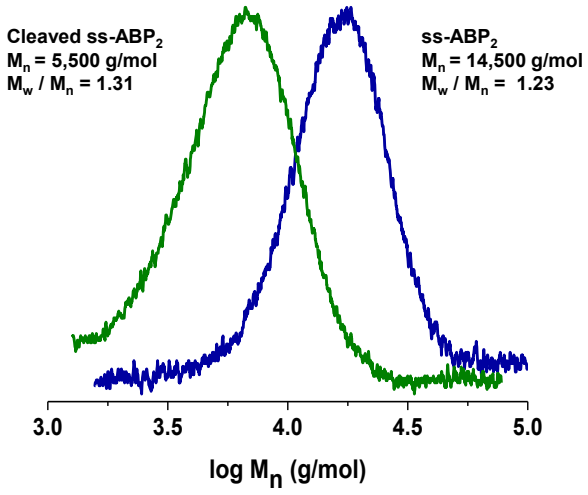

Figure 4.5. GPC traces of ss-ABP_2 before and after reductive cleavage of disulfide linkages in the presence of Bu_3P.

4.7. Reductively-degradable ss-ABP_2 micellar aggregates

Thiol-responsive degradation of self-assembled micelles through disulfide-thiol exchange in the presence of DL-dithiothreitol (DTT) was examined using AFM and DLS. Micellar dispersion was prepared at the concentration of 1.0 mg mL^{-1}. Aliquots of micellar dispersion were mixed with DTT as the mole equivalent ratio of DTT/disulfide = 1/1. As seen in Figure 4.6, the color of the mixtures changed from turbid to lightly blue-tint over 24 hrs. DLS results indicate that particle diameter was ≈ 109 nm in the absence of DTT (Figure 4.6a), and then decreased to 70.4 nm when DTT was added (Figure 4.6b). DLS data were collected from a single sample measured 3 times with 60 runs in each measurement; the particle diameter were calculated using the data collected from the 3 measurements. Further, the change of morphology in response to reductive reactions with DTT in water was explored using AFM. The dispersion without and with

DTT/ disulfide = 1/1 were spin-cast on mica surface. The AFM measurements were done by Dr. R. Schmidt in the Centre for NanoScience Research at Concordia University. AFM image of the micelles without DTT shows the presence of large particles along with small particles (Figure 4.6c). The average diameter was calculated to be 255.5 ± 128.7 nm, which is larger than particle size determined by DLS. The difference is attributed to flattening of the particles on the mica during the casting process. In the presence of DTT, the AFM image of micelles shows fairly uniform distribution of small particles with the average diameter = 97.8 ± 21.8 nm (Figure 4.6d). These results suggest the cleavage of disulfides in the micellar cores to the corresponding thiol-terminated degraded products in presence of DTT. These degraded polymers are still amphiphilic, and thus could re-aggregate to smaller-sized assembled structures in water.

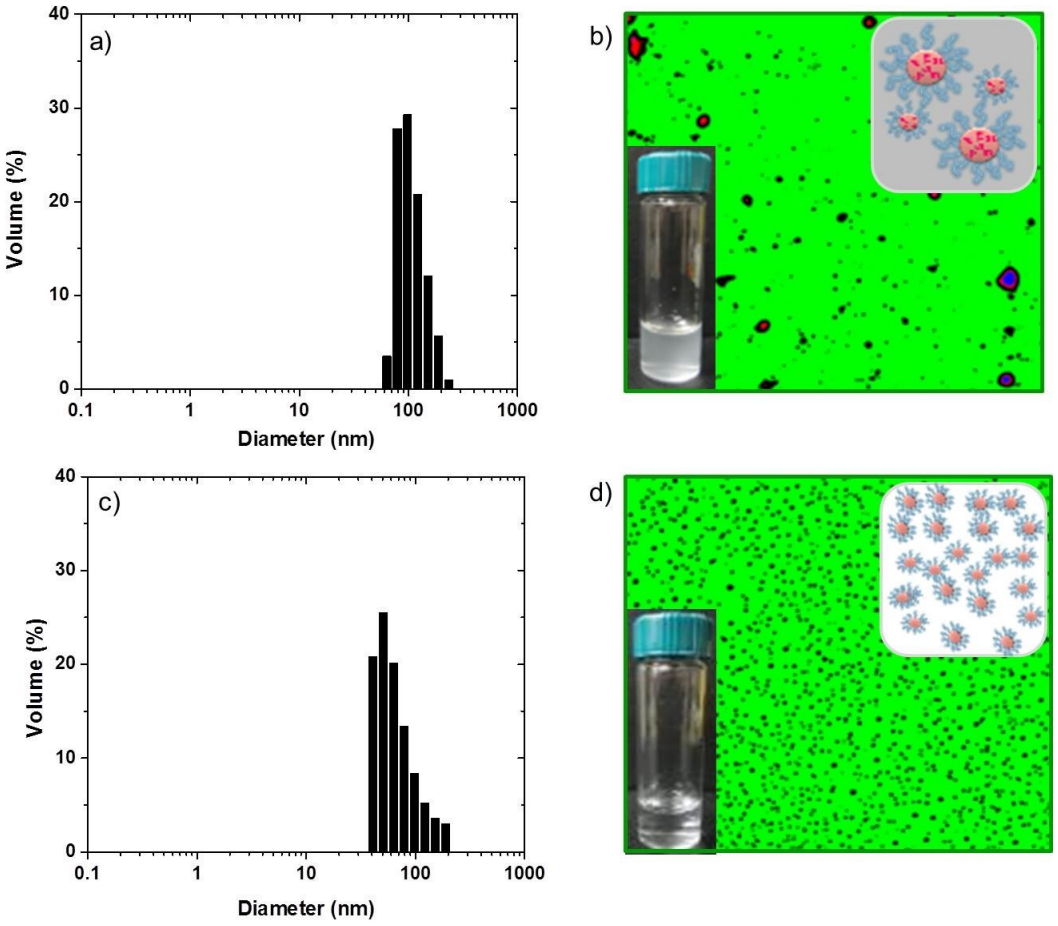

Figure 4.6. For ss-ABP_2 symmetric triblock copolymers, DLS diagrams based on % volume and AFM images with the size = 10 µm × 10 µm before (a and b) and after (c and d) addition of DTT defined as DTT/disulfide = 1/1 in water (insets; digital images of micellar dispersions in water).

4.8. Conclusions

New thiol-responsive symmetric triblock copolymer having single disulfide linkages in the middle blocks were synthesized using AGET ATRP. These mono-cleavable copolymers consist of hydrophobic PAP and hydrophilic POEOMA. Polymerizations were well-controlled, yielding both ss-$(PAP\text{-}Br)_2$ and ss-ABP_2 with monomodal and narrow molecular weight distributions with PDI as low as M_w/M_n <

1.23. Due to the amphiphilic nature, ss-ABP_2 self-assembled, through aqueous micellization, to form micellar aggregates at concentrations above CMC. For reductive cleavage of single disulfides in the mono-cleavable copolymers and micelles, GPC results suggest that copolymers in the presence of Bu_3P were cleaved to corresponding HS-terminated $PAP_{1/2}$-b-POEOMA with a half molecular weight. The AFM and DLS analyses suggest the degradation of ss-ABP_2 micelles to small amphiphilic thiols, leading to the formation of smaller-sized assembled structures in water.

Chapter 5

Glutathione-Responsive Micelles Having Pendant Disulfide Linkages

5.1. Introduction

Pendant multi-cleavable micelles are a promising class of drug delivery nanocarriers. These micelles are based on well-defined ABPs having pendant disulfide linkages as side chains. Of the strategies for the synthesis of thiol-responsive degradable nanosized assemblies, as reviewed in chapter 1 (Figure 1.7), amphiphilic block copolymer containing pendant disulfides in hydrophobic cores can be cleaved in response to excess reducing agents, causing the destabilization of micellar aggregates through the change in hydrophobic/hydrophilic balance.[107] Alternatively, these micelles are converted to core-crosslinked micelles with disulfide crosslinks through intermolecular thiol-disulfide polyexchange reactions in the presence of catalytic amount of reducing agents. This feature can enhance colloidal stability upon dilution below CMC, thus preventing premature release of encapsulated drugs during circulation in the body.

Several examples of reduction-sensitive core-crosslinked nanogels or micelles have been reported. Random copolymers prepared from dextran-lipoic acid derivatives (Dex-LAs)[108] and poly(ethyleneglycol) (PEG) and poly(ε-caprolactone) (PCL) were used to prepare crosslinked nanogels that contained two lipoyl functional groups at their interfaces.[109] Redox-responsive micelles composed of various ABPs with pendant multi-

cleavable functionalities have also been reported. ABPs consisting of poly(N-(2-hydroxypropyl)methacrylamide) (PHPMA) and poly(2-(pyridyldisulfide)ethyl methacrylate),[110] and well-defined ABPs consisting of PEG and L-lactide(LA)-co-2-(2,4-dinitrophenylthio)ethyl-5-methyl-2-oxo-1,3-dioxane-5-carboxylate (MTC) (mPEG-b-P(LA-co-MTC)) have been studied.[111] Another example includes well-controlled core-crosslinked PEG-b-PHPMA-lipoic acid conjugates (PEG-b-PHPMA-LA) micelles prepared by reversible addition fragmentation chain transfer (RAFT) polymerization.[112] Also recently cross-linked polyester micelles based on monomethoxy poly(ethylene glycol)-b-poly(Tyr(alkynyl)-OCA), a biodegradable amphiphilic block copolymer was developed.[113]

Recently, our research group has reported the synthesis of new ABPs having pendant disulfides positioned at the hydrophobic block as illustrated in Figure 5.1.[64] These ABPs consist of hydrophilic poly(ethylene oxide) (PEO) and hydrophobic pendant disulfide-labeled polymethacrylate (PHMssEt) blocks. They were synthesized by atom transfer radical polymerization (ATRP) of a novel pendant disulfide-functionalized methacrylate (HMssEt) in the presence of PEO-Br macroinitiator. The self-assembled micellar nanostructures of well-defined PEO-b-PHMssEt exhibited tunable release of encapsulated model drugs such as Nile Red in aqueous solution with morphology changes, depending upon the amount of added thiols such as D,L-dithiolthreitol (DTT).[64]

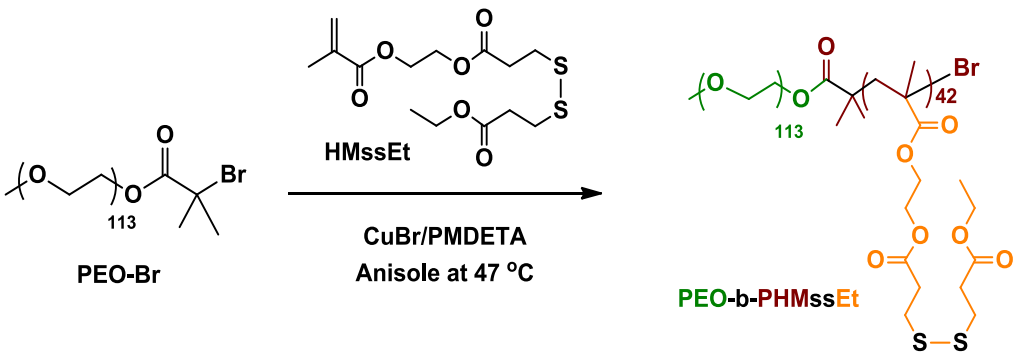

Figure 5.1. Preparation of well-controlled PEO-b-PHMssEt via ATRP (PMDETA: N,N,N′,N′,N″-pentamethyldiethylenetriamine).

This chapter describes the results obtained from my in-depth evaluation of thiol-responsive degradable PEO-b-PHMssEt micelles as effective intracellular delivery nanocarriers of anticancer drugs. In response to cellular GSH, the destabilization of these micelles upon cleavage of pendant disulfide linkages was monitored by dynamic light scattering (DLS) technique. This micellar destabilization led to enhanced release of encapsulated doxorubicin (DOX) as a model anticancer drug. Further, GSH-responsive degradation of DOX-loaded micelles was investigated in cellular environments using flow cytometry and confocal laser scanning microscopy (CLSM) for cellular uptake (Figure 5.2).

This chapter comprises material published in *Biomacromolecules*, **2013**, *14*, 2103-2111. Part of this text is adapted from the original source material.

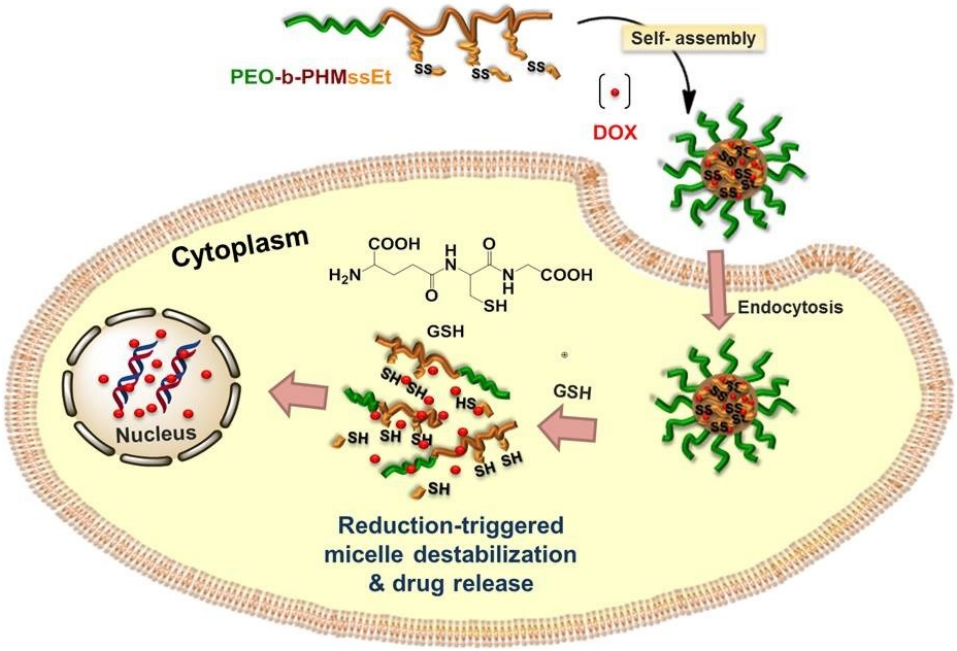

Figure 5.2. Illustration of PEO-b-PHMssEt micelles as effective intracellular drug delivery nanocarriers exhibiting enhanced release of DOX in response to GSH in cancer cells.

5.2. Experimental section

The detailed procedures of synthesis and characterization are described in Appendix C.

5.3. Synthesis and aqueous micellization of PEO-b-PHMssEt

Well-defined PEO-b-PHMssEt was previously synthesized by Dr. Q. Zhang in our group.[64] The polymer was characterized by GPC, and found to have M_n = 25,400 g mol^{-1} and M_w/M_n = 1.11, along with DP = 42 as determined by ^{1}H-NMR; thus PEO_{113}-b-$PHMssEt_{42}$ having 42 pendant disulfide linkages per each polymer chain.

The resulting PEO-b-PHMssEt is amphiphilic and self-assembled to form micellar aggregates in aqueous solution. Its critical micellar concentration (CMC) was

determined to be 49 μg mL^{-1} using tensiometry, has been reported in our previous publication.[64] Here, aqueous micellization of PEO-b-PHMssEt in dimethylformamide (DMF) through a dialysis method was examined to prepare micellar aggregates at 0.9 mg mL^{-1} concentration. As seen in Figure 5.3, DLS results indicate their number average diameter (D_n) to be 145.2 ± 0.7 nm with relatively narrow size distribution (polydispersity, $D_w/D_n < 1.13$). DLS data was collected from a single sample measured 3 times with 12 runs in each measurement. The average and standard deviation were calculated using the data collected from the 3 measurements (Figure 5.3). The above results suggest that PEO-b-PHMssEt can form spherical micelles with suitable size for drug delivery (< 200 nm).

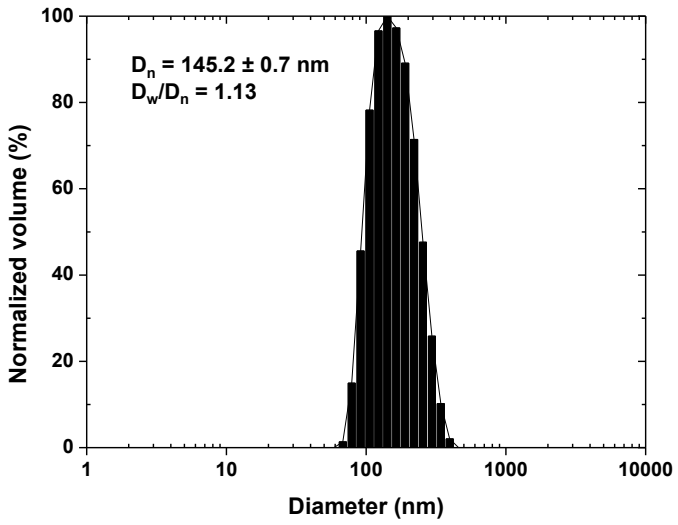

Figure 5.3. DLS diagram of PEO-b-PHMssEt micelles prepared using dialysis method in water.

5.4. Redox-trigger destabilization of PEO-b-PHMssEt micellar Aggregates

The resulting micellar aggregates of PEO-b-PHMssEt contain 42 pendant disulfide linkages in hydrophobic cores. The reductive cleavage of PEO-b-PHMssEt

micelle thus results in a change of hydrophobic/hydrophilic balance, leading to the destabilization of micelles. To study the response of PHMssEt blocks in micellar cores to reductive environment, micelles were treated with a 10 mM aqueous glutathione (GSH) solution. DLS was used to monitor the change in size distribution of aqueous micellar aggregates in the absence and presence of GSH at different time intervals (Figure 5.4).

As a control experiment, no significant change in size distribution was observed in the absence of GSH over 20 hrs. In the presence of 10 mM GSH, the average diameter of micelles increased from 145 nm to several hundred nanometers (diameter > 1 μm) with a broad and bimodal particle size distribution in 2 hrs. Further, the distribution became broader as the population of the large aggregates increased over 20 hrs (Appendix C, Figure C.1.). Such variations in micelle size suggest that micellar aggregates are destabilized due to the cleavage of disulfide linkages in the presence of GSH.

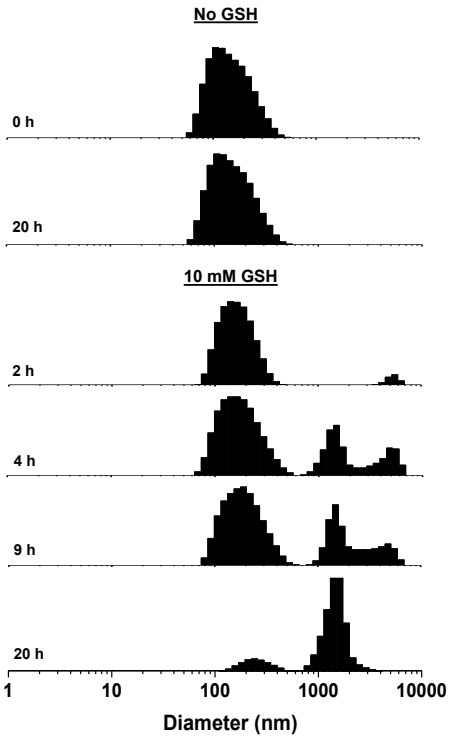

Figure 5.4. Evolution of DLS diagrams (volume %) of PEO-b-PHMssEt micellar aggregates in aqueous buffer solution as control and in 10 mM aqueous GSH buffer solution over time.

5.5. Preparation of DOX-loaded micelles

Doxorubicin (DOX) is one of the most potent anticancer therapeutics, which is widely used to treat various solid tumors. DOX can inhibit proliferation of cancerous cells by interacting with DNA, causing intercalation and inhibition of macromolecular biosynthesis.[114] Here, DOX was encapsulated in hydrophobic micellar cores using the dialysis method. A mixture of DOX and PEO-b-PHMssEt was dissolved in DMF and added into water. Free DOX and DMF were then removed by intensive dialysis using a dialysis tubing (MWCO = 12,000 g mol^{-1}) over 5 days (Appendix C, Figure C.2.). The removal of free DOX was monitored by measuring the absorbance of DOX at 497 nm in the outer dialysis water.

The size and morphology of aqueous DOX-loaded micellar aggregates were examined using DLS and TEM at a micellar concentration of 2.5 mg/mL. DLS results suggest the presence of two populations with z-average diameter based on light scattering intensity to be 174 ± 16 nm. The main population (> 95% by volume) consists of smaller-sized aggregates with D_n = 190 ± 31 nm and relatively broad size distribution (D_w/D_n > 1.33), while a smaller population (< 5% volume) is composed of larger-sized aggregates with the diameter > 1 μm. DLS data was collected from multiple samples (6 samples) each measured 3 times with 12 runs in each measurement. Average and standard deviation were calculated using the collective data of each sample from each measurement (Figure 5.5a). TEM images also indicate a broad distribution of spherical micelles with average diameter = 81.3 ± 25.9 nm (Figure 5.5b). The micelle size obtained by TEM was smaller than found using DLS. The difference is attributed to the dehydrated state of the micelles for TEM measurements.[94]

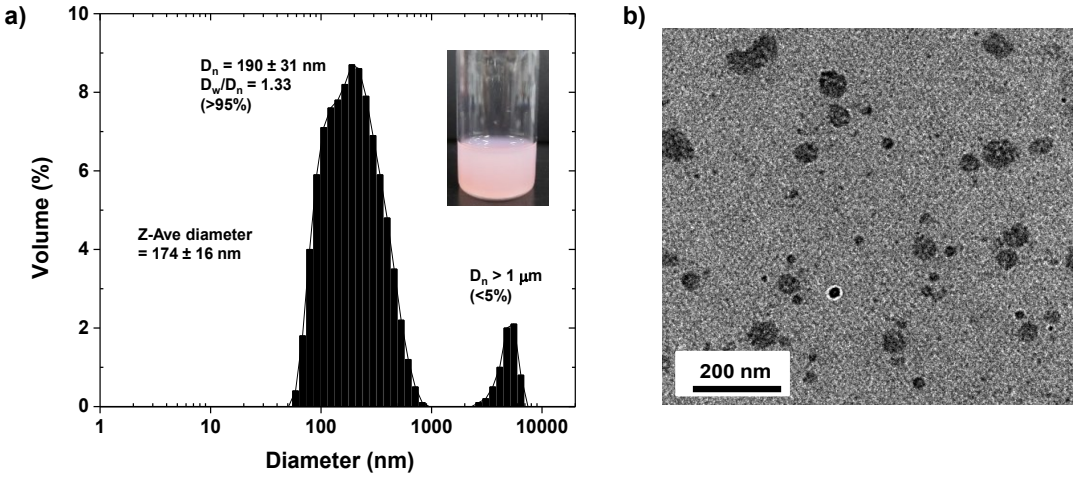

Figure 5.5. DLS diagram (a) and TEM images (b) of DOX-loaded micelles of PEO-b-PHMssEt at 2.5 mg/mL concentration prepared by dialysis method (inset of (a): digital picture of DOX-loaded micellar dispersion).

The loading level of DOX for DOX-loaded micelles was determined using UV/Vis spectroscopy. The extinction coefficient of DOX in DMF was first determined to be ε = 11,700 M^{-1} cm^{-1} at λ_{max} = 480 nm (Appendix C, Figure C.3.). Next, aliquots of DOX-loaded micellar dispersions were taken and water was removed by rotary evaporation. The residues were then dissolved in DMF to form clear solutions of DOX and PEO-b-PHMssEt. Figure 5.6 is an example of UV/Vis spectrum of DOX-loaded micelles in DMF which showed a strong absorption of DOX at λ_{max} = 480 nm. The spectrum is similar to that of free DOX in DMF, suggesting no signification change in the structure of DOX encapsulated in hydrophobic micellar cores. Using the Beer-Lambert equation with the absorbance at λ_{max} = 480 nm and the extinction coefficient, the loading level of DOX was determined to be 0.44 ± 0.07% for MDOX-1 and 0.81 ± 0.07% for MDOX-2 (Table 5.1). Similarly, the DOX loading level increased when the feed ratio of the initial amount of DOX to copolymer was increased.

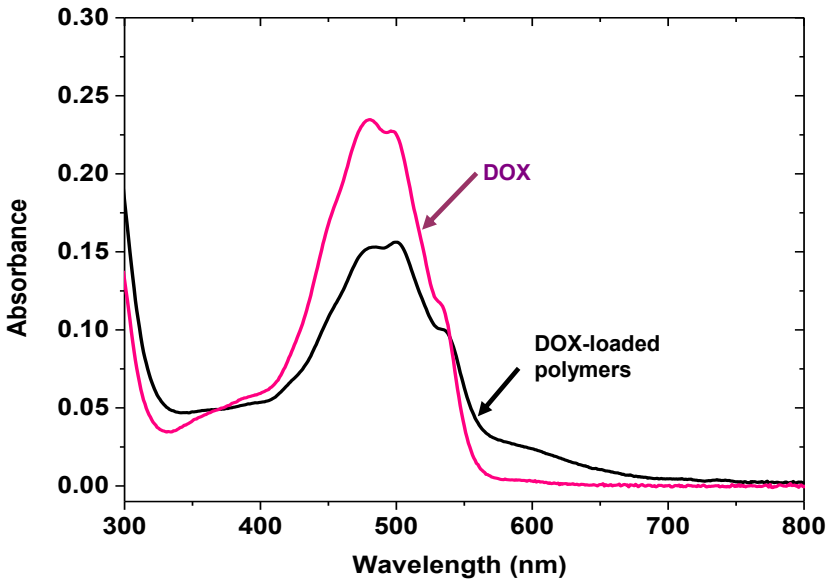

Figure 5.6. A typical UV/Vis spectrum of DOX-loaded micelles after the removal of water, compared with that of free DOX (19.5 µmol mL^{-1}) in DMF.

Table 5.1. Loading level of DOX for DOX-loaded PEO-b-PHMssEt micelles prepared by dialysis method over 5 days.

Sample	DOX/polymer (mg mg^{-1})	water/polymer (mL mg^{-1})	DOX-loaded micelles (mg mL^{-1})	Loading (%)
MDOX-1	1/20	5/20	2.8	0.44 ± 0.07
MDOX-2	2/20	10/20	1.7	0.81 ± 0.07

5.6. GSH-triggered release of DOX from DOX-loaded micelles

To examine GSH-responsive release of DOX from DOX-loaded micelles in the presence of GSH, an aliquot of DOX-loaded micellar dispersion was dialyzed against 10 mM aqueous GSH solution buffered with KH_2PO_4 at pH = 7. A control experiment without GSH was also conducted. Figure 5.7 shows % DOX released from DOX-loaded micelles in the absence and presence of 10 mM GSH. In the absence of GSH, no significant change in UV absorbance was observed, suggesting no significant release of DOX; because DOX is presumably confined in small micellar cores. In the presence of 10 mM GSH, the UV absorbance gradually increased over time and > 70 % DOX was released from the micelles within 4 hrs. This result suggests DOX-loaded micelles degrade to the corresponding water-soluble PEO-b-PHMSH, causing the enhanced release of encapsulated DOX to aqueous solution.

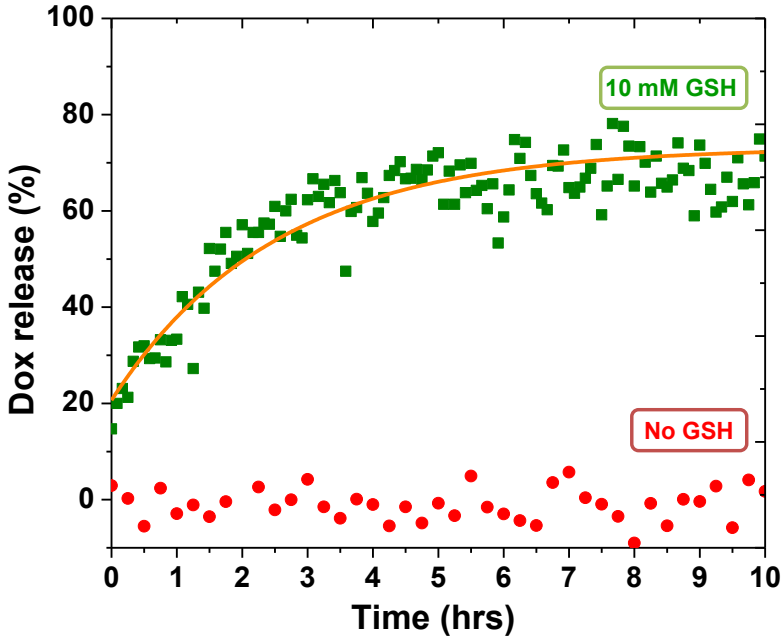

Figure 5.7. Release of DOX from DOX-loaded micelles in 10 mM aqueous GSH solution buffered with KH_2PO_4 at pH = 7.0, and aqueous KH_2PO_4 buffer solution at pH = 7.0 as a control.

5.7. GSH-responsive intracellular release of DOX upon degradation

To evaluate the efficiency of PEO-b-PHMssEt micelles as drug delivery nanocarriers at a cellular level, intracellular release of DOX in response to cellular GSH for HeLa cancer cells after internalization was investigated using flow cytometry and confocal laser scanning microscopy (CLSM). Figure 5.8 shows flow cytometric histograms of HeLa cells. Compared to cells only as a control, the histograms for HeLa cells incubated with DOX-loaded micelles were shifted to the direction of high fluorescence intensity, suggesting effective internalization of DOX-loaded micelles in HeLa cells in 2 hrs.

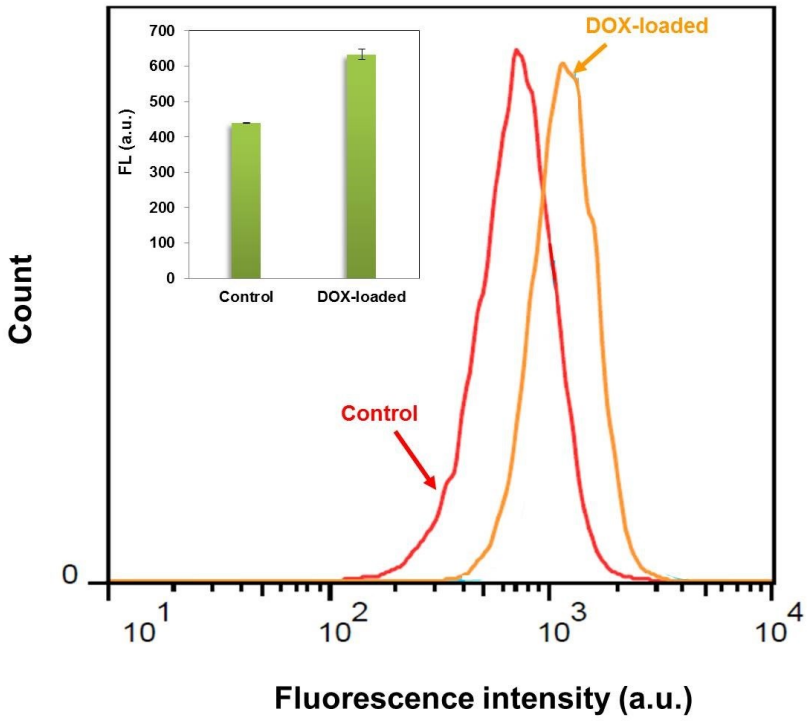

Figure 5.8. Flow cytometric histograms of HeLa cells incubated with DOX-loaded PEO-b-PHMssEt micelles for 2 hrs.

Intracellular release of DOX was further investigated using CLSM (Figure 5.9). Hela cells were incubated with DOX-loaded micelles for 24 hrs. HeLa nuclei were then stained with DAPI. The image from DOX fluorescence suggests that DOX-loaded micelles were internalized and DOX was released to reach the cell nuclei. This observation is in good agreement with the results obtained from flow cytometry.

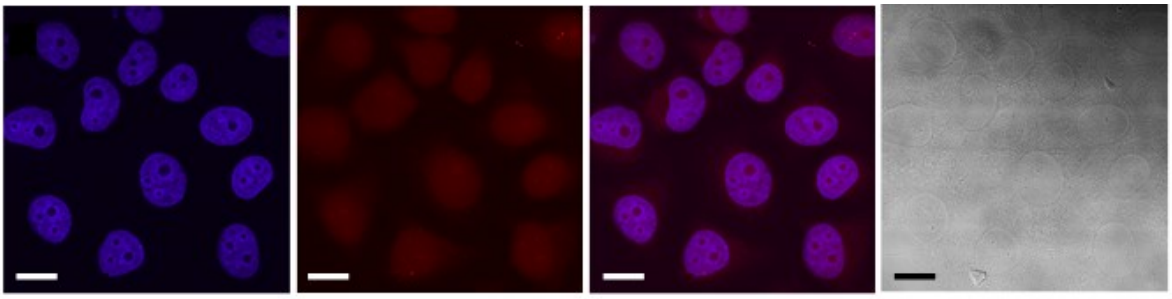

Figure 5.9. CLSM images of HeLa cells incubated with DOX-loaded PEO-b-PHMssEt micelles for 24 hrs. The images from left to right show cell nuclei stained by DAPI (blue), DOX fluorescence in cells (red), overlays of two images, and differential interference contrast (DIC) image. Scale bar = 20 μm.

5.8. *In vitro* cytotoxicity of DOX-loaded micelles

The efficiency of inhibition of cell proliferation of DOX-loaded micelles against tumor cells was evaluated. MTT colorimetric assay was used to evaluate the cytotoxicity of DOX-free (or blank) and DOX-loaded PEO-b-PHMssEt based micelles against HeLa cells. First, blank PEO-b-PHMssEt micelles exhibited > 80% viability of HeLa cells after 48 hrs incubation with micelles, suggesting non-toxicity of PEO-b-PHMssEt micelles to cells up to 510 μg mL^{-1}. Next, the cytotoxicity of DOX-loaded micelles upon their GSH-responsive degradation was examined. Here, HeLa cells were incubated with various amounts of DOX-loaded micelles for 48 hrs. For comparison, cells were also incubated with free DOX. As seen in Figure 5.10, the viability decreased with an increasing amount of both free and encapsulated DOX, suggesting inhibition of cell proliferation in the presence of DOX. The viability in the presence of DOX-loaded micelles was lower, compared to blank micelles; this could be due to the presence of GSH found in HeLa cancer cells that can trigger the degradation of DOX-loaded micelles. This result suggests

the release of DOX from DOX-loaded micelles triggered by intracellular GSH, thus enhancing the inhibition of the cellular proliferation after internalization.

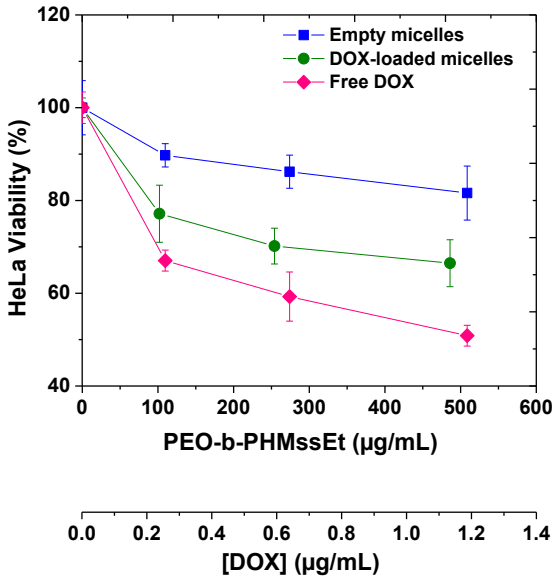

Figure 5.10. Viability of HeLa cells incubated with different amounts of empty micelles, DOX-loaded micelles, and free DOX for 48 hrs. Data are presented as average ± standard deviation (n = 12).

5.9. Conclusions

New redox-responsive PEO-b-PHMssEt ABPs having pendant disulfide linkages were synthesized and self-assembled to form micellar aggregates in aqueous solution at concentration of above CMC of 49 µg mL^{-1}. These micelles consist of hydrophobic PHMssEt core surrounded with hydrophilic PEO coronas. In the presence of cellular GSH, pendant disulfide linkages in micellar cores were rapidly cleaved, causing the destabilization of micelles, confirmed by DLS and UV/Vis spectroscopy measurements. The results of flow cytometry, CLSM and cell viability demonstrated intracellular release of anticancer drugs to inhibit the cellular proliferation after internalization into HeLa

cells. These results suggest that GSH-responsive PEO-b-PHMssEt micelles hold great promise as intracellular nanocarriers exhibiting the enhanced release of encapsulated anticancer drugs through biodegradation in response to cellular GSH.

Chapter 6

Conclusion and Future Works

Stimuli-responsive degradable block copolymer micelles are able to provide significant advantages for multifunctional drug delivery. These advantageous include enhanced release of encapsulated biomolecules as well as changes in morphologies of micellar nanocarriers. Advanced techniques such as control radical polymerization (CRP) allow for the synthesis of ABPs with chemical flexibility which may be engineered to incorporate stimuli-responsive degradable moieties. Examples of degradable linkages include acid-labile and disulfides bonds. These degradable covalent linkages make nanocarriers capable of undergoing changes in one or more physical properties in response to external triggers; thereby, triggering the programmed release of encapsulated biomolecules, particularly anticancer therapeutics. The objective of my master research was to explore stimuli-responsive degradation by designing new types of amphiphilic block copolymers. The obtained results contributed to a better understanding of the structure-property relationship between morphological variance and stimuli-responsive degradation. In this thesis, three different types of stimuli-responsive degradable micelles were developed exhibiting pH or thiol-responsive degradation through atom transfer radical polymerization (ATRP).

First, well-defined OH-terminated HO-POEOMA-b-PtBMA block copolymers were synthesized by consecutive ATRP of oligo(ethylene oxide) monomethyl ether methacrylate (OEOMA) and t-butyl methacrylate (tBMA) in the presence of a HO-

terminated alkyl halide initiator. ^{1}H-NMR and GPC results suggest that polymerizations preceded in a living fashion, yielding both HO-MI and HO-ABP with monomodal and narrow molecular weight distributions as low as $M_w/M_n < 1.25$. Self-assembly of these ABPs was first studied in aqueous solution using DLS and TEM. The encapsulation of small molecules within the hydrophobic micellar core of these micelles was investigated by loading the micelles with Nile Red (NR), and up to 1.1 wt% loading within micelles was observed. Hydrolytic cleavage of t-butyl group of PtBMA resulted in doubly hydrophilic HO-POEOMA-b-PMAA block copolymers. In acidic pH, HO-ABP micelles were gradually destabilized to form large aggregates. To demonstrate bioconjugation, the terminal OH groups were functionalized with biotin through a facile carbodiimide coupling reaction. These preliminary studies were encouraging, however, more work is required in order to increase HO-ABPs' sensitivity to acidic environment. In addition, by varying the nature of the pendant group, micelle destabilization kinetics can be tuned to occur at a more rapid rate and at a pH more representative of a cancer tissue's environment.

As detailed in chapter 4, a novel type of amphiphilic mono-cleavable triblock copolymer having single disulfide linkages in the hydrophobic main chains was synthesized and utilized to study redox-responsiveness of micelle in the presence of reducing agents. The mono-cleavable copolymer consisted of hydrophobic poly(oligo(propylene oxide) monononylphenyl ether acrylate (PAP) and hydrophilic POEOMA, thus attaining amphiphilicity and having a bush-like structure. Consecutive (activator generated by electron transfer) AGET ATRP of OEOMA in the presence of ss-$(PAP\text{-}Br)_2$ macroinitiators yielded well-defined ss-ABP_2 triblock copolymers, as

confirmed by GPC and ^{1}H-NMR. Formation of micellar aggregates in aqueous solution was studied by tensiometry and DLS. Their thiol-responsive degradation by cleavage of disulfide linkages in their micelle cores led to the change in morphologies to smaller aggregate structures, which was confirmed by DLS and AFM measurements. As the results presented in chapter 4 were merely preliminary, more work still needs to be done on the current system in order to utilize its potential as controlled delivery vehicles.

Another class of thiol-responsive degradable micelles, which consisted of block copolymers with disulfide linkages in side chains (pendant multi-cleavable micelles), was presented in chapter 5. Well-controlled PEO-b-PHMssEt ABPs was previously synthesized in our group. Self-assembly of PEO-b-PHMssEt to form micellar aggregates in aqueous solution was confirmed by DLS. Further investigation by TEM revealed the formation of spherical micelles. The encapsulation of anticancer drug within the hydrophobic micellar core of micelles was investigated by loading the micelles with doxorubicin, and up to 0.8% loading within the micelles was observed. The loading level is a modest, yet encouraging level of encapsulation. The micelles were designed to exhibit reduction-responsive degradation properties; consequently, pendant disulfide linkages in micellar cores were cleaved in the presence of GSH, resulting in degradation or destabilization of micellar nanocarriers. Such degradation led to the enhanced release of encapsulated anticancer drugs in aqueous solutions, which was monitored by DLS and UV absorbance measurements. *In vitro* release of doxorubicin to HeLa cellular environments was also performed. The efficiency of therapeutic release, was analyzed using MTT-based cell viability measurements. Intracellular release of anticancer drugs after internalization into HeLa cancer cells was evidenced by flow cytometry and CLSM.

Although these results suggest that PEO-b-PHMssEt micelles hold great promise as intracellular nanocarriers, more work needs to be done in order to develop the the medicinal value of these GSH-responsive micelles. Therefore, PEO-b-PHMssEt structure may be tailored and better-optimized to suit its desired application. Additionally, one possibility would be to conjugate drugs through a cleavable site to the hydrophobic core. This would enhance drug loading efficiency and prevent premature drug release.

Future work with these stimuli-responsive degradable micelles also should involve the testing of their stability over time in biological conditions. The ability of the proposed nanosized polymeric micelles to accumulate in tumor cells primilarily relied upon the enhanced permeability and retention (EPR) effect for passive targeting of tumors. By introducing active targeting moieties, particularly through the attachment of a cancer cell selective targeting moiety to their surface, the activity of these nanoparticles could be further enhanced. The epidermal growth factor receptor (EGFR) is one target that is commonly used for active targeting. EGa1 is a small antibody with specific binding to the EGFR receptor.[115] Hence, it would be encouraging to see the development of PEO-b-PHMssEt functionalized with EGa1 in order to improve their therapeutic efficacy. Also, it would be extremely beneficial to develop multifunctional amphiphilic block copolymers for many purposes such as drug delivery and diagnostics with the ability to respond to several stimuli. Such a system could find far-reaching applications in medicine by taking advantage of the unique properties of these polymers. Regardless of the many advances, many challenges and opportunities remain for making an impact in the field of smart polymers. While new stimuli-responsive degradable polymeric micelles are continually being developed and the ability to prepare complex

macromolecules architectures is growing, many underused stimuli will take on greater roles in the next generation of smart polymeric nanomaterials.

Appendix A

Experimental Section of Chapter 3

A.1. Materials

Ethylene glycol (EG), 2-bromoisobutyric acid (Br-iBuA), N,N′-dicyclohexyl carbodiimide (DCC), N,N-dimethylaminopyridine (DMAP), N-(3-dimethylaminopropyl)-N′-ethylcarbodiimide hydrochloride (EDC), N,N,N′,N″,N″-pentamethyldiethylenetriamine (PMDETA, >98%), 2,2′-bipyridyl (bpy), copper(I) bromide (CuBr, >99.99%), copper(I) chloride (CuCl, >99.99%), trifluoroacetic acid (CF_3COOH), avidin from egg white, biotin (>99%, lyophilized powder), 2-(4-hydroxyphenylazo)-benzoic acid (HABA), and potassium hydrogen phthalate (KHP) were used as received from Aldrich. For cell viability assay, Dulbecco's modified eagle medium (DMEM, 100 μL) and fetal bovine serum (FBS) were used as received from Wisent and 3-(4,5-dimethylthiazol-2-yl)-2,5-diphenyltetrazolium bromide (MTT, a yellow tetrazole) was used as received from Promega. OEOMA with MW = 300 g mol^{-1} and pendant ethylene oxide (EO) units ≈ 5 and tBMA from Aldrich were purified by passing it through a column filled with basic alumina to remove inhibitors.

A.2. Synthesis and purification of 2-hydroxyethyl-2′-bromoisobutyrate (OH-iBuBr)

The 2-Hydroxyethyl-2′-bromoisobutyrate (OH-iBuBr) was synthesized as described elsewhere.[92] Briefly, Br-iBuA (11.4 g, 68.7 mmol) was mixed with EG (6.4

g, 103.1 mmol, 1.5 equivalents to hydroxyl groups) in the presence of DCC (15.1 g, 72.7 mmol) and a catalytic amount of DMAP (0.7 g) in THF (250 mL) at room temperature overnight. After the removal of dicyclohexyl urea formed as a by-product, the product was collected as the third of the total four bands off a silica gel column by column chromatography using 1/4 to 2/3 v/v mixture of diethyl ether/hexane. Yield = 5.6 g (54.7%). R_f = 0.3 on silica (1/4 diethyl ether/hexane). ^{1}H-NMR ($CDCl_3$, ppm): 1.92 (s, 6H, -C(CH_3)$_2$Br), 3.82 (t, 2H, -CH_2OH), 4.28 (t, 2H,-OCH_2CH_2OH). ^{13}C-NMR ($CDCl_3$, ppm) 30.7, 55.8, 60.8, 67.4, 171.9.

A.3. Synthesis of HO-POEOMA-Br macroinitiator (HO-MI)

A series of ATRP of OEOMA was conducted in the presence of HO-iBuBr under various conditions. Here is an example of the detailed procedure for HO-MI with $[OEOMA]_0/[OH\text{-}iBuBr]_0/[CuBr]_0/[bpy]_0$ = 50/1/0.5/1; OH-iBuBr (0.42 g, 2.0 mmol), OEOMA (30.0 g, 100.0 mmol), bpy (0.32 g, 2.0 mmol), acetone (25 mL), and anisole (0.3 mL) were added to a 100 mL Schlenk flask. The mixture was degassed by three freeze-thaw cycles to remove any dissolved oxygen. The flask was filled with nitrogen and then CuBr (0.14 g, 1.0 mmol) was added to the frozen content. The flask was immediately degassed by vacuum and then was sealed under nitrogen. The mixture was allowed to melt and the schlenk flask was immersed in an oil bath preheated to 47 °C to start the polymerization. Aliquots were withdrawn at different time intervals during the polymerization to monitor conversion by ^{1}H-NMR and molecular weight by GPC. The polymerization was stopped by exposing the reaction mixture to air. In order to remove residual copper species and unreacted monomers, the viscous polymer solutions of HO-POEOMA-Br in acetone were precipitated (twice) into hexane (300 mL). To remove

copper species, the precipitate was then dissolved in THF and passed through a column filled with basic aluminum oxide. The polymer was isolated by evaporation of solvent via rotary evaporation and residual solvents were further dried in a vacuum oven at 50 °C overnight.

A.4. Synthesis of HO-POEOMA-b-PtBMA (HO-ABP) block copolymer

The detailed procedure for HO-ABP with $[tBMA]_0/[HO\text{-}POEOMA\text{-}Br]_0/[CuBr]_0/[bpy]_0$ = 200/1/0.5/1 is described as follows; purified, dried HO-POEOMA-Br (1.9 g, 0.49 mmol), tBMA (14 g, 98.4 mmol), bpy (76.9 mg, 0.49 mmol), and acetone (14 mL) were added to a 50 mL Schlenk flask. The mixture was degassed by three freeze-thaw cycles to remove any dissolved oxygen. The flask was filled with nitrogen and then CuBr (35.3 mg, 0.25 mmol) was added to the frozen content. The flask was closed, evacuated with vacuum and backfilled with nitrogen once. The mixture was thawed and the flask was then immersed in an oil bath preheated to 47 °C to start the polymerization. The polymerization was stopped at 5 hrs by exposing the reaction mixture to air. The resulting HO-ABP was purified as described above.

A.5. Aqueous micellization by solvent evaporation

Dried HO-ABP (10 mg) was dissolved in THF (2 mL), and then distilled water was added drop-wise into copolymer mixture. The resulting dispersion was stirred for >12 hrs to remove THF, yielding colloidally stable micellar dispersions at 0.5 mg mL^{-1} concentrations.

A.6. Determination of CMC using a NR probe

Fluorescence measurements were performed with Nile Red (NR) to determine the CMC. Different dilutions were prepared from a stock solution of NR in THF at 5.0 mg mL^{-1} and a stock solution of HO-ABP in THF at 1.0 mg mL^{-1} to obtain a series of NR-loaded micelles at various concentrations of HO-ABP ranging from 10^{-4} to 0.1 mg mL^{-1}. Water (12 mL) was drop-wise added into mixtures consisting of the same amount of the stock solution of NR (20 μL, 0.1 mg NR) and various amounts of the stock solution of HO-ABP. The resulting dispersions were stirred for 12 hrs to remove THF, and then were subjected to filtration using 0.45 μm Polyethersulfone (PES) filters to remove excess NR. Their fluorescence spectra were recorded with λ_{ex} = 480 nm and the fluorescence intensity was recorded at maximum λ_{em} = 620 nm.

A.7. Hydrolytic cleavage of t-butyl groups of PtBMA blocks in acidic conditions

PtBMA blocks in HO-ABP were hydrolyzed in the presence of CF_3COOH in dichloromethane (CH_2Cl_2) at room temperature. Typically, HO-ABP (100 mg, 0.5 μmol COOH) dissolved in CH_2Cl_2 (1.6 mL) was mixed with CF_3COOH (321.6 μL, 4.3 mmol) under stirring for 15 hrs. The degraded product was precipitated from hexane (10 mL). The white solids were isolated and further dried in a vacuum oven at 50 °C overnight.

A.8. pH-responsive destabilization of HO-ABP micelles at low pH

Using the same procedure described before, micellar dispersion was prepared at 5 mg mL^{-1}. Three aliquots were taken from micellar dispersion. Using KHP buffer solution at pH = 3, pH of two aliquots were adjusted to 5 and 3.2. pH of another aliquots

was adjusted to pH = 7 and used as a control sample. Then their size and size distribution was characterized by DLS.

A.9. Loading of NR into HO-ABP micelles

Purified HO-ABP (50 mg) was dissolved in a stock solution of NR in THF (5 mg mL^{-1}, 1 mL). Then water (100 mL) was added drop-wise into the solution. The THF and part of water were evaporated by stirring the resulting mixture overnight to reach the final concentration of NR-loaded micelles at 0.5 mg mL^{-1}. Then the solution was subjected to centrifugation (8,000 rpm × 15 min × 4 °C) to precipitate non-dissolved NR. The supernatant was further filtered using a 0.25 μm PES filter to remove residual NR. In order to determine the loading level of NR in micelles, an aliquot of NR-loaded micellar dispersion (30 mL) was taken and water was removed by a rotary evaporation. The remaining residues were further dried in a vacuum oven at 50 °C for 2 hrs, and then dissolved in THF (10 mL). The UV/Vis spectrum was recorded to measure the absorbance at a maximum λ_{abs} = 527 nm. Similar procedure was repeated three times with freshly-prepared NR-loaded micelles to obtain reproducible data.

A loading level of NR (%) was determined by the weight ratio of NR encapsulated in micelles to dried polymers. A loading efficiency (L.E., %) was calculated by the weight ratio of NR encapsulated in micelles to NR initially added.

A.10. Bioconjugation of HO-ABP with biotin

To the dried HO-ABP (80 mg, 8×10^{-3} mol), was added biotin (1.9 mg, 8×10^{-3} mmol), EDC (1.5 mg, 8×10^{-3} mmol) and DMF (3 mL). The mixture was allowed to stir for 48 hrs at the room temperature and was then dialyzed against aqueous $NaHCO_3$

solution for 3 days to remove free biotins. Rotary evaporation of the solution gave a white solid of biotinylated ABP for characterization.

A.11. Avidin-HABA binding assay studies

The availability of biotin on micelle was determined by Avidin-HABA assay. First, polymeric micelles were prepared as follow. The dried biotinylated ABP (200 mg) was dissolved in THF (2.5 mL) and added drop-wise into deionized water (41 mL). The resulting dispersion was kept under stirring overnight to remove THF, yielding an aqueous dispersion of micelles of biotinylated ABP at 5.0 mg mL^{-1} concentration. Avidin-HABA complex solution was prepared as follows; HABA (5.0 mg) was dissolved in water (8 ml) and undissolved species were removed using a 0.2 μm PES filter. Avidin (5.0 mg) was added to an aliquot of the HABA solution (5 ml). The resulting Avidin-HABA solution was equilibrated at room temperature for 2 hrs. For control experiment, in a 3 mL cuvette, 1.0 g of Avidin-HABA solution was pipetted, and mixed with 1.0 g of water, then the absorbance was measured at λ_{abs} = 500 nm ($A_{500}^{\text{Avidin-HABA}}$) by UV/Vis spectrophotometer. In another cuvette 1.0 g of Avidin-HABA solution was added and mixed with 1.0 g of sample (biotinylated micellar solution), the absorbance was recorded at λ_{abs} = 500 nm ($A_{500}^{\text{Avidin-HABA+sample}}$). The amount of the available biotin was calculated by the following formula[98]: μmol biotin/mL = $(\Delta A_{500}/34) \times 10$.

A.12. MTT cell viability assay

HEK293T and HeLa cells were plated at 5×10^5 cells/well into a 96-well plate and incubated for 24 hrs in DMEM (100 μL) containing 10% FBS. They were then treated with various amounts of HO-ABP micelles for another 48 hrs. Blank control

without micelles was run simultaneously. Cell viability was measured using CellTiter 96 Non-Radioactive Cell Proliferation Assay kit (MTT, Promega) according to manufacturer's instruction. Briefly, a solution of MTT supplied by Promega (20 μL) was added into each well, and then cell media were carefully removed after 4 hrs. Stop solution (100 μL) was added into each well in order to dissolve MTT crystals, and then the absorbance was recorded at λ = 570 nm using Powerwave HT Microplate Reader (Bio-Tek). Each concentration was 12-replicated. Cell viability was calculated as the percent ratio of absorbance of mixtures with micelles to control.

A.13. Supporting figures

Figure A.1. For HO-MI-3, kinetic plot (a) and evolution of molecular weight and molecular weight distribution over conversion (b) for ATRP of OEOMA in acetone at 47 °C under $[OEOMA]_0/[HO\text{-}iBuBr]_0/[CuBr]_0/[bpy]_0$ = 50/1/0.5/1; OEOMA/acetone = 1.5/1 wt/wt. The dotted lines in (a) are linear fits, and the straight lines in (b) are the theoretically predicted molecular weight over conversion.

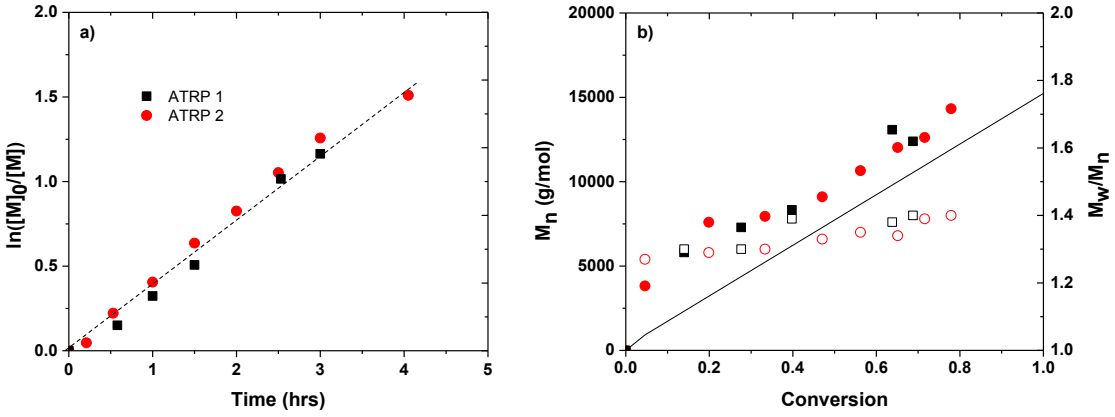

Figure A.2. UV spectra of different concentrations of NR in THF to determine its extinction coefficient at λ_{max} = 527 nm.

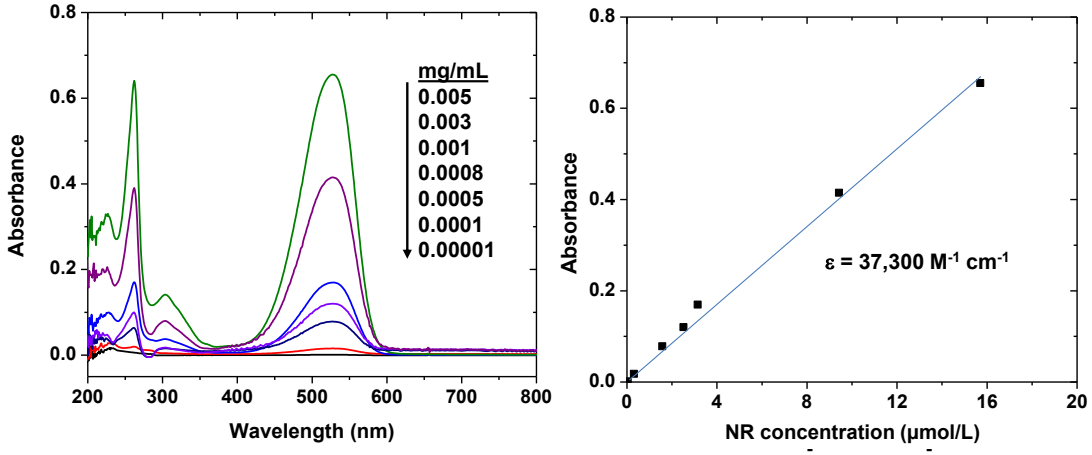

Figure A.3. An example of UV spectra of HO-ABP and NR-loaded HO-ABP micelles dissolved in THF.

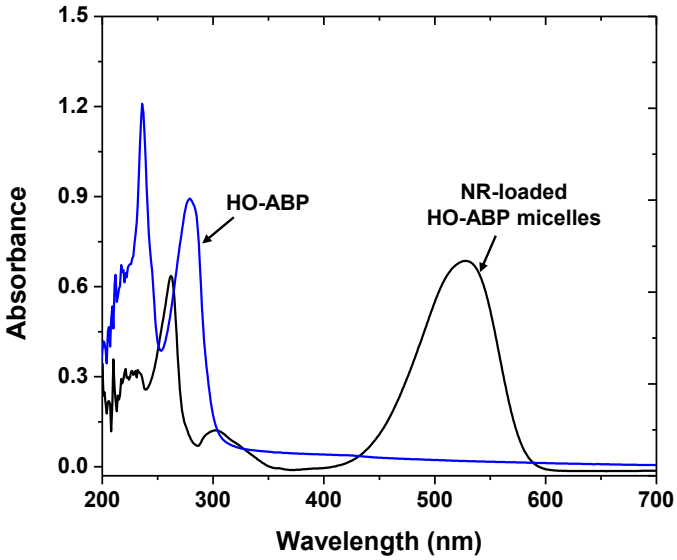

Figure A.4. DLS diagram of an example of NR-loaded HO-ABP micelles in water.

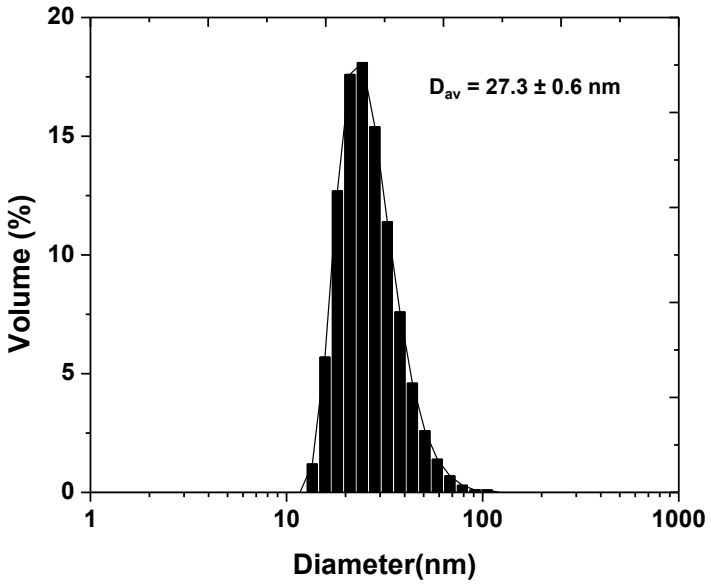

Appendix B

Experimental Section of Chapter 4

B.1. Materials

2-Hydroxyethyl disulfide, 2-bromoisoburylic acid, N,N′-dicyclohexyl carbodiimide (DCC), 4-dimethylaminopyridine (DMAP) as a catalyst, *N*,*N*,*N*′,*N*″,*N*″-pentamethyldiethylenetriamine (PMDETA, >98%), copper (II) chloride ($CuCl_2$, >99.99%), tin (II) 2-ethylhexanonate ($Sn(Oct)_2$, >95%), tributyl phosphine (Bu_3P, 97%), and anisole from Aldrich were used as received. copper(II) bromide ($CuBr_2$, >99.99%) and D_L-dithioerythritol (DTT, 99%) was purchased from Acros Organics. Oligo(propylene oxide) monononylphenyl ether acrylate (AP) with MW = 419 g mol^{-1} and pendent PO units DP ≈ 3 and oligo(ethylene oxide) monomethyl ether methacrylate (OEOMA) with MW = 300 g mol^{-1} and pendent EO units DP ≈ 5 from Aldrich were purified by passing them through a column filled with basic alumina to remove inhibitors. Spectra/Por dialysis tubing (MWCO = 3,500 g mol^{-1}) was purchased from SpectrumLab.

B.2. Synthesis of bis[2-(2-bromoisobutyryloxy)ethyl] disulfide (SS-DBr)

2-bromoisoburylic acid (12.0 g, 71.9 mmol) dissolved in tetrahydrofuran (THF, 50 mL) was drop-wise added to a solution of 2-hydroxyethyl disulfide (5.0 g, 32.5 mmol), DCC (14.7 g, 71.2 mmol), a catalytic amount of DMAP, and THF (130 mL) at 0 °C over 20 min. The resulting solution was stirred at room temperature for overnight. White solids (dicyclohexyl urea) formed during the reaction were removed by a vacuum

filtration. The solvent was then removed by a rotary evaporation. For further purification, the product was dissolved in hexane and undissolved dicyclohexyl urea (DCU) was removed by vacuum filtration. The pure product was isolated by removal of hexane and further dried in vacuum oven at 50 °C overnight to form oily residue. ^{1}H-NMR ($CDCl_3$, ppm) 4.5 (t, 4H, -CH_2O(O)C-), 3.0 (t, 4H, -CH_2-SS-),1.9 (s, 6H, Br-C(CH_3)$_2$).

B.3. Synthesis of ss-(PAP-Br)$_2$ macroinitiators

A series of ATRP of AP was conducted in the presence of SS-DBr difunctional initiator. The typical procedure for the preparation of ss-(PAP-Br)$_2$ is as follows; SS-DBr (40.0 mg, 0.14 mmol), AP (5.8 g, 13.8 mmol), PMDETA (57.8 mL, 0.28 mmol), CuBr2 (61.8 mg, 0.28 mmol), and acetone (4.9 mL) were added to a 25 mL Schlenk flask. The resulting transparent solution was deoxygenated by purging with nitrogen for 30 min at room temperature. The flask was immersed in an oil bath preheated to 80 °C. A nitrogen-purged solution of Sn(Oct)$_2$ (291.4 mg, 0.72 mmol) in anisole (0.5 mL) was added to start the polymerization. Aliquots were removed at different time intervals during the polymerization to measure conversion by ^{1}H-NMR and molecular weight using GPC. The polymerization was stopped by exposing the catalyst to air.

B.4. Synthesis of ss-ABP$_2$ triblock copolymers

Dried, purified ss-(PAP-Br)$_2$ ($M_{n,theo}$ = 10,000 g mol^{-1}, 0.5 g, 0.05 mmol), OEOMA (1.5 g, 5.0 mmol), PMDETA (20.9 mL, 0.10 mmol), $CuCl_2$ (13.4 mg, 0.10 mmol), and anisole (1.3 mL) were added to a 25 mL Schlenk flask. The resulting transparent solution was deoxygenated by purging with nitrogen for 30 min at room temperature. The flask was immersed in an oil bath preheated to 80 °C. A nitrogen-

purged solution of $Sn(Oct)_2$ (105 mg, 0.26 mmol) in anisole (0.3 mL) was added to start the polymerization. Aliquots were removed at different time intervals during the polymerization to measure conversion and molecular weight using GPC. The polymerization was stopped by exposing the catalyst to air. For purification of ss-ABP_2, anisole was removed from reaction mixture by rotary evaporation. The residues were dissolved in THF and dialyzed using a dialysis tubing with MWCO = 3,500 g mol^{-1} (SpectrumLab) over a mixture of MeOH/water (5/5 v/v) to remove unreacted OEOMA. The GPC trace suggests that < 5% unreacted OEOMA remained in the purified ss-ABP_2.

B.5. Aqueous micellization by solvent evaporation

An aliquot of the purified, dried ss-ABP_2 (92 mg) was dissolved in THF (2.6 mL). The clear polymer solution (0.30 mL) was drop-wise added into deionized water (10 mL). The resulting dispersion was kept under stirring overnight to remove THF, yielding colloidally stable micellar dispersions at 1mg mL^{-1} concentration.

B.6. Determination of CMC of ss-ABP_2 in water by tensiometry

An aliquot of the purified, dried ss-ABP_2 (20 mg) was dissolved in THF (1.0 mL). The clear polymer solution was drop-wise added into deionized water (20 mL). The resulting dispersion was kept under stirring overnight to remove THF, allowing for colloidally stable micellar dispersion. The final concentration of the dispersion was calculated to be 1.4 mg mL^{-1}. Then, aliquots of the aqueous stock solution were diluted with different amounts of deionized water to form a series of aqueous solutions of ss-ABP_2 at different concentrations from 10^{-3} to 1.4 mg mL^{-1}. A tensiometry was used to measure the osmotic pressure (mN/m) of the solutions as follows; an aliquot of each

solution (600 μL) was carefully placed on each well and equilibrated before measurements. The tensiometer was calibrated using air and water.

B.7. Degradation of ss-ABP_2 triblock copolymers and micelles

An aliquot of purified, dried ss-ABP_2 (50 mg) was dissolved in THF (5 mL). To the mixture was added Bu_3P (0.85 mL) defined as the ratio of Bu_3P/disulfide = 1/1. The mixture was magnetically stirred and aliquots of the mixture were injected into GPC to determine molecular weight of degraded products.

For micellar dispersion, an aliquot of micellar dispersion at 2.3 mg mL^{-1} (100 mL) was diluted with water (2.0 mL). The amount of disulfide linkages in micelles can be calculated to be 18.1 nmol using $M_{n,theo}$ = 12,700 g mol^{-1} of ss-ABP_2. An aliquot of the micellar dispersion (1.0 mL) was mixed with an aqueous stock solution of DTT (0.5 mg mL^{-1}, 2.7 mL) defined as the ratio of DTT/disulfide = 1/1 under magnetic stirring. Aliquots were taken for atomic force microscopy.

B.8. Supporting figures

Figure B.1. ^{1}H-NMR spectra of SS-DBr after (a) and before (b) precipitation from hexane (purification).

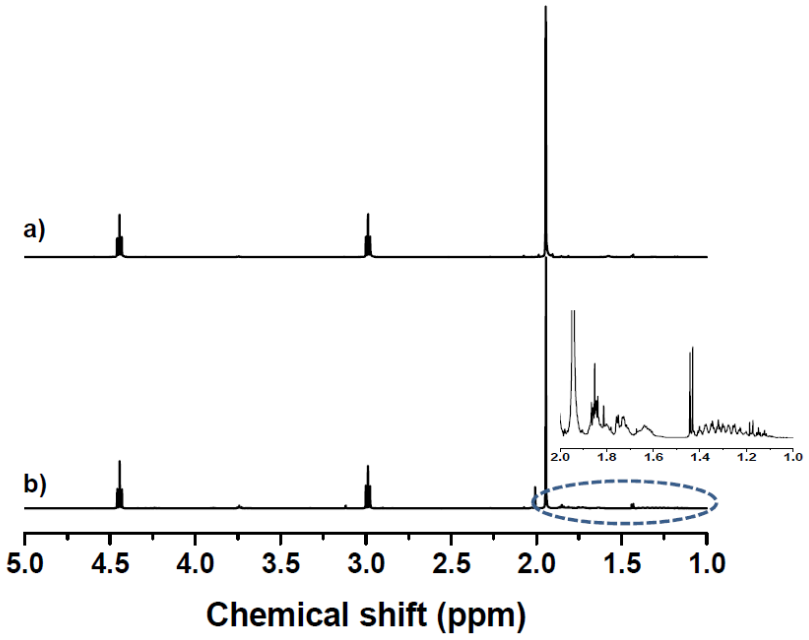

Appendix C

Experimental Section of Chapter 5

C.1. Materials

PEO-b-PHMssEt block copolymer was synthesized by Dr. Q. Zhang.[64] Doxorubicin hydrochloride (DOX.HCl, > 98%), L-glutathione (GSH) reduced form, triethylamine (Et_3N, > 99.5 %) and dimethylformamide (DMF) were purchased from Aldrich and used as received. Spectra/Por dialysis tubing (MWCO = 12,000 g mol^{-1}) was purchased from SpectrumLab. For cell viability assay, Dulbecco's modified eagle medium (DMEM) and fetal bovine serum (FBS) were used as received from Wisent and 3-(4,5-dimethylthiazol-2-yl)-2,5-diphenyltetrazolium bromide (MTT, a yellow tetrazolium) was used as received from Promega. 4',6-diamidino-2-phenylindole (DAPI) and mounting medium were used as received from Aldrich.

C.2. Aqueous micellization by dialysis method

Water (9 mL) was added drop-wise to a clear solution of PEO-b-PHMssEt (10 mg) dissolved in DMF (2 mL). The resulting mixture was stirred for 2 hrs, and then dialyzed in a dialysis tubing (MWCO = 12,000 g mol^{-1}) against water for 3 days to remove DMF. The outer water (500 mL) was changed twice a day, yielding colloidally-stable micellar aggregates in aqueous solution at 1 mg mL^{-1} concentration.

C.3. Preparation of DOX-loaded micelles

Similar procedure for aqueous micellization through the dialysis method was used. For the preparation of the sample of MDOX-1, water (5 mL) was added dropwise to the solution consisting of the purified, dried PEO-b-PHMssEt (20 mg), DOX (1 mg), and Et_3N (3 mol equivalent to DOX) in DMF (2 mL). The resulting dispersion was dialyzed over water (500 mL) for 5 days, yielding DOX-loaded micellar dispersion at 2.6 mg mL^{-1} concentration. For the MDOX-2 at 1.7 mg mL^{-1}, a similar procedure was used except for the use of increasing amounts of PEO-b-PHMssEt (20 mg), DOX (2 mg), DMF (3 mL), and water (10 mL).

C.4. Determination of loading level of DOX using UV/Vis spectroscopy

A calibration curve of absorbance (A) at λ_{max} = 480 nm over various concentrations of DOX in DMF was first constructed as follows. A stock solution of DOX in DMF (1 mg mL^{-1}, 1.7 mmol L^{-1}) was first prepared by dissolving DOX (1 mg, 1.7 μmol) in DMF (1 mL). Aliquots of the stock solution were then diluted with DMF to form a series of solutions of DOX ranging from 5.6 to19.5 μmol L^{-1}. Their UV/Vis spectra (λ_{ex} = 480 nm) were recorded. To determine the loading level of DOX in DOX-loaded micelles, aliquots of DOX-loaded micellar dispersion (1 mL) were taken. After the removal of water using a rotary evaporation, the residues of DOX and copolymers were dissolved in DMF (2 mL) to form clear solution. Their UV/Vis spectra were recorded and the loading level of DOX was calculated by the weight ratio of loaded DOX to dried polymers. The extinction coefficient of DOX in DMF was determined to be ε = 11,700 M^{-1} cm^{-1} at λ_{max} = 480 nm.

C.5. GSH-triggered destabilization of PEO-b-PHMssEt micelles

Aliquots of aqueous micellar dispersion (1 mg mL^{-1}, 10 mL) were mixed with GSH (30 mg, 97 μmol, 10 mM) under stirring. An aliquot was taken to analyze their size distributions using DLS.

C.6. GSH-triggered release of DOX from DOX-loaded micelles

Aliquots of DOX-loaded micellar dispersion (2.5 mg mL^{-1}, 3 mL) were transferred into a dialysis tubing (MWCO = 12,000 g mol^{-1}) and immersed in aqueous KH_2PO_4 buffer solution (50 mL, pH = 7.0) as a control and 10 mM aqueous GSH solution buffered with KH_2PO_4 at pH = 7.0 under stirring. The absorbance of DOX in outer water was recorded at an interval of 5 min using a UV/Vis spectrometer equipped with an external probe at λ = 497 nm. For quantitative analysis, DOX (20 μg) was dissolved in aqueous GSH solution buffered with KH_2PO_4 (10 mM, pH = 7.0). The UV/Vis spectrum of DOX in the solution was recorded and the absorbance at 497 nm was used for normalization.

C.7. Cell viability using MTT assay

HEK293T and HeLa cells were plated at 5×10^5 cells/well into a 96-well plate and incubated for 24 hrs in DMEM (100 μL) containing 10% FBS. They were then incubated with various concentrations of micellar dispersions of PEO-b-PHMssEt for 48 hrs. Blank controls without micelles (cells only) were run simultaneously. Cell viability was measured using CellTiter 96 Aqueous Non-Radioactive Cell Proliferation Assay kit (Promega) according to manufacturer's instruction. Briefly, 3-(4,5-dimethylthiazol-2-yl)-2,5-diphenyltetrazolium bromide (MTT) solutions (15 μL) was added into each well and

after 4 hrs incubation the medium containing unreacted MTT was carefully removed. The formed blue formazan crystals were dissolved in 100 μL per well stop solution, and the absorbance was measured at 570 nm using Powerwave HT Microplate Reader (Bio-Tek). Viability was calculated as the percent ratio of absorbance of mixtures with micelles to control (cells only).

C.8. Intracellular DOX release and HeLa cells viability

HeLa cells were plated at 1×10^5 cells/ well into a 96-well plate and incubated for 24 hrs in 100 μL complete medium. They were then incubated with different amounts of DOX-loaded micellar dispersion (2.8 mg mL^{-1}) for 48 hrs. Cells only without micelles were run simultaneously as blank controls. Viability was calculated as the percent ratio of absorbance of mixtures with micelles to control (cells only).

C.9. Cellular uptake using flow cytometry and Confocal laser scanning microscopy (CLSM)

C.9.1. Flow cytometry

Cells plated at 5×10^5 cells/well into a 6-well plate and incubated for 24 hrs in DMEM (2 mL) and then incubated with DOX-loaded micelles (200 μL for DOX = 1.9 μg mL^{-1}) at 37 ºC for 1 hr. After culture medium was removed, cells were washed with PBS buffer three times and then treated with trypsin. The cells were suspended in DMEM (300 μL) for flow cytometry measurements. Data analysis was performed by means of a BD FACSCANTO II flow cytometer and BD FACSDiva software.

C.9.2. Confocal laser scanning microscopy (CLSM)

HeLa cells plated at 2×10^5 cells/well into a 24-well plate and incubated for 24 hrs in DMEM (100 μL) and then incubated with DOX-loaded micelles (DOX = 5.1 μg mL^{-1}) at 37 ºC for 24 hrs. After culture medium was removed, cells were washed with PBS buffer three times. After the removal of supernatants, the cells were fixed with cold methanol (-20 ºC) for 20 min at 4 ºC. The slides were rinsed with TBST (tris-buffered saline tween-20) for three times. Cells were stained with 2-(4-amidinophenl)-6-indolecarbamidine (DAPI) for 5 min. The fluorescence images were obtained using a LSM 510 Meta/Axiovert 200 (Carl Zeiss, Jena, Germany).

C.10. Supporting figures

Figure C.1. Evolution of z-average diameter of PEO-b-PHMssEt micelles in aqueous 10 mM GSH solution over time.

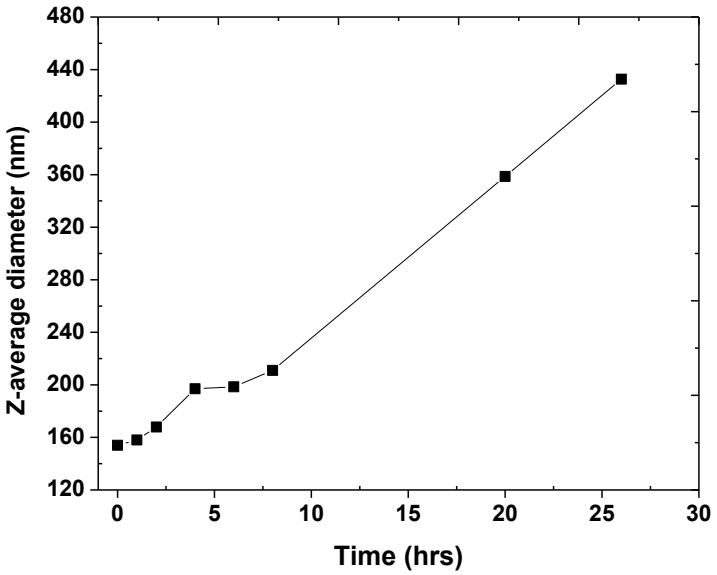

Figure C.2. UV absorbance at λ= 497 nm of free DOX in outer water during extensive dialysis.

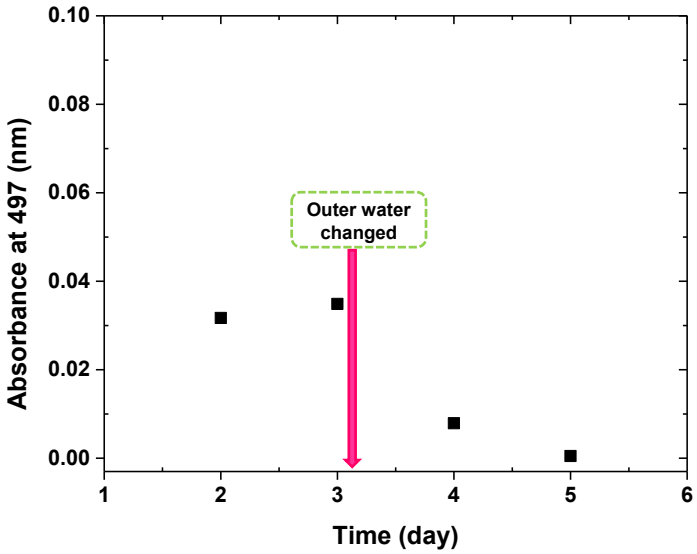

Figure C.3. Overlaid UV spectra (a) and absorbance at λ_{max} = 480 nm (b) of DOX at various concentrations (μmol L^{-1}) in DMF to construct a calibration curve.

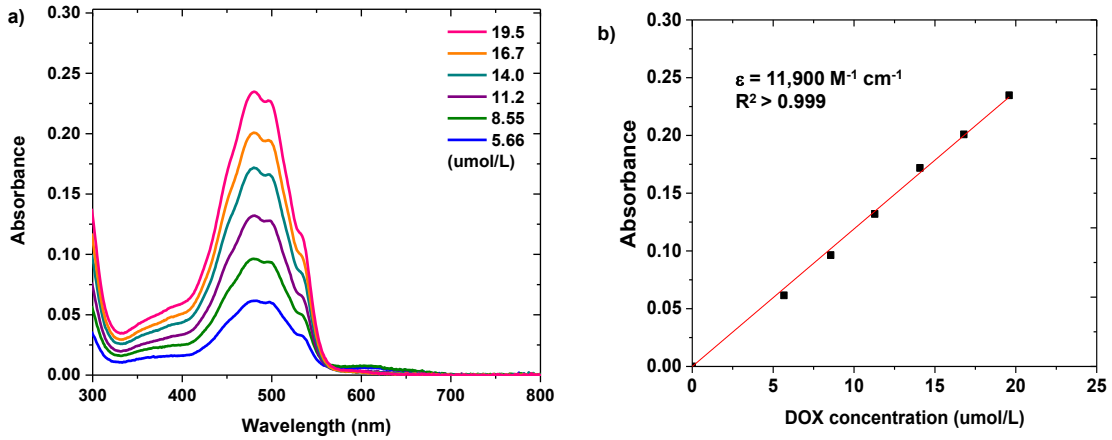

Figure C.4. Absorption (—) and emission (- - -) spectra of 0.01 mg mL–1 free DOX, and emission spectrum of 0.2 mg mL–1 micellar-encapsulated DOX (····), all in aqueous solution.[116]

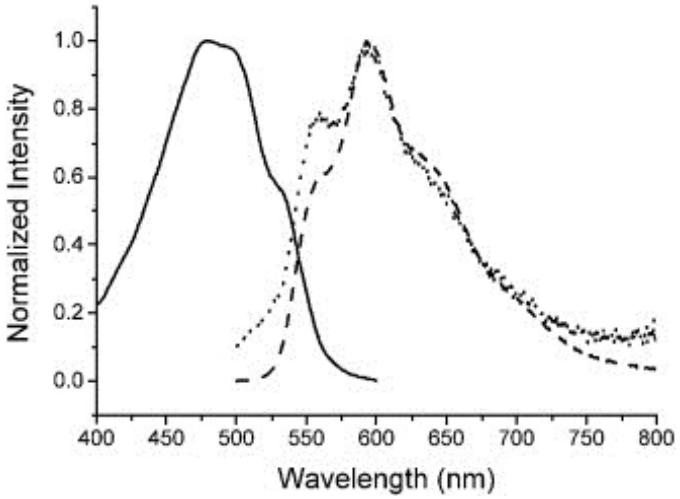

Figure C.5. Absorption spectra of MTT and commercially prepared MTT-formazan dissolved in DMSO. Also shown is the spectrum of MTT-formazan produced by incubation of L-DAN cells with MTT (5 mg ml-1) for 4 h.[82]

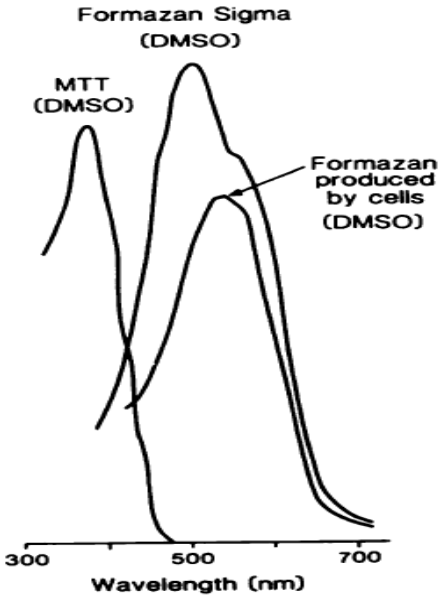

References

[1] R. Langer, *Science* **1990**, *249*, 1527-1533.
[2] A. K. Bajpai, S. K. Shukla, S. Bhanu, S. Kankane, *Progress in Polymer Science* **2008**, *33*, 1088-1118.
[3] T. Okano, 1 ed., Academic press, San Diego, **1998**, p. 257.
[4] M. M. Frank, L. F. Fries, *Immunology Today* **1991**, *12*, 322-326.
[5] H. M. Patel, *Critical Reviews in Therapeutic Drug Carrier Systems* **1992**, *9*, 39-90.
[6] D. E. Owens Iii, N. A. Peppas, *International Journal of Pharmaceutics* **2006**, *307*, 93-102.
[7] K. Strebhardt, A. Ullrich, *Nature Reviews Cancer* **2008**, *8*, 473-480.
[8] D. Peer, J. M. Karp, S. Hong, O. C. Farokhzad, R. Margalit, R. Langer, *Nat Nano* **2007**, *2*, 751-760.
[9] H. Maeda, J. Wu, T. Sawa, Y. Matsumura, K. Hori, *Journal of Controlled Release* **2000**, *65*, 271-284.
[10] F. Schué, *Polymer International* **2000**, *49*, 236-236.
[11] M. E. Fox, F. C. Szoka, J. M. J. Fréchet, *Accounts of Chemical Research* **2009**, *42*, 1141-1151.
[12] S. Zalipsky, *Bioconjugate Chemistry* **1995**, *6*, 150-165.
[13] Y. Cheng, Z. Xu, M. Ma, T. Xu, *Journal of Pharmaceutical Sciences* **2008**, *97*, 123-143.
[14] A. S. Hoffman, *Advanced Drug Delivery Reviews* **2012**, *64, Supplement*, 18-23.
[15] A. Blanazs, S. P. Armes, A. J. Ryan, *Macromolecular Rapid Communications* **2009**, *30*, 267-277.
[16] J. Khandare, T. Minko, *Progress in Polymer Science* **2006**, *31*, 359-397.
[17] Q. Zhang, N. Re Ko, J. Kwon Oh, *Chemical Communications* **2012**, *48*, 7542-7552.
[18] H. B. D. A. Tomalia, J. Dewald, M. Hall, G. Kallos, S. Martin, J. Roeck, J. Ryder and P. Smith, *Polym. J. (Tokyo)*, *17*, 117 - 132
[19] S. M. Grayson, M. Jayaraman, J. M. J. Frechet, *Chemical Communications* **1999**, *0*, 1329-1330.
[20] J. K. Oh, R. Drumright, D. J. Siegwart, K. Matyjaszewski, *Progress in Polymer Science* **2008**, *33*, 448-477.
[21] S. Aleksanian, B. Khorsand, R. Schmidt, J. K. Oh, *Polymer Chemistry* **2012**, *3*, 2138-2147.
[22] R. Obeid, C. Scholz, *Biomacromolecules* **2011**, *12*, 3797-3804.
[23] J. K. Oh, *Soft Matter* **2011**, *7*, 5096-5108.
[24] K. Letchford, H. Burt, *European Journal of Pharmaceutics and Biopharmaceutics* **2007**, *65*, 259-269.
[25] J. N. Israelachvili, *Intermolecular & Surface Forces*, 2nd ed., Academic Press, London, **1991**.
[26] S. I. Jeon, J. D. Andrade, *Journal of Colloid and Interface Science* **1991**, *142*, 159-166.
[27] L. A. Aliabadi Hamidreza Montazeri, *Expert Opinion on Drug Delivery* **2006**, *3*, 139-162.
[28] D. Sutton, N. Nasongkla, E. Blanco, J. Gao, *Pharmaceutical Research* **2007**, *24*, 1029-1046.
[29] K. Mondon, R. Gurny, M. ller, *CHIMIA International Journal for Chemistry* **2008**, *62*, 832-840.
[30] Z. Sezgin, N. Yüksel, T. Baykara, *European Journal of Pharmaceutics and Biopharmaceutics* **2006**, *64*, 261-268.

[31] M. L. Adams, A. Lavasanifar, G. S. Kwon, *Journal of Pharmaceutical Sciences* **2003**, *92*, 1343-1355.
[32] K. J. Holmberg, B.; Kronberg, B.; Lindman, B. , *Surfactants and Polymers in Aqueous Solution* Second Edition ed., John Wiley & Sons, Ltd, , **, 2003.**
.
[33] G. S. O. Kwon, T., *Advanced Drug Delivery Reviews* **1996**, *21*, 107.
[34] C. Allen, D. Maysinger, A. Eisenberg, *Colloids and Surfaces B: Biointerfaces* **1999**, *16*, 3-27.
[35] R. Nagarajan, K. Ganesh, *The Journal of Chemical Physics* **1989**, *90*, 5843-5856.
[36] E. Fleige, M. A. Quadir, R. Haag, *Advanced Drug Delivery Reviews* **2012**, *64*, 866-884.
[37] Z. Qian, A. Samuel, C. Alexander, O. Jung Kwon, in *Progress in Controlled Radical Polymerization: Materials and Applications, Vol. 1101*, American Chemical Society, **2012**, pp. 287-302.
[38] A. W. Jackson, D. A. Fulton, *Macromolecules* **2012**, *45*, 2699-2708.
[39] H. Fan, J. Huang, Y. Li, J. Yu, J. Chen, *Polymer* **2010**, *51*, 5107-5114.
[40] S. Li, C. Ye, G. Zhao, M. Zhang, Y. Zhao, *Journal of Polymer Science Part A: Polymer Chemistry* **2012**, *50*, 3135-3148.
[41] W. Gao, J. M. Chan, O. C. Farokhzad, *Molecular Pharmaceutics* **2010**, *7*, 1913-1920.
[42] F. Meng, Z. Zhong, J. Feijen, *Biomacromolecules* **2009**, *10*, 197-209.
[43] S. Sengupta, D. Eavarone, I. Capila, G. Zhao, N. Watson, T. Kiziltepe, R. Sasisekharan, *Nature* **2005**, *436*, 568-572.
[44] S. Aryal, C.-M. J. Hu, L. Zhang, *ACS Nano* **2009**, *4*, 251-258.
[45] H. Mok, J. W. Park, T. G. Park, *Bioconjugate Chemistry* **2008**, *19*, 797-801.
[46] A. P. Griset, J. Walpole, R. Liu, A. Gaffey, Y. L. Colson, M. W. Grinstaff, *Journal of the American Chemical Society* **2009**, *131*, 2469-2471.
[47] B. Wang, C. Xu, J. Xie, Z. Yang, S. Sun, *Journal of the American Chemical Society* **2008**, *130*, 14436-14437.
[48] Z. Xu, W. Gu, L. Chen, Y. Gao, Z. Zhang, Y. Li, *Biomacromolecules* **2008**, *9*, 3119-3126.
[49] E. R. Gillies, J. M. J. Frechet, *Chemical Communications* **2003**, *0*, 1640-1641.
[50] K. Ulbrich, V. r. Šubr, *Advanced Drug Delivery Reviews* **2004**, *56*, 1023-1050.
[51] W. Chen, F. Meng, F. Li, S.-J. Ji, Z. Zhong, *Biomacromolecules* **2009**, *10*, 1727-1735.
[52] E. R. Gillies, T. B. Jonsson, J. M. J. Fréchet, *Journal of the American Chemical Society* **2004**, *126*, 11936-11943.
[53] H. S. Yoo, E. A. Lee, T. G. Park, *Journal of Controlled Release* **2002**, *82*, 17-27.
[54] Y. Bae, S. Fukushima, A. Harada, K. Kataoka, *Angewandte Chemie International Edition* **2003**, *42*, 4640-4643.
[55] F. Meng, W. E. Hennink, Z. Zhong, *Biomaterials* **2009**, *30*, 2180-2198.
[56] F. Q. Schafer, G. R. Buettner, *Free Radical Biology and Medicine* **2001**, *30*, 1191-1212.
[57] G. Saito, J. A. Swanson, K.-D. Lee, *Advanced Drug Delivery Reviews* **2003**, *55*, 199-215.
[58] A. Russo, W. DeGraff, N. Friedman, J. B. Mitchell, *Cancer Research* **1986**, *46*, 2845-2848.
[59] H. Sun, B. Guo, R. Cheng, F. Meng, H. Liu, Z. Zhong, *Biomaterials* **2009**, *30*, 6358-6366.
[60] H. G. Sun, B.; Li, X.; Cheng, R.; Meng, F.; Liu, H.; Zhong, Z., *Biomacromolecules* **2010**, *11*, 848-854.
[61] L.-Y. Tang, Y.-C. Wang, Y. Li, J.-Z. Du, J. Wang, *Bioconjugate Chemistry* **2009**, *20*, 1095-1099.
[62] J. Liu, Y. Pang, W. Huang, Z. Zhu, X. Zhu, Y. Zhou, D. Yan, *Biomacromolecules* **2011**, *12*, 2407-2415.

[63] A. Nelson-Mendez, S. Aleksanian, M. Oh, H.-S. Lim, J. K. Oh, *Soft Matter* **2011**, *7*, 7441-7452.
[64] Q. Zhang, S. Aleksanian, S. M. Noh, J. K. Oh, *Polymer Chemistry* **2013**, *4*, 351-359.
[65] M. Szwarc, M. Levy, R. Milkovich, *Journal of the American Chemical Society* **1956**, *78*, 2656-2657.
[66] M. Szwarc, *Nature* **1956**, *178*, 1168-1169.
[67] C. J. Hawker, A. W. Bosman, E. Harth, *Chemical Reviews* **2001**, *101*, 3661-3688.
[68] J.-S. Wang, K. Matyjaszewski, *Journal of the American Chemical Society* **1995**, *117*, 5614-5615.
[69] A. B. Lowe, C. L. McCormick, *Progress in Polymer Science* **2007**, *32*, 283-351.
[70] M. Kato, M. Kamigaito, M. Sawamoto, T. Higashimura, *Macromolecules* **1995**, *28*, 1721-1723.
[71] W. Jakubowski, K. Matyjaszewski, *Macromolecules* **2005**, *38*, 4139-4146.
[72] I. F. Uchegbu, in *Polymers in Drug Delivery*, CRC Press, **2006**.
[73] N. Rapoport, *Progress in Polymer Science* **2007**, *32*, 962-990.
[74] P. Goon, C. Manohar, V. V. Kumar, *Journal of Colloid and Interface Science* **1987**, *119*, 177-180.
[75] I. Astafieva, X. F. Zhong, A. Eisenberg, *Macromolecules* **1993**, *26*, 7339-7352.
[76] J. Jiang, X. Tong, D. Morris, Y. Zhao, *Macromolecules* **2006**, *39*, 4633-4640.
[77] M. Stoddart, in *Mammalian Cell Viability, Vol. 740* (Ed.: M. J. Stoddart), Humana Press, **2011**, pp. 1-6.
[78] S. A. Altman, L. Randers, G. Rao, *Biotechnology Progress* **1993**, *9*, 671-674.
[79] R. Supino, in *In Vitro Toxicity Testing Protocols, Vol. 43* (Eds.: S. O'Hare, C. Atterwill), Humana Press, **1995**, pp. 137-149.
[80] T. Mosmann, *Journal of Immunological Methods* **1983**, *65*, 55-63.
[81] J. Carmichael, W. G. DeGraff, A. F. Gazdar, J. D. Minna, J. B. Mitchell, *Cancer Research* **1987**, *47*, 936-942.
[82] J. A. Plumb, R. Milroy, S. B. Kaye, *Cancer Research* **1989**, *49*, 4435-4440.
[83] N. G. Papadopoulos, G. V. Z. Dedoussis, G. Spanakos, A. D. Gritzapis, C. N. Baxevanis, M. Papamichail, *Journal of Immunological Methods* **1994**, *177*, 101-111.
[84] P. Decherchi, P. Cochard, P. Gauthier, *Journal of Neuroscience Methods* **1997**, *71*, 205-213.
[85] K. Engin, D. B. Leeper, J. R. Cater, A. J. Thistlethwaite, L. Tupchong, J. D. McFarlane, *International Journal of Hyperthermia* **1995**, *11*, 211-216.
[86] T. J. Martin, K. Procházka, P. Munk, S. E. Webber, *Macromolecules* **1996**, *29*, 6071-6073.
[87] S.-i. Yusa, Y. Shimada, Y. Mitsukami, T. Yamamoto, Y. Morishima, *Macromolecules* **2003**, *36*, 4208-4215.
[88] X. Huang, F. Du, J. Cheng, Y. Dong, D. Liang, S. Ji, S.-S. Lin, Z. Li, *Macromolecules* **2009**, *42*, 783-790.
[89] X. Huang, F. Du, R. Ju, Z. Li, *Macromolecular Rapid Communications* **2007**, *28*, 597-603.
[90] L. Brannon-Peppas, *Journal of Controlled Release* **2000**, *66*, 321.
[91] B. Khorsand, J. K. Oh, *Journal of Polymer Science Part A: Polymer Chemistry* **2013**, *51*, 1620-1629.
[92] T. Sarbu, K.-Y. Lin, J. Spanswick, R. R. Gil, D. J. Siegwart, K. Matyjaszewski, *Macromolecules* **2004**, *37*, 9694-9700.
[93] A. Lavasanifar, J. Samuel, G. S. Kwon, *Journal of Controlled Release* **2001**, *77*, 155-160.
[94] V. T. Huynh, P. de Souza, M. H. Stenzel, *Macromolecules* **2011**, *44*, 7888-7900.
[95] A. Rösler, G. W. M. Vandermeulen, H.-A. Klok, *Advanced Drug Delivery Reviews* **2001**, *53*, 95-108.

[96] R. Sinha, G. J. Kim, S. Nie, D. M. Shin, *Molecular Cancer Therapeutics* **2006**, *5*, 1909-1917.
[97] J. K. Oh, D. J. Siegwart, H.-i. Lee, G. Sherwood, L. Peteanu, J. O. Hollinger, K. Kataoka, K. Matyjaszewski, *Journal of the American Chemical Society* **2007**, *129*, 5939-5945.
[98] K. Qi, Q. Ma, E. E. Remsen, C. G. Clark, K. L. Wooley, *Journal of the American Chemical Society* **2004**, *126*, 6599-6607.
[99] aD. Han, X. Tong, Y. Zhao, *Langmuir* **2012**, *28*, 2327-2331; bY. Kim, M. H. Pourgholami, D. L. Morris, M. H. Stenzel, *Journal of Materials Chemistry* **2011**, *21*, 12777-12783.
[100] D. Han, X. Tong, Y. Zhao, *Macromolecules* **2011**, *44*, 437-439.
[101] aB. Khorsand Sourkohi, A. Cunningham, Q. Zhang, J. K. Oh, *Biomacromolecules* **2011**, *12*, 3819-3825; bT.-B. Ren, Y. Feng, Z.-H. Zhang, L. Li, Y.-Y. Li, *Soft Matter* **2011**, *7*, 2329-2331; cT.-B. Ren, W.-J. Xia, H.-Q. Dong, Y.-Y. Li, *Polymer* **2011**, *52*, 3580-3586.
[102] B. Khorsand Sourkohi, R. Schmidt, J. K. Oh, *Macromolecular Rapid Communications* **2011**, *32*, 1652-1657.
[103] L. Sun, W. Liu, C.-M. Dong, *Chemical Communications* **2011**, *47*, 11282-11284.
[104] D.-L. Liu, X. Chang, C.-M. Dong, *Chemical Communications* **2013**, *49*, 1229-1231.
[105] N. V. Tsarevsky, K. Matyjaszewski, *Macromolecules* **2005**, *38*, 3087-3092.
[106] D. A. Shipp, J.-L. Wang, K. Matyjaszewski, *Macromolecules* **1998**, *31*, 8005-8008.
[107] L. Yuan, J. Liu, J. Wen, H. Zhao, *Langmuir* **2012**, *28*, 11232-11240.
[108] Y.-L. Li, L. Zhu, Z. Liu, R. Cheng, F. Meng, J.-H. Cui, S.-J. Ji, Z. Zhong, *Angewandte Chemie International Edition* **2009**, *48*, 9914-9918.
[109] Y. Xu, F. Meng, R. Cheng, Z. Zhong, *Macromolecular Bioscience* **2009**, *9*, 1254-1261.
[110] Z. Jia, L. Wong, T. P. Davis, V. Bulmus, *Biomacromolecules* **2008**, *9*, 3106-3113.
[111] L. Yan, W. Wu, W. Zhao, R. Qi, D. Cui, Z. Xie, Y. Huang, T. Tong, X. Jing, *Polymer Chemistry* **2012**, *3*, 2403-2412.
[112] R. Wei, L. Cheng, M. Zheng, R. Cheng, F. Meng, C. Deng, Z. Zhong, *Biomacromolecules* **2012**, *13*, 2429-2438.
[113] Z. Zhang, L. Yin, C. Tu, Z. Song, Y. Zhang, Y. Xu, R. Tong, Q. Zhou, J. Ren, J. Cheng, *ACS Macro Letters* **2012**, *2*, 40-44.
[114] R. L. Momparler, M. Karon, S. E. Siegel, F. Avila, *Cancer Research* **1976**, *36*, 2891-2895.
[115] S. Oliveira, R. M. Schiffelers, J. van der Veeken, R. van der Meel, R. Vongpromek, P. M. P. van Bergen en Henegouwen, G. Storm, R. C. Roovers, *Journal of Controlled Release* **2010**, *145*, 165-175.
[116] X. Dai, Z. Yue, M. E. Eccleston, J. Swartling, N. K. H. Slater, C. F. Kaminski, *Nanomedicine: Nanotechnology, Biology and Medicine* **2008**, *4*, 49-56.

List of publications

N. Chan, **B. Khorsand**, S. Aleksanian, J. K. Oh* "Dual location stimuli-responsive degradation strategy of block copolymer nanocarriers for accelerated release"**,** *Chemical Communications*, **2013**, *49*, 7534-7536.

B. Khorsand, G. Lapointe, C. Brett, J. K. Oh* "Intracellular drug delivery nanocarriers of glutathione-responsive degradable block copolymers having pendant disulfide linkages"**,** *Biomacromolecules*, **2013**, *14*, 2103-2111.

B. Khorsand, J. K. Oh* "pH-responsive destabilization and facile bioconjugation of new hydroxyl-terminated block copolymer micelles"**,** *Journal of Polymer Science Part A: Polymer Chemistry*, **2013**, *51*, 1620-1629. (**Selected as spotlight article of the issue**)

S. Aleksanian, **B. Khorsand**, R. Schmidt, J. K. Oh* "Rapidly thiol-responsive degradable block copolymer nanocarriers with facile bioconjugation"**,** *Polymer Chemistry*, **2012**, *3*, 2138-2147.

B. Khorsand, A. Cunningham, Q. Zhang, J. K. Oh* "Biodegradable block copolymer micelles with thiol-responsive sheddable coronas"**,** *Biomacromolecules*, **2011**, *12*, 3819–3825. (**One of the top 5 most-read articles in Biomacromolecules in 2011**)

B. Khorsand, R. Schmidt, J. K. Oh* "New thiol-responsive mono-cleavable block copolymer micelles labeled with single disulfides"**,** *Macromolecular Rapid Communications*, **2011**, *32*, 1652–1657.